The role of feedback in maintaining robustness and modulation across scales:

Insights from cellular and network neurophysiology

Julie Dethier

Supervised by Professor Rodolphe Sepulchre

Systems and Modeling Research Unit
Department of Electrical Engineering and Computer Science
Faculty of Applied Sciences
University of Liège, Belgium

A thesis submitted for the degree of
Doctor of Philosophy in Engineering Sciences

August 2015

The present dissertation has been supervised by

Prof. R. Sepulchre	University of Liège, Belgium

The present dissertation has been evaluated by the members of the Jury (sorted by alphabetical order):

Prof. R. Bogacz		University of Oxford, UK
Prof. J.-M. Goaillard		University of Aix-Marseille, France
Prof. G. Kerschen	(Chair)	University of Liège, Belgium
Prof. P. Maquet		University of Liège, Belgium
Prof. R. Sepulchre	(Advisor)	University of Liège, Belgium
Prof. V. Seutin		University of Liège, Belgium

The research described in the present dissertation was financially supported by the Belgian F.R.S.-FNRS (National Fund for Scientific Research), and by the Belgian Network DYSCO (Dynamical Systems, Control, and Optimization), funded by the Interuniversity Attraction Poles Programme initiated by the Belgian Science Policy Office.

Abstract

The brain is a complex system made of many components acting at very different resolution levels, from the microsecond and nanometer scales with ion channels to hours and brain-wide scale with proteins. The brain dynamics and functions emerge from the interactions between these resolution levels. Mathematical modeling is a powerful ally to uncover some of the brain organizing principles and mechanisms. From this perspective, the question of which cellular details must be retained at the network level is largely open.

Motifs simplify systems by approximating the wiring diagram and by taking advantage of the timescale separation between processes. Yet, motifs study each resolution level separately and neglect couplings between levels. This approach falls short of system-level questions and multiresolution intrinsic properties.

The present dissertation aims at narrowing the gap by looking at the *interplay between resolution levels*. We propose to extract essential elements, in the form of feedback loops, to be maintained from one resolution to the next in the hope of a better understanding of brain functions and diseases. The focus is on the spatiotemporal upscaling from the neuron to the network level and, in particular, on the maintenance of modulation and robustness properties across scales. This approach is used in a two-neuron network and is extended to a prospective multiresolution excitability framework. The main contributions of this dissertation are the following.

We identify the key role of *a cellular feedback loop for network oscillation robustness and modulation*. Rhythms are crucial in the brain functioning but much awaits to be understood regarding their control, regulation, and function. In a mutually-inhibitory network, we isolate an essential cellular property—a positive feedback loop in the slow timescale—to be retained at the network level to ensure modulation and robustness of network oscillations.

We highlight the peculiar role that *a cellular feedback loop can play for the regulation of network switches*. We identify that a cellular positive feedback loop brings localization properties, both temporally and spatially, to network oscillations. The emerging picture suggests a basal ganglia network model valid both in healthy movement-related oscillations and in parkinsonian conditions.

Multiresolution excitability emerges due to localization properties of excitable systems: different excitability resolution windows can be superposed and interact, generating multiresolution systems. In each window, the system is characterized via its transfer properties and input-output behavior. Signal processing properties appear in these multiresolution systems and endow multiresolution objects with gating and multiplex signaling capabilities.

In conclusion, the present dissertation provides novel insights on the importance of the interplay between cellular and network levels. This multiresolution motif perspective is thought to be general and not specific to neuroscience. Finally, exploiting the concept in multiresolution technologies is suggested.

Résumé

Le cerveau est un système complexe composé d'éléments actifs à des niveaux de résolution très différents, de la microseconde et nanomètre avec les canaux ioniques, à l'heure et l'échelle du cerveau avec les protéines. La dynamique et les fonctions du cerveau émergent des interactions entre les différents niveaux de résolution. La modélisation mathématique est un allié puissant pour dévoiler certains des principes organisationnels et mécanismes cérébraux. Dans ce contexte, la question de savoir quels détails cellulaires doivent être conservés au niveau du réseau reste largement ouverte.

Les motifs décomplexifient les systèmes en simplifiant le schéma de connexion et en exploitant la séparation des échelles de temps entre processus. Cependant, les motifs étudient chaque niveau séparément et négligent les couplages entre niveaux. Cette approche passe à coté des questions systémiques et des propriétés intrinsèques de multirésolution.

Cette thèse a pour but de rapprocher les deux domaines en étudiant les *interactions entre niveaux de résolution*. Nous proposons d'extraire les éléments principaux, sous la forme de boucles de feedback, à maintenir d'une résolution à la suivante dans l'espoir d'une meilleure compréhension des functions et maladies cérébrales.

L'accent est placé sur le changement d'échelle spatiotemporelle, du niveau neuronal au niveau réseau, et en particulier sur le maintien des propriétés de modulation et de robustesse à travers les échelles. Cette approche est utilisée dans le cas particulier d'un réseau de deux neurones et est étendue à un cadre théorique plus spéculatif d'excitabilité multirésolution. Les principales contributions de cette thèse sont les suivantes.

Nous identifions le rôle clé joué par *une boucle de feedback cellulaire pour la modulation et la robustesse des oscillations réseaux*. Les rythmes sont cruciaux pour le fonctionnement du cerveau mais leurs contrôles, régulations, et fonctions sont loin d'être compris. Dans un réseau avec inhibition mutuelle, nous isolons une propriété cellulaire essentielle—une boucle de feedback positive dans l'échelle lente—à maintenir au niveau réseau afin d'assurer des oscillations réseaux modulables et robustes.

Nous soulignons le rôle particulier qu'*une boucle de feedback cellulaire peut jouer dans la régulation des interrupteurs réseaux*. Nous identifions qu'une boucle de feedback positive apporte des propriétés de localisation, à la fois temporellement et spatialement, aux oscillations réseaux. Ces propriétés suggèrent un nouveau modèle réseau des ganglions de la base, valide dans l'état sain pour les oscillations liées au mouvement ainsi que dans l'état parkinsonien.

L'*excitabilité multirésolution* émerge dû aux propriétés de localisation des systèmes excitables : des fenêtres d'excitabilité de résolution différente sont superposées et interagissent, créant des systèmes multirésolutions. Dans chaque

fenêtre, le système est caractérisé par ses propriétés de transfert et par son comportement entrée-sortie. Des propriétés de traitement du signal apparaissent dans ces systèmes multirésolutions et dotent les objets multirésolutions de capacités de blocage et de multiplexage des signaux.

En résumé, cette thèse offre un nouvel aperçu de l'importance du couplage entre le niveau cellulaire et réseau. Le concept de motif multirésolution semble être général et non limité aux neurosciences. Enfin, l'exploitation du concept en technologies multirésolutions est suggérée.

Acknowledgements

A doctoral dissertation is a personal journey. However, this journey would have been impossible without the help and support from many people to whom I would like to express my sincere gratitude.

First and foremost, I heartily thank my advisor, Rodolphe Sepulchre, for his scientific enthusiasm and his ever pertinent guidance. I am very grateful to Rodolphe for his precious advice and support, both scientifically and personally. His permanent optimism and his passion for novelty in research succeeded in providing me with the motivation and self-confidence necessary to accomplish this journey. I am especially appreciative of the stimulating international work environment he established in Liège and Cambridge and his support and encouragements for my research stay in Princeton.

I am also indebted to my (former and present) colleagues. Many thanks to my friends and colleagues at the University of Liège. I enjoyed very much working and exchanging with them in a pleasant and friendly atmosphere. Special thanks go to Guillaume Drion for his sound advice and suggestions throughout this journey. I am also grateful to the team at Cambridge University for their warm welcome, help, and support during my research stays. Finally, I want to thank the team at Princeton University and especially Prof. Naomi Leonard for her guidance and the exciting work environment I benefited from during this past year.

I wish to express my sincere appreciation to the members of the Jury for devoting time and interest to the reading and evaluation of this manuscript. The members of the thesis committee are also acknowledged for their advices during the progress of this work.

I gratefully acknowledge the financial support from the Belgian National Fund for Scientific Research (FNRS), Wallonie-Bruxelles International, the Lear Foundation, and the Belgian Network DYSCO (Dynamical Systems, Control, and Optimization), funded by the Interuniversity Attraction Poles Programme, initiated by the Belgian State, Science Policy Office.

Last, but not least, my enormous gratitude goes to my family and friends. I owe my parents many thanks for their unconditional support and love which consistently pushed me to challenge myself. I am grateful to my sisters and family-in-law for helping me to disconnect from research when needed and offering me so many pleasant moments. I want to thank my friends, especially the ones who shared this journey with me at the University, for cheering me up when I needed so. Finally, my deepest gratitude goes to my loving, supportive, encouraging, and patient husband Thomas, whose faithful support has been, by far, the most precious encouragement. Having him by my side encourages me to undertake the most ambitious of the projects. Thank you.

Contents

1 Introduction **1**
- 1.1 Research context . . . 2
- 1.2 Contributions of the dissertation . . . 2
- 1.3 Outline of the presentation . . . 5
- 1.4 Publications . . . 5

2 Modeling the brain, from ion channels to functions **7**
- 2.1 The brain: components, functions, and models . . . 8
  - 2.1.1 Resolution levels of the brain . . . 8
  - 2.1.2 Brain rhythms and functions . . . 8
  - 2.1.3 Resolution levels in models . . . 11
- 2.2 Neurodynamics and excitability . . . 13
  - 2.2.1 Hodgkin-Huxley neuron model . . . 13
  - 2.2.2 Excitability . . . 17
- 2.3 Motif approach . . . 18
  - 2.3.1 Positive and negative feedback loops . . . 18
  - 2.3.2 Generality of the motif approach . . . 19
  - 2.3.3 Excitability motif . . . 20
- 2.4 Excitability motif in neuroscience . . . 21
  - 2.4.1 Excitability in neurons . . . 21
  - 2.4.2 Excitability in networks . . . 23
- 2.5 Temporal superposition of excitable motifs . . . 24
  - 2.5.1 Burst-firing pattern . . . 24
  - 2.5.2 Three-timescale bursting neuron model . . . 25
  - 2.5.3 Excitability motif in two temporal resolutions . . . 26
- 2.6 Interacting motifs . . . 26
  - 2.6.1 Half-center oscillators . . . 27
  - 2.6.2 Excitatory-inhibitory circuits . . . 28
- 2.7 Neuron-level and network-level motifs . . . 29
  - 2.7.1 Interactions between resolution levels . . . 29
  - 2.7.2 Neuron resolution level in networks . . . 29

2.8 Summary 30

3 Cellular feedback for network modulation and robustness 31
3.1 Slow activation of T-type calcium channels is critical to robustness of network rhythmic activity 32
3.2 Robust modulation of network properties requires slow regenerativity 36
3.3 Robustness of network oscillations requires PIR with slow regenerativity 40
3.4 Discussion 44
3.4.1 Complementarity between the two types of PIR currents 44
3.4.2 Positive feedback as a source of endogenous activity . . 44
3.4.3 Slow regenerativity in half-center oscillator models . . . 45
3.5 Summary 46

4 Cellular feedback for transient oscillations in networks 47
4.1 The role of T-type calcium channels in underlying a cellular excitability switch 48
4.2 Hyperpolarized-induced bursting relies on slow activation and ultraslow inactivation 50
4.3 The three-timescale bursting model captures the cellular switch 52
4.4 The cellular switch induces a network switch 53
4.5 Robustness and modulation of the network rhythmic activity . 54
4.6 Temporal and spatial localization of the network switch 56
4.7 Discussion 58
4.7.1 The cellular-based network switch yields physiologically relevant applications 58
4.7.2 Comparison with experimental data 62
4.7.3 Comparison with previous models 63
4.8 Summary 64

5 Localized transfer properties of excitable behaviors 65
5.1 Excitable systems have an exogenous and an endogenous behavior 66
5.2 Monoresolution excitability motif 67
5.3 Bursting as coexisting fast and slow excitability 70
5.4 Circuit spike as coexisting fine and coarse excitability 72
5.5 Multiplex signaling 73
5.6 Discussion 76
5.6.1 Localization and hierarchical sources of feedback 76
5.6.2 Physiological implications 77
5.7 Summary 80

6 Conclusion **83**
6.1 Summary . . . 83
6.2 Prospects . . . 86
6.2.1 A neuromorphic gating control mechanism for information transfer . . . 86
6.2.2 Hardware implementation . . . 89
6.2.3 Multiresolution excitability in technology . . . 91

A Numerical tools **93**
A.1 Conductance-based model . . . 93
A.1.1 Neuron model . . . 93
A.1.2 Network model . . . 95
A.2 Reduced model . . . 96
A.2.1 Neuron model . . . 96
A.2.2 Network model . . . 96
A.3 Tools for simulation analysis . . . 98
A.3.1 Variability . . . 98
A.3.2 Network rhythm . . . 98
A.3.3 Noise . . . 99
A.3.4 Local field potential and time-average . . . 99
A.3.5 Spectrogram . . . 100
A.3.6 Correlations . . . 100
A.4 Simulation details . . . 100
A.4.1 Chapter 3 . . . 100
A.4.2 Chapter 4 . . . 101
A.4.3 Chapter 5 . . . 102

B Omitted derivations **105**
B.1 State-space model . . . 105
B.2 Linear state-space model . . . 107
B.3 System of equations for T_{osc} and T_{burst} . . . 108

Chapter 1

Introduction

> *"...comparing the capacity of computers to the capacity of the human brain, I've often wondered, where does our success come from? The answer is synthesis, the ability to combine creativity and calculation, art and science, into a whole that is much greater than the sum of its parts."*
>
> *Garry Kasparov (1963)*

This quote from the famous Russian chess Grandmaster and former World Chess Champion highlights the intrinsic complexity of the brain: the emergence of complex brain activity dynamics and functions from the interactions of its many composing elements.

In this dissertation, we aim at simplifying the picture by extracting similar organizing principles, in the form of motifs, that are at play at different resolution levels in the brain. The interactions between these different resolution levels, in particular the cellular and network levels, is under scrutiny to investigate how system-level properties are maintained across scales. This approach is pursued in the hope of a better understanding of brain functions and diseases.

1.1 Research context

Mathematical tools are powerful allies to gain insights on brain functions and underlying mechanisms. Pioneering steps in this direction can be traced to the work of people such as Louis Lapicque, Hodgkin & Huxley, and David Marr, among others. Mathematical models are used to capture essential features of the system under study and to frame hypotheses that can later be verified experimentally.

The brain is a complex system made of many components—e.g., ion channels, neurons, or brain regions—and each of these components is shaping the brain activity and functions at a distinct resolution level. Mathematical models capture the activity of these components in their respective resolution. However, emphasis on the interactions between the different resolution levels, and more precisely on the impact of higher resolutions on the behavior at lower resolutions levels, is scarce in the literature. The question to determine which details from high resolution levels must be retained at lower resolution levels is largely open, especially when it comes to understand system-level questions such as robustness and modulation properties. For closed systems, many reduction tools exist. But for open systems, reduction methods are not well understood except for linear time-invariant (LTI) systems.

Motifs have been widely used in systems biology to identify shared design principles [4, 249]. The motif approach consists in adopting an engineer's mindset to control systems by identifying simple patterns of activation and inhibition among a small number of components that carry out specific functions [3, 94, 234, 246, 249]. Motifs help for generalization purposes: a motif captures the recurring patterns of interactions in a system and simplifies the picture [3, 94]. However, motifs characterize the dynamics in each resolution level independently and the interactions between resolution levels are ignored.

1.2 Contributions of the dissertation

In the above context, the present dissertation proposes to investigate the interplay between resolution levels to gain some insights on how elements at high resolution levels impact lower resolution levels. The simplification of systems to the description of solely their coarser elements results in the suppression of finer resolution levels and the destruction of intrinsic multiresolution characteristics. At the other side of the spectrum, highly detailed models at very high resolution levels are not computationally tractable and analyzable for large systems. The approach we follow aims at narrowing the gap between those two extremes and at extracting essential elements, in the form of feedback loops, to be maintained from one resolution to the next to preserve intrinsic multiresolution properties. The focus lies on the transition in spatiotemporal scale from

the neuron level—fast and fine scales—to the network level—slow and coarse scales.

In particular, this dissertation includes the following specific contributions.

As a conceptual contribution, we propose to study the *interplay between motifs at different resolution levels*. To motivate this approach, we identify brain resolution levels, in physiology and in models, and provide two instantiations of the limitation of the motif approach when considered at a unique resolution level. In the dissertation, the interaction of interest is between the neuron and the network levels: in particular, how system-level properties, mainly modulation and robustness, are maintained in the coupling between these two levels. The importance of the interplay between motifs at different resolutions is thought to be of general interest, beyond the specific on neuroscience systems in the present dissertation.

A methodological contribution is to illustrate how this approach helps to determine the key role of *a cellular positive feedback loop for network oscillation robustness and modulation*.

Biological rhythms play a major role in the functioning of the brain. However, the generation mechanisms and functions of these rhythms are still under debate. We isolate a basic cellular property, a positive feedback loop in the slow timescale, to be retained at the network level in modeling network robustness and modulation. The importance of this cellular property is assessed in one of the simplest and best understood network oscillation mechanisms, the anti-phase rhythm observed between two populations of neurons mutually connected by inhibitory synaptic connections.

In a neurophysiological context, our work suggests a novel and perhaps fundamental complementarity between two ionic currents in post-inhibitory rebound (PIR) mechanisms, a cellular level excitability property at the core of network oscillations. Our results predict that PIR per se is not sufficient to ensure modulation and robustness of network oscillations. In addition, the slow positive feedback nature of the current dynamics must be retained as an important parameter. However, this important aspect is frequently lost in existing reduced models.

Another methodological contribution lies in the identification of the peculiar role that *a cellular feedback loop can play for the regulation of network switches*. We distinguish PIR from hyperpolarized-induced bursting (HIB), i.e., the ability to switch between a single-spike discharge mode to a burst-firing mode when the membrane is hyperpolarized and a permanent source of endogenous behavior, and we show that HIB is a source of localization properties, both temporally and spatially, in network oscillations.

Rhythmic brain activities are robust to parameter heterogeneity and noise and can undergo modulation to adapt to changing environmental conditions.

The physiological driving example takes place in the basal ganglia, a group of subcortical nuclei involved in movement initiation and learning. The cellular feedback loop endows network with cellular-based network switch capabilities for transient network oscillations.

The proposed mechanism is simple, generic, and robust, and suggests the orchestration of network oscillations via a cellular switch mediated by neurotransmitters. The emerging picture suggests a basal ganglia network model switch independent from synaptic changes and applicable in both healthy conditions associated to movement control and persistent pathological parkinsonian oscillations.

The approach is generalized to explore the multiresolution aspect of the excitability motif and to propose the prospective *multiresolution excitability* framework.

The general contribution consists in associating input-output behavior characteristics to a motif and in characterizing its transfer properties with traditional correlation measures to quantify the behavior of excitable systems. We identify that the excitability motif possesses localization properties—in time, space, and amplitude—and that a superposition principle can be applied to form multiresolution excitable systems: different excitability resolution windows can be superposed and interact, generating multiresolution objects.

The importance of the hierarchy in feedback loops, in addition to the sign, is emphasized: cellular positive feedback gives rise to localization properties and therefore allows for spatial and temporal modulation, whereas network positive feedback produces a general and permanent switch. Physiological implications of this hierarchical organization are explored in the physiologically relevant thalamocortical network.

Finally, repercussions for *signal processing capabilities* of excitable systems are highlighted.

The transient network oscillations suggest a *gating function mechanism*: a transient increase in neuromodulator level controls the network state (an endogenous oscillatory OFF state which filters incoming signals and an exogenous transfer ON state receptive to peripheral signals). Potential engineered applications exploiting this function are proposed.

Our results suggest that multiresolution excitable systems are endowed with *multiplex signaling* capabilities: the input controls the spatial and temporal scales in which the communication (fine grain or coarse grain) takes place.

The specific contributions of the thesis are highlighted at the end of each chapter introduction.

1.3 Outline of the presentation

The dissertation is organized as follows.

Chapter 2 presents the concept of resolution levels in brain physiology and models, and describes the motif approach. Emphasis is set on the excitability motif, with examples in neuroscience, at the neuron and network level. The motivation for the dissertation is provided with two examples where the motif approach leads to modeling limitations when ignoring the coupling between resolution levels. The novel approach suggests to investigate the interplay between resolution levels to extract critical mechanisms, in the form of feedback loops, from high resolution levels for the activity at lower resolutions.

Chapter 3 introduces the cellular PIR property and the two major ionic currents that underlie it. Those two currents are differentiated by their dynamical feedback loops as well as by their impact on the modulation and robustness properties of network oscillations. The generality of the approach is discussed and the implications for mathematical models are highlighted.

Chapter 4 captures a cellular excitability switch in a conductance-based model and in a reduced version. It highlights the distinction between PIR and HIB. In this chapter, we propose a cellular-based network switch and study its robustness, modulation, localization, and gating properties. The physiological basal ganglia application is detailed and its physiological relevance, both in healthy and diseased conditions, is investigated. A comparison to previous models of the basal ganglia is given.

Chapter 5 is more speculative and proposes to study multiresolution excitability with an input-output behavior perspective by investigating transfer properties. Localization properties in excitable systems are highlighted and a superposition principle is applied. Monoresolution and multiresolution characteristics are studied at three resolution levels: spike, burst, and circuit excitability. An analysis of multiplex signaling is provided for multiresolution objects. Finally, the thalamus is given as a physiological relevant illustration of multiresolution excitable system.

Chapter 6 concludes the dissertation, summarizes the major contributions, and offers perspectives for future work.

Appendix A provides the numerical tools and details for the models, simulations, and analyses presented in the manuscript. Appendix B collects derivations omitted in the general dissertation.

1.4 Publications

The main results of this dissertation are presented in the following publications and conference proceedings:

- J. Dethier, G. Drion, A. Franci, and R. Sepulchre. A positive feedback at the cellular level promotes robustness and modulation at the circuit level. *J Neurophysiol*, 2015. In Press
- J. Dethier, G. Drion, A. Franci, and R. Sepulchre. Cellular control of network oscillations. In preparation (preprint http://arxiv.org/abs/1311.2238)
- G. Drion, A. Franci, J. Dethier, and R. Sepulchre. Dynamic input conductances shape neuronal spiking. *eneuro*, 2015
- J. Dethier, D. Ernst, and R. Sepulchre. Neuromorphic reinforcement learning. In *Proc 31st Benelux Meeting on Systems and Control*, Heijen/Nijmegen, 2012
- J. Dethier, G. Drion, A. Franci, and R. Sepulchre. Impacts of a unicellular mechanism on network behaviors. In *Proc 32nd Benelux Meeting on Systems and Control*, Houffalize, 2013
- J. Dethier, G. Drion, A. Franci, and R. Sepulchre. Modulation of beta oscillations during movement initiation: modeling the ionic basis of a functional switch. In *Proc 43rd Annual Meeting of the Society for Neuroscience*, San Diego, CA, 2013
- J. Dethier, G. Drion, and R. Sepulchre. Contrasting the role of Ih and ICaT currents in post-inhibitory rebound mechanisms in reciprocal-inhibitory networks. In *Proc 44th Annual Meeting of the Society for Neuroscience*, Washington, DC, 2014
- G. Drion, T. O'Leary, J. Dethier, A. Franci, and R. Sepulchre. Neuronal behaviors: a control perspective. In *Proc 54th IEEE Conference on Decision and Control*, Osaka, Japan, 2015

In addition, a collaboration with the Brains in Silicon laboratory, Stanford, lead to the following publication (not included in this dissertation):

- J. Dethier, P. Nuyujukian, S. I. Ryu, K. V. Shenoy, and K. Boahen. Design and validation of a real-time spiking-neural-network decoder for brain-machine interfaces. *J Neural Eng*, 10(3):036008, 2013

Chapter 2

Modeling the brain, from ion channels to functions

The brain is a complex system made of many components and each of these components is shaping the brain activity and functions at a distinct resolution level. Mathematical models capture the activity of these components in their respective resolution.

The interactions between the different resolution levels, and more precisely the impact of higher resolutions on the robustness and modulations properties at lower resolution levels is somewhat obscure.

The focus of this thesis is to study the interplay between different resolution levels. In this perspective, we extract particular elements, in the form of feedback loops, at high resolution levels and investigate their impact at lower resolution levels.

The chapter is organized as follows. Section 2.1 introduces the concept of resolution levels in brain physiology and models. Section 2.2 presents the seminal work of neurodynamics: the description by Hodgkin and Huxley of the initiation and propagation of action potentials. This section also extracts a fundamental concept of neuroscience: *excitability*. Section 2.3 describes the motif approach. The positive and negative feedback loops—the major building blocks of motifs—are depicted, and the generality of the motif approach is illustrated. Emphasis is set on the excitability motif. Section 2.4 provides instances of the excitability motif in neuroscience, separately at the neuron level and at network level. Section 2.5 presents neuronal bursting and highlights the interplay between excitability motifs at two different temporal resolutions. Section 2.6 stresses, with two examples, the importance of studying interactions between motifs at different spatiotemporal resolution levels. Section 2.7 presents the approach followed in this dissertation: the study of the interplay

between different resolution levels, in particular the neuron and the network levels.

Contributions. The main objective in this chapter is (i) to identify brain resolution levels, in physiology and in models, (ii) to present a fundamental concept of neuroscience, excitability, and its motif representation, the +FB then –FB motif, and (iii) to motivate the need to study the interplay between different resolution levels.

2.1 The brain: components, functions, and models

2.1.1 Resolution levels of the brain

Electrical activity in the brain span a broad range of temporal scales, from milliseconds (action potentials), seconds (calcium dynamics) to hours (protein synthesis) and a broad range of spatial scales, from nanometers (ion channels), micrometers (neurons) to millimeters (brain regions). Figure 2.1 represents the molecular, cellular, network, and organ levels, with activity in each level at specific spatial, temporal, and amplitude scales.

To monitor these brain activities at multiple spatial and temporal levels, recording methods with 'sufficient' spatial and temporal resolution are required. The definition of 'sufficient' in this context depends on the system under study as every existing methods has to compromise between spatial and temporal resolution [28, 29]. At each resolution level, the mechanisms at play are generally understood: the molecular, developmental, and functional properties of neurons are mostly known; at the opposite resolution level, behaviors can be correlated to brain imaging [198]. However, how to close the explanatory gap between the different levels is far from being understood; in particular, which aspects from a finer/faster resolution level should be kept to describe a coarser/slower resolution are still largely unknown.

2.1.2 Brain rhythms and functions

Neuronal rhythms are ubiquitous features of the brain but their underlying physiological mechanisms and associated functions remain elusive [28, 34, 94, 106, 241, 250, 253]. In this dissertation, we focus specifically on electrical activities, by contract other type of rhythmic activities, e.g., hormonal or circadian. Since the invention of the electroencephalogram (EEG) by Hans Berger in the 1920's, electrical rhythmic activities have been known to emerge in various structures of the brain [28, 106, 241]. These rhythms differ in many ways, such as frequency (ranging from 0.02 hertz to 600 hertz), origin, and reactivity to environmental changes [241]. The precise role of these oscillations remains

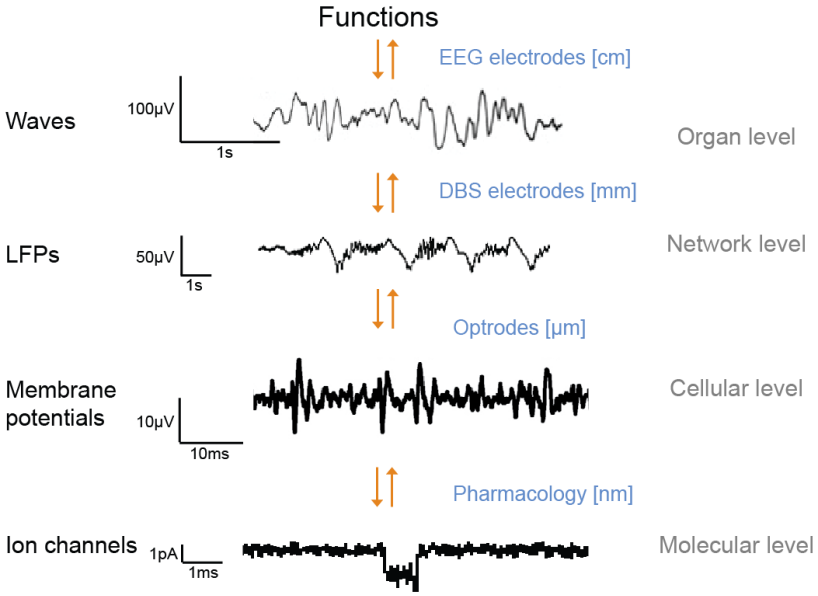

Figure 2.1 – The brain resolution levels. Activity in the brain takes place at distinct levels with specific temporal, spatial, and amplitude scales. Example with four resolution levels: molecular, cellular, network, and organ levels. The resolution at which the brain activity is recorded depends on the system under study.

unclear but their relationship with specific cognitive processes is now well accepted [34, 106, 241].

Rhythms emerge from complex interactions between cellular and network mechanisms and their specific characteristics depend on the properties of their constituent elements [28, 94, 106, 253]. Unfortunately, the exact mechanisms of most rhythms are uncertain. In addition, different rhythms, via modulatory mechanisms, can emerge from one brain area [34, 94].

These neuronal oscillations are highly correlated with cognitive functions, e.g., perceptual grouping, sensory coding, attentional gain modulation, routing of signals, sensory-motor integration, working memory, and perceptual awareness [34,106,241,250,253]. One role of the oscillations seems to be the grouping and coordination of interactions between large numbers of neurons for sculpting temporal coordination of neural activity in the brain-wide network, supporting information multiplexing and inter-area communication [106, 241, 250, 253].

Rhythmic brain activities have been classified, following Berger's tradition, in frequency bands labeled with Greek letters [28]. It is out of the scope of the present dissertation to review and classify all the neuronal oscillations discovered so far. Rather, we draw a non-exhaustive list of brain oscillations to highlight their wide frequency ranges, origins, and putative functions:

- Delta oscillations (0.5–4 hertz): slow-wave sleep emerging from the thalamus [176], hippocampal rhythms involved in signal detection and decision making [242].

- Theta oscillations (4–8 hertz): oscillations in the hippocampus in relation to cognitive processing [242], cortical oscillations for tasks engaging working memory [71, 134].

- Alpha oscillations (8–12 hertz): thalamocortical oscillations for propofol-induced loss of consciousness [38], cortical oscillations associated with memory clearance [71], cortical oscillations reflecting attention selection and control [142, 172, 182].

- Beta oscillations (12–30 hertz): in the cerebral motor cortex prior to an expected postural challenge [7], in relation to impaired movement [23], in the striatum of awake behaving monkeys [44], in the basal ganglia as a measure of the likelihood for the need of actuation for a new voluntary action [133].

- Gamma oscillations (>30 hertz): in many brain regions during both waking and sleep states [30].

Brain disorders, such as schizophrenia, epilepsy, autism, Alzheimer's disease, and Parkinson's, have also been associated with strong rhythmic activities

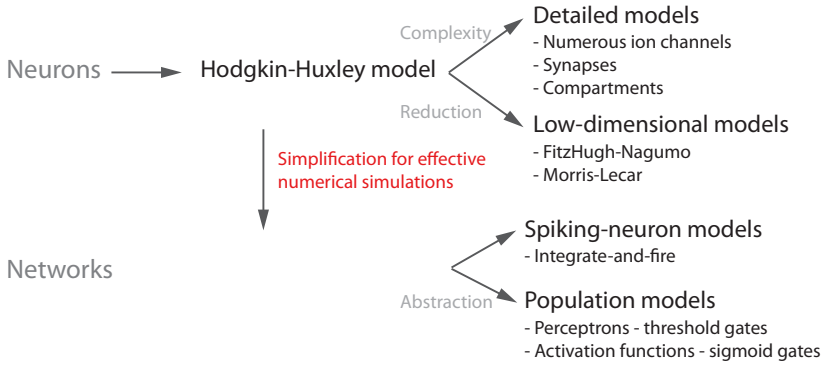

Figure 2.2 – Model resolution levels. The spatiotemporal scales of the models cover the resolution levels of the brain and depend on the mechanism under study. Focus on the neuron and network levels for brain models.

in the brain [250]. EEG studies support that schizophrenia is related to impaired neural synchrony in the beta- and gamma-frequency range. By contrast, large-amplitude fluctuations in the EEG reveal that epilepsy is correlated with abnormal neural synchronization, especially in the gamma-band, in extensive brain regions. Several fMRI studies have highlighted the reduced functional connectivity, reflecting reduced neural synchronization, with the dysfunctional integrative symptoms of autism. Patients suffering from Alzheimer's disease see a relative increase in the theta- and delta-band activity simultaneously with a reduction in the alpha- and beta-band activity. Finally, Parkinson's disease correlates with an enhanced synchronized beta-band activity. The study of these abnormal oscillations is also instructive for our understanding of normal brain functions.

2.1.3 Resolution levels in models

Mathematical modeling is essential to advance the understanding of the brain organizing principles and mechanisms. In this approach, models are used to capture the essential features of the biological system and to frame hypotheses that can later be verified experimentally. The spatiotemporal scales of the models cover the resolution levels of the brain (see section 2.1.1) and depend on the mechanism under study. In this dissertation, we focus on the neuron and network levels (see Figure 2.2).

At the neuron level, we distinguish two types of models: detailed—or conductance-based—neuron models and reduced—or low-dimensional—neuron models. Detailed neuron models trace back to the seminal work of Hodgkin and Huxley on the giant axon of the squid [120] (see section 2.2.1). Action

potentials result from the passage of currents through ion channels in the cell membrane. Hodgkin and Huxley managed to measure those currents and to derive a set of differential equations to describe their dynamics. Over the years, the biological complexity of detailed models has increased with the insertion of numerous ion channels, different types of synapse, and the specific spatial geometry of individual neurons [49, 93]: electrophysiologists have described a realm of different ion channels, different from one neuron to the next, synaptic transmission is modeled as specific ion channels, and the complex geometry of the neuron has been taken into account in multi-compartment models.

Complex high-dimensional nonlinear models involving thousands of coupled differential equations are difficult to analyze and to visualize. This obstacle is tackled by reducing high-dimensional models to a set of low-dimensional differential equations where the power of the phase-plane analysis can be exploited [49, 93]. Examples of low-dimensional models include the FitzHugh-Nagumo model and the Morris-Lecar model (these models are described in section 2.4.1).

At the network level, simplification of neuron models can accelerate simulations drastically at the expense of the explicit description of the biophysical mechanisms responsible for action potentials. One such simplification instantiates in the integrate-and-fire model, which is part of the broader category of spiking-neuron models [49, 93]. In these models, spikes are fully characterized by their firing time defined by a threshold criterion. There exist different complexity levels in spiking-neuron models, including e.g., multi-compartment models, non-linear models with voltage-dependent parameters, and spike-rate adaptation [49, 93].

When describing large and homogeneous networks, it is sensible to use a mean-field approximation and to describe the mean activity of the neuronal population, i.e., the mean-firing rate or probability density of firing [49, 93, 160](see section 2.4.2). The first generation of such models is based on the McCulloch-Pitts neurons—i.e., perceptrons or threshold gates—whose output is all-or-none (0 or 1). The second generation is based on computational units with an activation function, typically the sigmoid function. These computational units, or sigmoidal gates, possess a continuous set of possible outputs.

The firing-rate models have numerous advantages compared to spiking-neuron models [49]. For instance, they are easier to simulate on computers, possess less free parameters, and introduce stochasticity. However, they eliminate the aspects of spike timing and spike correlations and they are restricted to simulations of uncorrelated firing neurons.

In practice, the type of model used depends on the problem under study and results from a tradeoff between biophysiological plausability and computational cost. For instance, Hopfield studied recurrent neural networks with threshold and sigmoidal gates [121, 122]. These ‘Hopfield nets’ are capable of

emulating an associative memory by storing and recalling memory patterns [49]. Recent projects have taken the opposite approach, emphasizing biological realism. Covering the entire range of the spectrum, from computational efficient to biophysiological plausible models, one can mention:

- the SyNAPSE project, a DARPA-funded program, which aims at building an electronic system that matches a mammalian brain in function, size, and power consumption;
- the SPAUN project, at the University of Waterloo, Canada, which consists in a 2.5-million-neuron model of the brain as an attempt to bridge the gap between neural activity and biological functions;
- the BRAIN Initiative, a US-based project, whose goal is to produce dynamic pictures of the brain that show how individual brain cells and complex neural circuits interact;
- the Human Brain Project, funded by the European Union, which targets the project to provide a human whole brain model through a collaborative informatics infrastructure.

We refer the interested reader to the respective project websites.

2.2 Neurodynamics and excitability

In the early fifties, Hodgkin and Huxley proposed a biophysical model to explain the ionic mechanisms underlying the initiation and propagation of action potentials in a nerve cell [120]. Their pioneering work in neurodynamics was the first to quantitatively record and mathematically describe excitability through the generation of an action potential.

2.2.1 Hodgkin-Huxley neuron model

The cell membrane that separates the cytoplasm from the extracellular medium is made of a phospholipid bilayer, which is permeable to small molecules and water but almost fully impermeable to ions and large molecules. Transmembrane proteins are embedded in the cell membrane, crossing it from side to side. These proteins are selectively permeable to one or several specific substances, depending on their structure, and regulate the transport of these subtances in and out of the cell.

The neuron electrical behavior is based on the movement of unequally distributed electric charges, carried by ions—in particular the sodium ions (Na^+) and the potassium ions (K^+)—across the cell membrane. The ion flow is

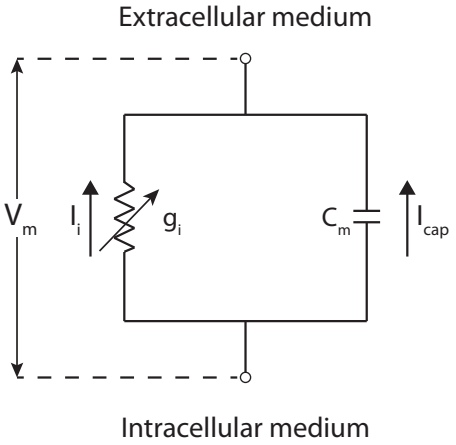

Figure 2.3 – The neuron membrane can be likened to the classic electrical RC circuit. The phospholipid cell membrane is likened to a capacitor of capacitance C_m and the transmembrane proteins to dynamic resistor g_i.

allowed by the transmembrane proteins. This flow can be passive via *ion channels*, which allow the flow following a concentration gradient, or active via *pumps*, which use cellular energy to move specific ions against their concentration gradient. The relative concentrations of ions across the cell membrane and the membrane permeability to these ions result in an electrical potential gradient across the membrane, called the *membrane potential* (V_m). Neuronal signaling results from abrupt variations in this membrane potential: typically, V_m is close to $-70mV$ at rest and rises up to $40mV$ during action potential (*membrane depolarization*).

The neuron membrane can be likened to the classic electrical *RC circuit* (Figure 2.3). The phospholipid cell membrane is impermeable to ions and only allows for the accumulation of charges on each side, acting as an electric capacitor. Its capacitance C_m is constant and function of the cell. Regarding transmembrane proteins, they are ion selective and can be likened to resistors, whose conductance g_i is dynamically regulated as the channels regulate their opening state.

Mathematical modeling is therefore particularly suited to describe the neuron membrane electrical behavior. The application of Kirchhoff's current law gives:

$$I_{cap} = -I_i + I_{app},$$

with

$$I_{cap} = C_m \frac{dV_m}{dt},$$
$$I_i = \sum_{ion} I_{ion},$$

where I_{ion} is the ionic current corresponding to a specific *ion* and I_{app} includes external stimulations.

Following Ohm's law, the ionic current I_{ion} depends on the conductivity of the channel g_{ion} (reflecting the fraction of open channels) and the difference between the membrane potential and ion reversal potential E_{ion} (the ion *reversal potential*, or *Nernst potential*, is the membrane potential at which the voltage driving force exactly balances the chemical driving force due to the asymmetric ion concentration):

$$I_{ion} = g_{ion} \left(V_m - E_{ion} \right).$$

By convention, an inward (resp. outward) ionic current has negative (resp. positive) sign. The general equation for n different ionic currents writes as follows:

$$C_m \frac{dV_m}{dt} = - \sum_n g_{ion} \left(V_m - E_{ion} \right) + I_{app}.$$

This equations is at the basis of electrophysiological modeling and neurodynamics.

In their early work, Hodgkin and Huxley characterized the tight regulation of ion channel opening states [120]. For practical reasons, they performed their experiments on the squid giant axon, a $1mm$-diameter cell which allows for manual experiments. Their first observation revealed that the necessary ions for action potentials are the sodium (Na^+) and the potassium (K^+) ions. Therefore, the general model described previously particularizes to the circuit of Figure 2.4 where the g_L conductance (L for leak) accounts for the passive diffusion occurring through the membrane independently of voltage-gated channels. The equation writes:

$$\begin{aligned} C_m \frac{dV_m}{dt} &= -I_{Na} - I_K - I_L + I_{app} \\ &= -g_{Na}(V_m - E_{Na}) - g_K(V_m - E_K) - g_L(V_m - E_L) + I_{app}. \end{aligned}$$

Hodgkin and Huxley also discovered that ionic channels are voltage-gated and that the ionic conductances g_{Na} and g_K are dynamically regulated by the membrane potential V_m. In order to find a mathematical expression for the dynamic regulation of these conductances, Hodgkin and Huxley performed

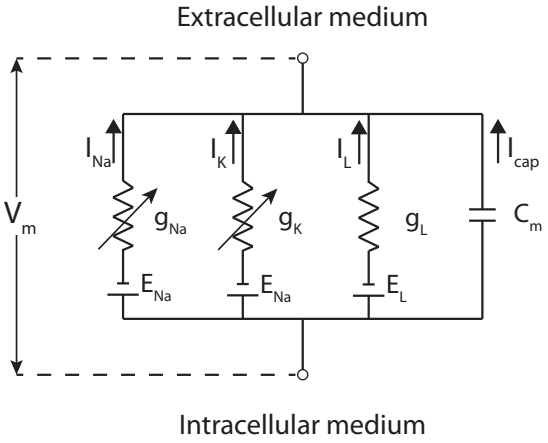

Figure 2.4 – The electrical model for the squid giant axon. The necessary ions for action potentials are the sodium (Na^+) and the potassium (K^+) ions. The g_L conductance accounts for the leak current.

space-clamp experiments, which consist in homogenizing the membrane potential along the axon to avoid any propagation effect. In parallel, they recorded the ionic currents flowing through the membrane via a technique called *voltage-clamp*: this technique consists in fixing the membrane potential to particular constant values and recording the ionic currents flowing through the membrane at these potentials.

Hodgkin and Huxley isolated the action of the sodium and potassium ion currents and fitted the experimental traces to get a mathematical expression for the dynamic conductances. The conductances vary between a totally closed state ($g_{ion} = 0$) and a totally open state ($g_{ion} = \overline{g}_{ion}$, the maximal conductance). This maximal conductance $\overline{g}_{ion}$ is only function of the ion channel density and is supposed constant for a given neuron. They hypothesized that dynamical variations between these two extreme values could be modeled following the law of mass action, with $n(V_m, t)$ the fraction of open channels, $n_\infty(V_m)$ the fraction of open channels at steady-state, and $\tau_n(V_m)$ the channel time constant:

$$\tau_\infty(V_m)\dot{n} = (n_\infty(V_m) - n)$$

with

$$n_\infty(V_m) = \frac{\alpha_n(V_m)}{\alpha_n(V_m) + \beta_n(V_m)},$$
$$\tau_\infty(V_m) = \frac{1}{\alpha_n(V_m) + \beta_n(V_m)},$$

where the functions $\alpha_n(V_m)$ and $\beta_n(V_m)$ vary for each ion channel type.

From the experimental measures, Hodgkin and Huxley chose the following model for the squid giant axon:

$$\begin{aligned} C_m\dot{V}_m &= -I_{Na} - I_K - I_L + I_{app}, \\ &= -\overline{g}_{Na}m^3h(V_m - E_{Na}) - \overline{g}_K n^4(V_m - E_K) - \overline{g}_L(V_m - E_L) + I_{app}, \\ \dot{m} &= \alpha_m(1-m) - \beta_m m, \\ \dot{h} &= \alpha_h(1-h) - \beta_h h, \\ \dot{n} &= \alpha_n(1-n) - \beta_n n, \end{aligned}$$

where V_m is the membrane potential in mV, $C_m = 1\mu F/cm^2$ is the membrane capacitance, I_{app} is the applied current in $\mu A/cm^2$, and m, h, and n are the gating variables (m and h are the activation and inactivation variables of sodium channels and n is the activation variable of potassium channels).

The specific functions α and β are, in units of $(ms)^{-1}$:

$$\begin{aligned} \alpha_m &= 0.1\frac{25 - V_m}{e^{(25-V_m)/10} - 1}, \\ \beta_m &= 4e^{-V_m/18}, \\ \alpha_h &= 0.07e^{-V_m/20}, \\ \beta_h &= \frac{1}{e^{(30-V_m)/10} + 1}, \\ \alpha_n &= 0.01\frac{10 - V_m}{e^{(10-V_m)/10} - 1}, \\ \beta_n &= 0.125e^{-V_m/80}. \end{aligned}$$

2.2.2 Excitability

Figure 2.5 shows the response of the Hodgkin-Huxley neuron model to two impulses of excitatory current: one 'subthreshold' and one 'superthreshold'. After a small subthreshold stimulation, only small variations around the resting potential are generated, whereas a large superthreshold stimulation results in a large excursion of the membrane potential before it resumes to its steady-state value after a time duration called a *refractory period*. This phenomenon defines *excitability* and the large excursion followed by the membrane potential is called an *action potential*.

The cascade of events composing the action potential relies on the kinetics of the membrane permeability changes, function of the particular kinetics of sodium and potassium channels. Figure 2.5 (Right) shows that, after a superthreshold excitatory stimulus, sodium channels open rapidly (m increases) which induces a massive flow of sodium ions into the cell, generating a strong

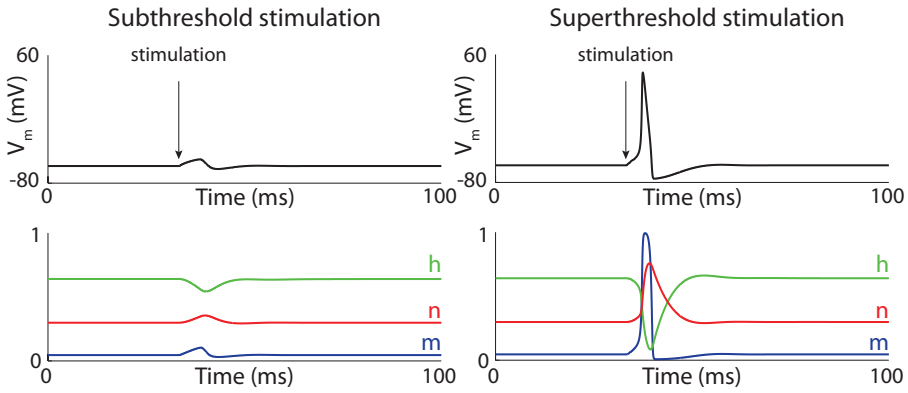

Figure 2.5 – Simulation of the Hodgkin-Huxley neuron model. (Left) Subthreshold stimulation. (Right) Superthreshold stimulation. Variations of membrane potential (top) and gating variables (bottom) over time.

membrane depolarization. On a slower timescale, sodium channels close (h decreases) and potassium channels open (n increases). Sodium ions stop coming into the cell and potassium ions flow out of the cell, repolarizing the membrane.

Therefore, the sodium current, I_{Na}, is rapidly activated but slowly inactivated by membrane depolarization. In contrast, the delayed-rectifier potassium current, I_K, is solely activated by membrane depolarization on a timescale similar to the sodium channel inactivation, slower than sodium channel activation. The gating timescales can be separated into the fast contribution (time-constant in the millisecond range) and the slow contribution (time-constant 5 to 10 times larger) [89]: the fast gating variable is the sodium channel activation m, and the slow gating variables are the sodium channel inactivation h and the potassium channel activation n.

The rapid action of the fast gating variable m and the slower action of the slow gating variables h and n can be captured with a motif representation.

2.3 Motif approach

2.3.1 Positive and negative feedback loops

Dynamics in biological systems can be described in the form of interactions between antagonist feedback loops [39]. With negative feedback loops (–FB), the response counteracts the effect of the stimulus, reflecting an auto-regulation mechanism and leading to homeostasis or oscillations [247]. In dynamical systems theory, negative feedbacks are known to linearize the behavior, acting as regulators with sigmoid-like characteristics. The output primarily reflects

the input and the system behavior is termed *exogenous*. In contrast, positive feedback loops (+FB), by which the response amplifies the effect of the stimulus, bring bistability to the system—i.e., the robust coexistence of two stable attractors—and lead to switch-like behaviors [247]. The output primarily reflects memory of the past and the system behavior is called *endogenous*.

In the 1960's, Jacob and Monod performed the first study of the interaction of positive and negative feedback loops for the control of gene expression [132]. At approximately the same time, Griffith studied the interaction of negative and positive feedback loops in networks [110,111]. In particular, Griffith showed that a two-state system with a negative feedback loop possesses a single stable equilibrium and that a system with a positive feedback loop undergoes oscillations under the strict condition of ultra-sensitivity.

The interplay of positive and negative feedback loops can generate complex behaviors, e.g., toggle switches and oscillators [203, 234, 247]: the positive feedback creates bistability, i.e., two stable steady states, and the negative feedback drives the system between those two states. Over the years, two main building blocks have emerged to explain biological oscillators: the *delayed-negative-feedback*—the local excitation is created by a time delay—presented by Goodwin to model enzymatic control [105] and the *hysteresis-and-adaptation*—the local excitation is generated by a dynamical hysteresis due to an autocatalytic feedback loop—for example at play in the FitzHugh-Nagumo model [86, 186]. For instance, those two distinct building blocks have been used to model the same mitosis mechanism responsible for the cell division cycle [98, 245], conjecturing drastically different underlying principles.

2.3.2 Generality of the motif approach

The motif approach consists in adopting an engineer's mindset to control systems by identifying simple patterns of activation (+) and inhibition (–) among a small number of components that carry out specific functions [3, 94, 234, 246, 249]. The description in term of motif is helpful for generalization purposes: a motif captures the recurring patterns of interactions in a system and simplifies the picture [3, 94]. Such motifs are found in a variety of fields, e.g., biochemistry (transcriptional gene regulation), ecology (food webs), neurobiology (neuron connectivity), and engineering (electronic circuits, World Wide Web) [180, 265]. In neuroscience, motifs have been used to describe structural and functional networks and characterize network building blocks that occur frequently in the human brain [229, 230].

The power of the motif approach is largely exploited in systems biology to identify shared design principles [4,249]. Motifs simplify the systems by approximating the wiring diagram and taking advantage of the strong separation of timescales between different processes [4]. Examples of biological motifs are the positive and negative feedback loops (Figure 2.6, Left and Center) described in

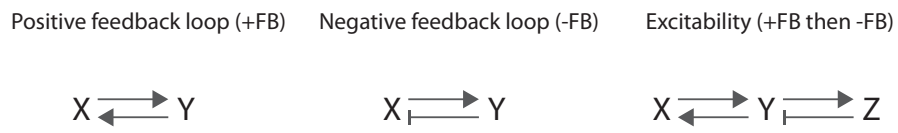

Figure 2.6 – Motifs. (Left) The positive feedback loop motif. (Center) The negative feedback loop motif. (Right) The excitability motif.

the previous section (2.3.1), but many other motifs have been identified [249].

2.3.3 Excitability motif

The seminal work of Hodgkin and Huxley introduced the concept of *excitability*, which refers to spatially distributed systems capable of propagating signals in time and in space [11]. An excitable system is characterized by a resting state, stable under small subthreshold perturbations. A superthreshold input evokes in the system a great excursion, orders of magnitude greater than the subthreshold response, before the system resumes to the resting state [11, 129]. From a dynamical system point of view, a system with a stable equilibrium is excitable if there is a large amplitude periodic pseudo-orbit passing near the equilibrium, i.e., a large-amplitude piece of trajectory that starts in a small neighborhood of the equilibrium, leaves the neighborhood, and then returns to the equilibrium [83, 128, 129].

The excitability motif is composed of a fast positive feedback loop (+FB)—or autocatalysis—and a slower negative feedback loop (–FB) and will be referred in the rest of the dissertation as the *+FB then –FB* motif (Figure 2.6, Right). In neuroscience, this +FB then –FB motif has been introduced as early as in the 1930's with the description of the action potential in nerves [119, 209] and later formalized in the work of FitzHugh-Nagumo [86, 186] (see section 2.4.1).

Many biological and chemical systems are excitable and use the +FB then –FB motif [11, 73, 140]. Examples of excitable dynamics include the action-potential propagation along axons [120], the Field-Noyes model of the Belousov-Zhabotinskii reaction [85], the pacemaker cells of the heart, the pancreatic beta-cells, and specific applications in systems biology such as the transient cellular differentiation [3, 235, 249].

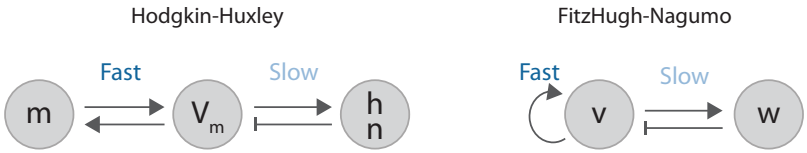

Figure 2.7 – The +FB then –FB excitability motif in neuron models. (Left) The excitability motif in the Hodgkin-Huxley neuron model. The fast regenerative gating variable m provides a positive feedback on membrane potential variations and the slow restorative gating variables h and n provide a negative feedback on membrane potential variations. (Right) The excitability motif in the FitzHugh-Nagumo neuron model. The fast excitation variable v provides a positive feedback via its autocatalysis and the slow recovery variable w provides a negative feedback on variations of v.

2.4 Excitability motif in neuroscience

2.4.1 Excitability in neurons

The +FB then –FB excitability motif emerged from the mathematical modeling of Hodgkin and Huxley and was later formalized by the work of FitzHugh and Nagumo.

Hodgkin-Huxley model

As detailed in section 2.2.2, the gating variables can be grouped in the fast gating variables (m) and the slow gating variables (h and n). The fast gating variable m generates the rapid upstroke of the action potential. It enhances a membrane potential variation by positive feedback and is *regenerative* in the sense defined in [89]. The slow gating variables h and n provide a negative feedback on membrane potential variations and are *restorative* in the sense defined in [89]. The +FB then –FB emerges from the Hodgkin-Huxley neuron model and is given in Figure 2.7 (Left).

One should notice that the restorative (resp. regenerative) nature of channels is not solely set by the outward (resp. inward) nature of the current [89]: for instance, the fast sodium channels are fast regenerative—they are responsible for the regenerative spike upstroke—but slow restorative because their slow variable inactivates an inward current. Delayed-rectifier potassium channels are slow restorative because they activate an outward current but there exist slow regenerative potassium channels, e.g., the A-type potassium channels, which decrease the outward current by their slow activation.

FitzHugh-Nagumo model

As stated in section 2.1.3, high-dimensional nonlinear systems are difficult to analyze and visualize. Reducing the complexity of the system allows for the use of dynamical system theory tools such as phase-plane techniques and for a better understanding of the underlying dynamics [140].

In the 1960's, FitzHugh reduced the four-dimensional Hodgkin-Huxley set of equations to a two-dimensional system by aggregating variables and exploiting the timescale separation [86]. In particular, the fast m and V_m variables are grouped in a fast autocatalytic variable v while the effect of the slow n and h variables is taken into account in a slow variable w. The fast variable v, the *excitation* variable, possesses a cubic nullcline, while the slow variable w, the *recovery* variable, has a monotonically increasing nullcline [140]. The equations for this dynamical system write:

$$\begin{aligned} \dot{v} &= v - \frac{v^3}{3} - w + I_{app}, \\ \tau \dot{w} &= v + a - bw. \end{aligned}$$

Nagumo created the equivalent circuit the year after [186], leading to the appellation: the FitzHugh-Nagumo model. This model extracts the essential mechanism of the Hodgkin-Huxley model and presents it in a simplified form while retaining many of the qualitative features [140]. This FitzHugh-Nagumo model captures also the basic elements for excitability and can be represented with the motif formalism (Figure 2.7, Right).

Morris-Lecar model

Another two-dimensional reduction of a neuronal spike dynamics was proposed in the 1980's by Morris and Lecar [183]. Their system includes the effect of potassium channels and voltage-gated calcium channels and writes:

$$\begin{aligned} C_m \dot{V} &= -\overline{g}_{Ca} m_\infty(V)(V - E_{Ca}) - \overline{g}_K n(V - E_K) - \overline{g}_L(V - E_L) + I_{app}, \\ &\equiv -I_{ion}(V, n) + I_{app}, \\ \dot{n} &= \phi(n_\infty(V) - n)/\tau_n(V), \end{aligned}$$

where

$$\begin{aligned} m_\infty(V) &= \frac{1}{2}\left[1 + tanh\left(\frac{V - V_1}{V_2}\right)\right], \\ n_\infty(V) &= \frac{1}{2}\left[1 + tanh\left(\frac{V - V_3}{V_4}\right)\right], \\ \tau_n(V) &= \frac{1}{cosh\left(\frac{V - V_3}{2V_4}\right)} \end{aligned}$$

with parameters V_1, V_2, V_3, V_4, and ϕ. The excitability motif representation for the Morris-Lecar model can be drawn similarly to the one for the FitzHugh-Nagumo model.

2.4.2 Excitability in networks

In neuroscience, the +FB then –FB excitability motif emerges at other resolution levels, e.g., at the network level with the mean-field network model of Wilson and Cowan.

Mean-field approach

The mean-field approach consists in simplifying large and complex stochastic models by approximating the effect of a large number of small components in a single averaged effect (see section 2.1.3). In neuroscience, the mean-field approach takes the form of neural field models [41]: the study, by taking the continuum limit, of a large population of neurons and synapses with a macroscopic state variable, the mean-firing rate, i.e., the number of firing neurons in a certain short time interval of few milliseconds. The first attempts in this direction are attributed to Beurle [13], and later to Griffith [108, 109]. Wilson and Cowan, and later Amari, extended this early work in populations of both inhibitory and excitatory neurons.

Firing-rate models make the assumption that the synaptic input current is a function of the pre-synaptic firing rate function and take the form [41, 264]:

$$\tau \dot{r}(x,t) = -r(x,t) + \phi\left(I(x,t) + \int dy J\left(|x-y|\right) r(y,t)\right)$$

where $r(x,t)$ is interpreted as a neural field representing the local activity of a population of neurons—firing-rate—at position x at time t, τ is the time constant of firing rate dynamics, $I(x,t)$ is the external input, $J(x,y)$ is the strength of synaptic connections between neurons at locations x and y. $\phi(.)$ is a static transfer function which can take various forms: the simplest being the Heaviside step function (for perceptrons or threshold gates) and the most famous the sigmoidal function (for sigmoidal gates) [263].

Wilson-Cowan model

In the 1970's, Wilson and Cowan proposed a firing-rate model of the cortical circuitry and dynamics [264]. It relied on the assumptions that cortical neurons can be subdivided into two classes: excitatory (E) neurons, primarily pyramidal cells, and inhibitory (I) interneurons. The simple network they proposed is given in Figure 2.8 (Left). The firing-rate model formulation given in the

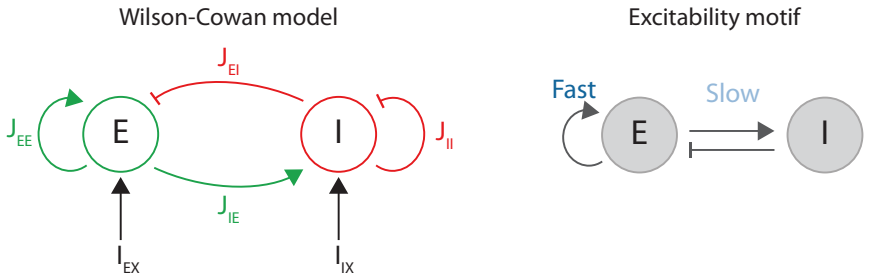

Figure 2.8 – The Wilson-Cowan network model. (Left) Connectivity diagram for the firing-rate model of the cortical circuitry and dynamics: excitatory (E) pool of neurons reciprocally connected to an inhibitory (I) pool of neurons. (Right) The excitability motif is present at the network level.

previous section leads to the set of equations:

$$\tau_E \dot{r}_E = -r_E + \phi_E \left(I_{EX} + J_{EE} r_E - J_{EI} r_I \right),$$
$$\tau_I \dot{r}_I = -r_I + \phi_I \left(I_{IX} + J_{IE} r_E - J_{II} r_I \right),$$

where r_E and r_I represent the proportions of excitatory and inhibitory cells, respectively, firing at time t. Neural fields with such connections exhibit all sort of complex dynamics such as spatially and temporally periodic patterns, localized regions of activity (bumps and multi-bumps), and traveling waves (fronts, pulses, target waves and spirals) [41].

Under certain conditions (notably J_{EE} and $J_{EI}J_{IE}$ sufficiently large), the E-I network develops an excitable dynamics [83, 262] and the +FB then –FB excitability motif can be extracted (Figure 2.8, Right). Local dynamics and spatial connectivity influence the type of dynamical pattern that develops in the network: travelling wave pulses or stationary pulses occur [83]. Amari extended this framework to a network with a 'Mexican hat' connectivity, i.e., local excitation and distal inhibition, for a mixed E-I population [5].

2.5 Temporal superposition of excitable motifs

2.5.1 Burst-firing pattern

The Hodgkin-Huxley model captures the fundamental property of neuronal excitability, through modeling an action potential. Depending on the time interval separating two successive action potentials, neurons are capable of exhibiting various firing patterns, for instance *burst firing*. Burst firing corresponds to the generation in alternance of high-frequency firing periods and quiescent periods. Many neurons are capable of switching between single-spike and burst-firing patterns (see for instance chapter 4).

There exist many types of burst-firing patterns in neurons expressing various ion channels and having different morphologies but the underlying mechanisms are strongly similar and happen on three sharply separated timescales [88]: the fast activation, corresponding the rapide spike upstroke, the slow recovery, corresponding to all gating variables that (in)-activate during the action potential, and the ultraslow adaptation, which modulates neuron excitability. A critical component of neuronal bursting relies on the presence of robust bistability between a resting state and a spiking state, allowing for transition between spiking and quiescent periods [88]. This robust bistable region is a signature of slow regenerative excitability, this bistable zone being fragile or even absent in slow restorative excitability [87]. Transitions between the two types of excitability can be regulated and corresponds to a switch between single-spike firing to burst firing. As a consequence, only four ion channel types are necessary for the generation of bursting [88]: (i) one fast depolarizing for the generation of the regenerative upstroke of action potentials, (ii) one slow restorative for the action potential downstroke, (iii) one slow regenerative for switching from restorative excitability to regenerative excitability, and (iv) one ultraslow hyperpolarizing for the adaptation of excitability during spiking. This physiologically relevant considerations can be captured in a three-timescale bursting neuron model.

2.5.2 Three-timescale bursting neuron model

The three-timescale bursting model is an abstract model of neuronal spiking based on the transcritical normal form [76,77,87–89]. It is inspired by the planar reduction of the Hodgkin-Huxley model augmented with calcium channels [77]. Calcium channels are essential to provide a source of positive feedback in a timescale that is significantly slower than the timescale of neuron excitability. The model exploits the three timescales of neuronal bursting [88]: fast—the timescale of the rapid action potential upstroke, slow—the timescale of intraburst spike frequency, and ultraslow—the timescale of interburst frequency:

$$\begin{aligned} \dot{v} = v^2 + bvx_s - x_s^2 \pm \overline{g}_s x_s - \overline{g}_{us} x_{us} + I_{app} + I_{static} \quad & \text{if } v \geq v_{th}, \text{then} \\ \tau_s \dot{x}_s = a_s v - x_s \quad & v \leftarrow c, x_s \leftarrow d_s, \\ \tau_{us} \dot{x}_{us} = a_{us} v - x_{us}, \quad & x_{us} \leftarrow x_{us} + d_{us}. \end{aligned}$$

where v merges the membrane potential and fast variables, x_s merges all slow recovery variables, and x_{us} all ultraslow adaptation variables. I_{app} represents the applied current and I_{static} the static current that determines the resting potential. The reduced model is in dimensionless units. The interested reader is referred to [77, 87] for more details about the model.

The model is composed of three feedback loops: one fast, one slow, and one ultraslow (Figure 2.9, Left) [76]. The fast feedback loop mainly accounts for the

fast autocatalysis achieved by sodium activation (positive feedback, i.e., fast regenerativity). The slow and ultraslow feedback loops correspond to two currents active in the respective timescales multiplied by their respective feedback gains, $\overline{g}_s$, and $\overline{g}_{us}$. The slow feedback gain $\overline{g}_s$ accounts for the net sum of the many slow currents, which can either be slow restorative (e.g., delayed-rectifier potassium channels) or slow regenerative (e.g., T-type calcium channels) [89]. The ultraslow feedback gain $\overline{g}_{us}$ accounts for the net sum of ultraslow currents and will be considered ultraslow restorative in this dissertation.

The balance between restorative and regenerative ion channels in the slow timescale, $\overline{g}_s$, corresponds to a physiologically meaningful modulation parameter [88]. $\overline{g}_s$ is physiologically modulated by the balance between restorative and regenerative channels: the positive sign models the case where regenerative channels are dominant, the negative sign models the case where restorative channels are dominant, and $\overline{g}_s = 0$ corresponds to an exact balance between restorative and regenerative channels.

2.5.3 Excitability motif in two temporal resolutions

The block diagram of Figure 2.9 (Left) can be abstracted with the motif approach: the fast feedback loop corresponds to a fast positive (autocatalytic) feedback, the slow feedback loop can either be slow negative for restorative excitability or slow positive for regenerative excitability, and the ultraslow feedback loop is ultraslow negative. The motif representation that emerges corresponds to two excitability motifs in two different timescales (Figure 2.9, Right): in the fast/slow timescale, the +FB then –FB motif is identical to the one described in single-spike firing (fast autocatalysis and slow recovery with slow restorative channels); in the slow/ultraslow timescale, the +FB then –FB motif is constituted by the slow positive feedback brought by slow regenerative channels and ultraslow negative feedback brought by ultraslow restorative channels.

The bursting pattern emerges from the interplay of the two motifs. To study the modulation and robustness properties of burst firing, it is primordial to keep the description of the mechanism at the two distinct resolution levels: fast/slow and slow/ultraslow.

2.6 Interacting motifs

In this section, we enlarge the concept introduced in the temporal dimension in the previous section to the interactions of motifs at different spatiotemporal resolution levels. Motifs in a given resolution level can emerge from the interplay of feedback loops at a different resolution level. For these systems, it is crucial to investigate the interactions between resolution levels rather than

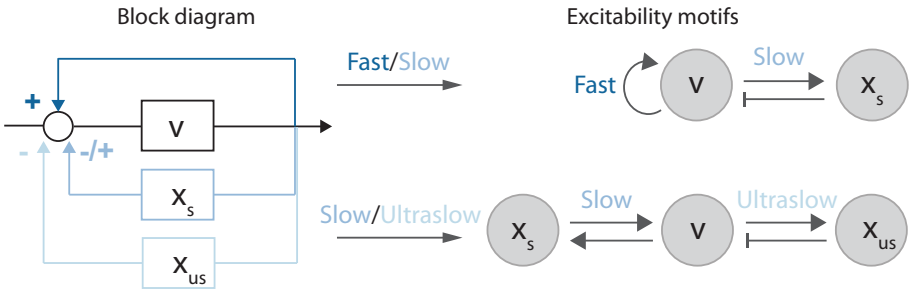

Figure 2.9 – The three-timescale bursting model. (Left) Block diagram with the three feedback loops, fast, slow, and ultraslow. The slow feedback loop can have either a positive or a negative sign, depending on the balance between restorative and regenerative channels. (Right) The excitability motif is present at two resolutions: the fast/slow timescales and the slow/ultraslow timescales.

each level separately. We give two examples where motifs at different resolution levels interact to produce the system behavior. Those examples emphasize the drawbacks of the motif approach when considered at a unique resolution level and drive the motivations for the dissertation.

2.6.1 Half-center oscillators

At the beginning of the last century, Brown suggested that the rhythmic walking pattern, i.e., the alternate flexion and extension of leg muscles, could originate from rhythmic central circuits [26]. Central pattern generators (CPGs) are neuronal circuits that, when activated, produce a rhythmic pattern for simple behaviors such as locomotion, mastication, and respiration [94, 112, 117, 168, 169]. From a dynamical system theory viewpoint, these CPGs produce stereotypical limit cycle oscillations in response to a constant input [262]. The rhythmic patterns provide specific timing information without receiving extrinsic phasic timing input. The dynamics of the network depend on the complex interplay between the neuron intrinsic membrane properties and the network—or synaptic—extrinsic properties [169, 262]. Neuromodulators often play a crucial role: they set the intrinsic and extrinsic parameters to render the networks functional [117]. Neuromodulators activate and modulate—both in frequency and phasing—the motor patterns produced by a given CPG to allow adaptation to changing environmental demands [168, 169]. For instance, some CPGs operate continuously (e.g., such as vertebrate respiration), some are activated and terminated at specific time points (e.g., for walking, running, flying and swimming), while others are rare and briefly seen (e.g., escape or scratch behaviors) [169].

Many CPGs incorporate a specific building block: a *half-center oscillator*

(HCO), i.e., two neurons mutually inhibiting each other [168, 262]. Although these two neurons, or neuronal populations, do not oscillate in isolation, they produce, when connected, alternating patterns of activity [26, 200, 214]. This circuit was first introduced by Brown to explain the control of antagonistic muscles during walking [26]. HCOs have been identified at the core of most endogenous rhythmic circuits, such as CPGs governing locomotion [26, 33, 47, 112, 200, 214] and respiration [27, 47].

HCOs embody prototypes of circuit behavior emerging from the interactions between cellular and network levels. When solely considered at the network level, the mutual-inhibition architecture takes the form of an I-I motif which captures the anti-phase property of the rhythm. This mean-field approach holds solely if the circuit coupling is much slower than the cellular dynamics. This observation highlights a limitation of the motif approach when considered at a unique resolution level: the complex interplay between neuron and network dynamics is completely lost in favor of simplicity. The robustness and modulation properties which emerge from the neuron (intrinsic) level are obliterated. Considering the +FB then –FB excitability motifs in both timescales at the cellular level allows for the investigation of system-level properties and highlights the necessity of a slow positive feedback loop at the cellular level (see chapter 3).

2.6.2 Excitatory-inhibitory circuits

Parkinson's disease is one of the most common disabling neurodegenerative disorder, second only to Alzheimer's disease, and affects tens of millions of people worldwide [116]. The core physiological signature is the degeneration of dopaminergic neurons in the substantia nigra pars compacta (SNc) of the midbrain and a consequent dopaminergic denervation of the striatum, the major input nucleus to the basal ganglia [116, 193, 212]. The hallmark feature of Parkinson's disease is severe motor symptoms: poverty of voluntary movements (akinesia), slowness and impaired scaling of voluntary movement (bradykinesia), muscle stiffness (rigidity), and tremor at rest [116, 212, 215, 259]. The relation between dopaminergic denervation and the motor symptoms is still unclear [116]. One of the patho-physiological characteristics of Parkinson's disease is the increase in firing rate of the output neurons of the basal ganglia, generating an excessive inhibition on the thalamus [193]. In addition, recent recordings, in both animal models and humans, have demonstrated abnormally synchronized oscillatory activity at multiple levels in the basal ganglia and cerebral cortex [20, 116].

One neuronal circuit hypothetically responsible for the oscillatory activity is the subthalamic nucleus - globus pallidus pars externa (STN-GPe) network of the basal ganglia, a mutually-connected excitatory-inhibitory (E-I) network [18]. According to the motif approach, this circuit is excitable in the

presence of an autocatalytic feedback loop. Generally speaking, at the network level, this autocatalysis can come from a reciprocal E-E or I-I coupling. However, the autocatalysis can also emerge from the cellular level, endowing network oscillations with specific modulation and localization properties (see chapter 4). This sets emphasis on the importance of studying motifs and their interplay in different resolution levels.

2.7 Neuron-level and network-level motifs

The approach emphasized in this dissertation is the use of motifs to capture the essential characteristics of phenomena at higher (finer/faster) resolution levels to study modulation and robustness properties at lower (coarser/slower) resolutions. We show that the interplay of motifs at different levels is primordial for studying system-level questions.

2.7.1 Interactions between resolution levels

As emphasized in section 2.1.3, there exist models at the different resolution levels of the brain, each model resolution capturing a specific spatiotemporal scale. However, from the two previous motivating examples, we see that eliminating the characteristics at finer/faster resolution levels is detrimental for analyses at coarser/slower resolutions. To palliate to this limitation, we suggest to investigate the interplay between motifs at different resolution levels.

Similarly to the strategy proposed in [198], we highlight the importance, at the network level, of including both the network organization and the functional properties of the cellular and synaptic components. Specifically, we extract from higher resolution levels the critical components—the motif representation and the feedback loops—for the activity at the lower resolution. We propose to use this approach in the modeling of the brain, i.e., to capture, in models, the mechanisms at different spatiotemporal resolution levels in order to develop of global understanding for specific activity patterns.

2.7.2 Neuron resolution level in networks

Similarly to what is done in the temporal scale for the neuron burst-firing pattern (section 2.5.3), we propose to study the interplay of motifs in the spatiotemporal scale, going from the neuron level to the network level.

In this dissertation, we consider two network-level systems: the mutual-inhibition (I-I) network of HCOs (chapter 3) and the E-I network of the basal ganglia (chapter 4). We examine system-level questions such as modulation, robustness, and function emergence. In particular, the impact, at the network level, of cellular feedback loops is studied. In the last chapter (chapter 5), the

analysis is extended to localized transfer properties of multiresolution excitability.

2.8 Summary

In this chapter, we introduced the concepts of resolution levels in the brain physiology and models. The seminal work of neurodynamics, the Hodgkin-Huxley neuron model, was depicted and introduced the excitability concept. The motif approach, a widely used methodology, was presented to extract important elements, in the form of feedback loops, in each resolution level. The interplay between excitability motifs at two different temporal levels was shown with the neuronal burst-firing pattern. The dissertation was motivated by the instantiation, in two neuronal circuits, of the limitation the motif approach when considered at a unique resolution level. Study of the motif interactions at different spatiotemporal resolutions was suggested to tackle system-level questions and to investigate the interplay of neuron and network resolution levels.

Chapter 3

Cellular feedback for network modulation and robustness

Biological rhythms play a major role in the functioning of the brain but much remains to be understood regarding their control, regulation, and function. Many advances in this important question have come from experimental and computational studies of central pattern generators (CPGs), which endogenously produce precise rhythmic outputs directly related to motor functions [94,112,117, 168,169]. In this effort, experimental work benefits from computational models but models at the circuit level usually rely on mathematical simplifications at the component level.

The question of which cellular details must be retained at the network level is largely open [170]. We use the approach presented in chapter 2 to investigate cellular properties to be preserved in the study of modulation and robustness of network rhythms.

Motivated by this general question, we highlight a simple feedback mechanism at the cellular level that has a key influence on circuit robustness and modulation. We illustrate this property via the computational study of an archetype model of CPG circuits, the *half-center oscillator* (HCO): two neurons, or neuronal populations, that do not oscillate in isolation, but oscillate in an anti-phase rhythm when reciprocally connected [26,200,214]. Because of the widespread occurrence of this circuit motif, the mechanisms have been extensively studied, both computationally and experimentally [33, 47, 117, 169, 223, 224, 255]. A specific cellular excitability property, the *post-inhibitory rebound* (PIR) [200], and its two specific ionic currents, I_H and $I_{Ca,T}$ [8], are well-known key players in circuit oscillations. Previous studies have focused on distinguish-

ing those two currents from their contribution to the escape or release mechanism [47, 223, 255] and their modulation of rhythmic activity [46, 74, 194, 228]. This chapter highlights that those two currents differ in another simple yet fundamental aspect: both generate a PIR, but only one of them acts as a source of positive feedback through its slow activation (in a timescale critical for the rhythm generation). The present chapter demonstrates through a computational study that this particular feedback is fundamental for the robustness and modulation properties of the circuit rhythm, and that its absence is detrimental both to robustness and modulation at the circuit level.

The chapter is organized as follows. Section 3.1 presents the cellular PIR property and the two major ionic currents that underlie it. Those two currents are differentiated by their dynamical feedback loops and the type of PIR they generate, Mechanism A or B. Section 3.2 separates Mechanism A and B PIR in the impact they have on modulation of the network rhythm. Sections 3.3 extends these results to investigate the robustness of network oscillations. In section 3.4, we discuss the generality of the approach and the implications for computational model of HCOs.

Contributions. The main contributions of this chapter are (i) the identification of an essential cellular property, a positive feedback loop in the slow timescale, to be retained at the network level in modeling network robustness and modulation and (ii) the suggestion of a novel and somewhat fundamental complementarity between the two ionic currents in PIR mechanisms.

The material of this chapter is greatly inspired from the publication in preparation [66].

3.1 Slow activation of T-type calcium channels is critical to robustness of network rhythmic activity

To assess the role of cellular properties in network rhythms, we consider one of the simplest and most studied networks: the half-center oscillator (HCO). The network rhythm results from the mutual inhibition (I) of two neurons that do not oscillate endogenously in isolation [26, 200, 214]. HCOs have been identified at the core of most endogenous rhythmic circuits, such as CPGs governing locomotion [26, 33, 47, 112, 200, 214] or respiration [27, 47]. Oscillations in HCOs can be triggered by an external pulse of hyperpolarizing current. When released from hyperpolarization, the cell generates a burst-like transient depolarization with one or more spikes. This activity hyperpolarizes the other cell via the inhibitory synaptic connection, which in turn triggers a transient burst. The cycle repeats leading to an anti-phase rhythm between the two neurons.

The transient depolarization following the termination of an hyperpolarizing input is an essential cellular property for the network rhythm, best known in the literature as post-inhibitory rebound (PIR) [200]. Two major ionic currents have been shown to underlie the PIR (Figure 3.1, Top): i) the hyperpolarization-activated cation current, I_H, an hyperpolarization-activated inward current that contributes to rebound responses in a diverse array of neurons in invertebrates and vertebrates [8]; ii) the low-threshold T-type calcium current, $I_{Ca,T}$, which is deinactivated by hyperpolarization and then activates upon release from inhibition [233]. Many studies have highlighted the distinction between these two currents in HCOs from an "escape or release" mechanism perspective, T-type calcium currents inducing the release mechanism and I_H-like currents promoting the escape mechanism [47, 223, 255]: either the active cell "releases" its inhibitory effect on the silent cell (release mechanism), or the silent cell "escapes" from inhibition via the activation of an I_H-like current (escape mechanism).

Separately, the two types of current generate similar PIR traces in single cells (Figure 3.1, Top; see appendix A.1 for cellular models and model difference between Mechanism A and B). While both mechanisms are redundant for the generation of oscillations in a two-neuron network with reciprocal inhibition (Figure 3.1, Center), we emphasize a fundamental difference between the two: in presence of physiological variability, i.e., variability in the intrinsic cellular properties and synaptic connections (see appendix A.3 for a description of variability), only the rhythm generated by Mechanism B is robust (Figure 3.1, Bottom). This robustness property highlights a fundamental difference between the two mechanisms.

This difference lies in the dynamical feedback loops generated by the gating variables of the two currents. Both currents generate an ultraslow (the ultraslow timescale is set by the interburst frequency) inward current in response to hyperpolarization, which is the foundation of the PIR. This inward current counteracts the external hyperpolarization and acts as a source of negative feedback on membrane potential variations—or restorativity in the terminology of [89]—in the ultraslow timescale (Figure 3.2, red feedback loops). But, in contrast to I_H, $I_{Ca,T}$ provides a slow *positive* feedback on membrane potential variations—or regenerativity in the terminology of [89]—via its slow activation variable (Figure 3.2, green feedback loop). This slow positive feedback is absent in Mechanism A. At the cellular level, the slow positive feedback is revealed by a specific signature during hyperpolarization [89]: a transient excitatory pulse that triggers a single spike in Mechanism A (I_H), triggers a burst in Mechanism B ($I_{Ca,T}$) (Figure 3.2, Left and Right). This signature reveals that bursts are endogenously generated with a PIR with slow regenerativity (Mechanism B), as opposed to a purely restorative—i.e., only I_H—PIR (Mechanism A).

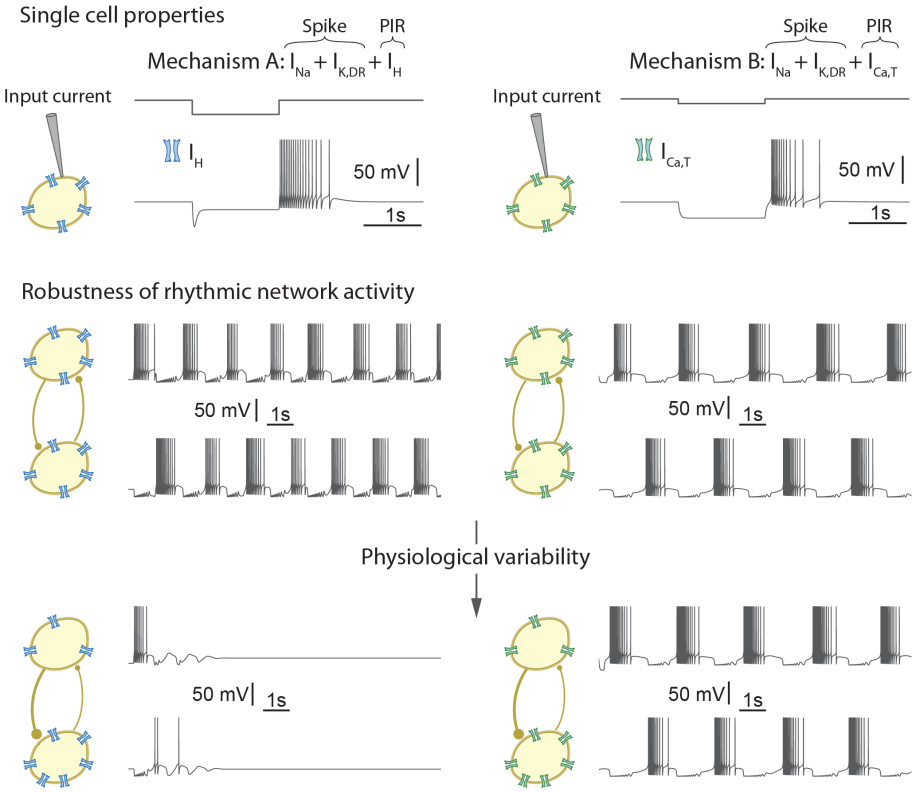

Figure 3.1 – Network rhythmic activities generated by distinct post-inhibitory rebound mechanisms strongly differ in their robustness properties. (Top) Mechanism A generates a PIR with a I_H-type current and Mechanism B generates a PIR with a slowly activating $I_{Ca,T}$-type current (see appendix A.1 for cellular models). (Center) In a half-center two-neuron network configuration, both mechanisms generate anti-phase oscillations. (Bottom) Physiological variability (see appendix A.3 for a description of variability) in both the synaptic (20% variability in $\overline{g}_{syn}$) and cellular (Left: 20% variability in $\overline{g}_H$; Right: 20% variability in $\overline{g}_{Ca,T}$) properties makes the oscillations unstable with Mechanism A but not with Mechanism B.

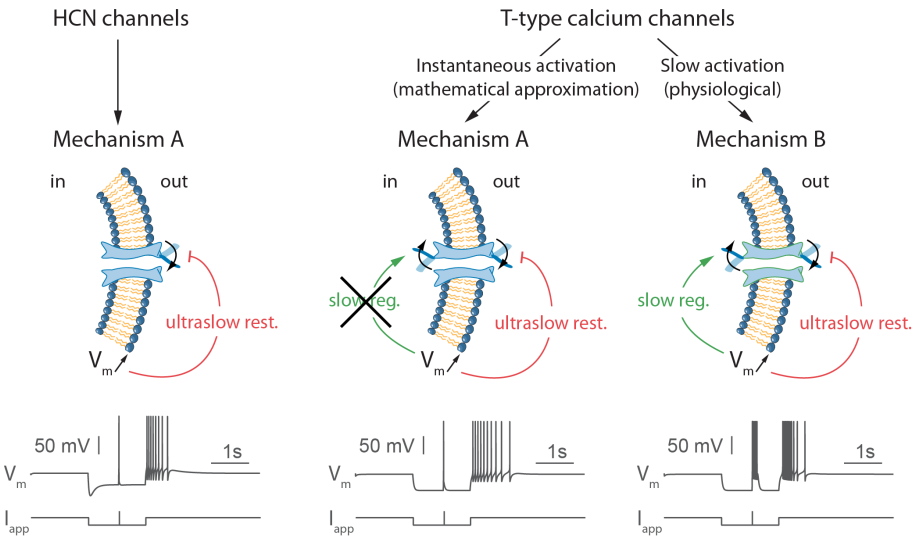

Figure 3.2 – The slow activation of T-type calcium channels is the distinctive difference between the two PIR mechanisms. (Top) Schemes representing ion channel gating in different cases. (Bottom) Responses of membrane potential (V_m) to a varying external applied current (I_{app}) for each case. Both mechanisms trigger a PIR via an ultraslow inward current in response to hyperpolarization, which brings ultraslow restorativity to the neuron (see appendix A.1 for cellular models). In addition, T-type calcium channels in Mechanism B, due to their slow activation, are a source of slow regenerativity. An instantaneous activation of the T-type calcium channels, i.e., steady-state approximation of their activation, suppresses this slow regenerativity and produces a Mechanism A PIR. Mechanism B PIR is endogenous as revealed by the specific signature during hyperpolarization.

A frequent modeling simplification is to neglect the slow activation kinetics of T-type calcium channels and to consider the activation at steady-state (i.e., instantaneous). It should be noted that the slow regenerativity is lost in this approximation, which eliminates the bursting signature observed in Mechanism B, as illustrated in Figure 3.2 (Center).

In the rest of the chapter, we investigate the impact of the difference between Mechanism A and B at the network level (see appendix A.4.1 for details). More specifically, we look at a few simple quantities that characterize the network rhythm in a two-neuron network: the network—or interburst—frequency, i.e., the inverse of the time duration between two burst onsets, the duty cycle, which is the ratio between the burst duration and the period, averaged over the two neurons, and the ratio between the duty cycle in neuron 1 (the neuron upon which acts the external hyperpolarization) and in neuron 2 (the other neuron). We also investigate to what extend the two mechanisms withstand robust oscillations in network with neuronal populations.

3.2 Robust modulation of network properties requires slow regenerativity

Experimentally, the network properties of CPGs, i.e., network frequency and duty cycle—or phase relation—can be modulated via both intrinsic neuron parameters (such as ionic conductances across neurons) and synaptic parameters (such as synaptic conductances) on multiple timescales [48, 70, 81, 84, 117, 118, 166, 171, 184]. In this section, we investigate how the rhythmic activity of a two-neuron network responded to these modulations, both with PIR without slow regenerativity and with PIR with slow regenerativity, and in presence of parameter variability (see appendix A for network description and details of the simulations).

Extrinsic parameters, i.e., the synaptic parameters $\overline{g}_{syn}$ and τ_{syn}, given intrinsic (cellular) characteristics, modulate the network frequency. Synaptic coupling is very plastic [49, 93] and synapses are a primary target of modulators [184]. Synaptic currents can be generated by the cooperation of several ion channel subtypes which have slightly different kinetics. Variation of the synaptic parameters results from a variation of the contribution of all the subtypes. Absolute variation of the different ion channels influences the maximal conductance whereas their relative variation can modulate the time constant of the synaptic current that aggregates all the different subtypes in a model (for instance, combination of $GABA_A$ and $GABA_B$ synapses). Therefore, both the synaptic magnitude, $\overline{g}_{syn}$, and the synaptic kinetics, τ_{syn}, can be sources of modulation.

Oscillations with cellular slow regenerativity can be modulated over a large

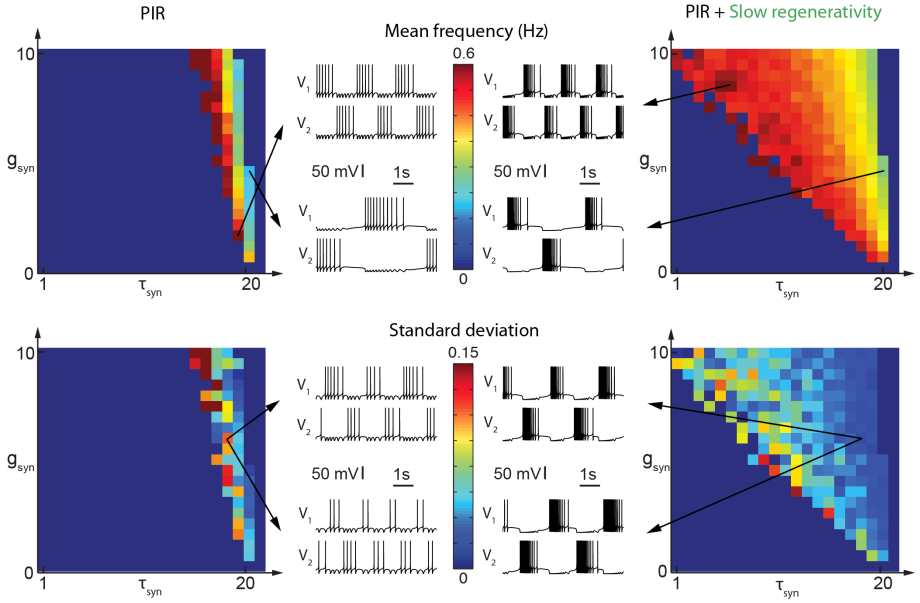

Figure 3.3 – Frequency modulation with extrinsic parameters is fragile without slow regenerativity. Modulation of the network frequency by varying synaptic parameters, $\overline{g}_{syn}$ (in $[mS/cm^2]$) and τ_{syn} (in $[ms]$), is robust with slow regenerativity but fragile without. (Left) PIR only. (Right) PIR + slow regenerativity. Mean frequency (Top) and standard deviation (Bottom) for ten simulations with 40% variability in $\overline{g}_{syn}$ and 20% variability in $\overline{g}_{PIR}$ (see appendix A.3 for a description of variability, mean frequency, and standard deviation). Membrane potentials (Top): maximal and minimal oscillation frequency, respectively, with parameters as indicated by the arrows. Membrane potentials (Bottom): two different simulations with the same $\overline{g}_{syn}$ and τ_{syn} parameters, $\overline{g}_{syn}$ and $\overline{g}_{PIR}$ affected by parameter variability.

range by extrinsic parameters (Figure 3.3, Right). Variation of the $\overline{g}_{syn}$ and τ_{syn} parameters generates a 150% increase in network frequency (see appendix A.3 for a description of mean frequency). Such a span of modulation is observed in physiological rhythms: for instance, there is a 150% increase in frequency from slow-wave sleep ($\approx 4Hz$) to sleep spindles ($\approx 10Hz$) and a 250% increase from beta-band oscillations ($\approx 20Hz$) to gamma-band oscillations ($\approx 70Hz$). In addition, with slow regenerativity, the network frequency is only weakly sensitive to the variability in parameters as shown with the standard deviation plot and the highly similar network frequencies in the membrane voltage traces (see appendix A.3 for a description of variability and standard deviation). In contrast, variations of $\overline{g}_{syn}$ without slow regenerativity allow for network frequency modulation for a much smaller parameter range (Figure 3.3, Left). Moreover, this modulation is very fragile and very sensitive to variability: the standard deviation reaches higher values than with slow regenerativity and membrane potential traces, for a same set of parameters but different simulations, are drastically different (Figure 3.3, bottom Left). Variation of τ_{syn} is almost impossible: τ_{syn} must lie in a very specific timescale for the oscillations to develop in the network. In the absence of positive feedback at the cellular level, the modulation requires a tight coupling between intrinsic and extrinsic parameters: the network oscillations are a direct image of the unicellular activity. The synaptic dynamics must be close to the neuron intrinsic dynamics and cannot deviate from a tiny range of parameters.

Intrinsic parameters, i.e., the cellular parameter $\overline{g}_{PIR}$ for each neuron ($\overline{g}_{PIR,1}$ for neuron 1—the neuron upon which acts the external hyperpolarization—and $\overline{g}_{PIR,2}$ for neuron 2—the other neuron), given extrinsic (synaptic) characteristics, modulate the duty cycle and duty cycle ratio (see appendix A.3 for a description of duty cycle and duty cycle ratio). Many neuromodulators act on the neuron intrinsic properties by altering the balance of conductances, modifying their excitability properties [171]. The maximal conductance of the PIR current is a natural candidate for modulation by intrinsic parameters.

The high robustness brought by cellular slow regenerativity allows also for the modulation by intrinsic parameters even in presence of variability in the network (Figure 3.4; see appendix A.3 for a description of variability). Covariation of the maximal PIR conductances, $\overline{g}_{PIR,1}$ and $\overline{g}_{PIR,2}$, leads to an increase in duty cycle of 100% (Figure 3.4, Top Right). Independent variation of the same parameters, i.e., varying $\overline{g}_{PIR,1}$ and $\overline{g}_{PIR,2}$ independently, modulates the duty cycle ratio up to a factor three (Figure 3.4, Bottom Right). Variation in phase relation have been observed for instance in cats, during normal locomotion, where the shortening, by a factor two or three, of one of the phase (the extensor phase) leads to faster walking [114]. In contrast, our computational model suggests that modulation with PIR without slow regenerativity is so fragile that it is physiologically unrealistic. Stable oscillations with variation

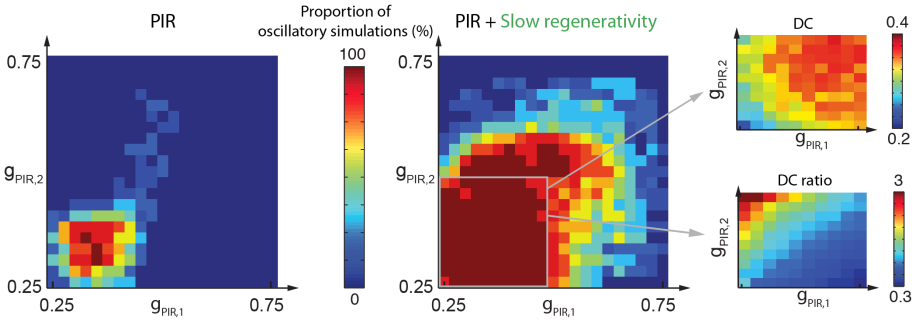

Figure 3.4 – Duty cycle modulation with intrinsic parameters is fragile without slow regenerativity. Modulation of the duty cycle (the ratio between the burst duration and the period) and duty cycle ratio (the ratio between the duty cycle in neuron 1 and in neuron 2) by varying intrinsic parameters of neuron 1, $\overline{g}_{PIR,1}$ (in $[mS/cm^2]$), and neuron 2, $\overline{g}_{PIR,2}$ (in $[mS/cm^2]$), is robust with slow regenerativity but fragile without. Proportion of simulations with stable rhythmic activity for ten simulations with 40% variability in $\overline{g}_{syn}$ and 20% variability in $\overline{g}_{PIR}$ (see appendix A.3 for a description of variability, detection of rhythm, and proportion of oscillatory HCOs). (Left) PIR only. (Center) PIR + slow regenerativity. (Right) For the case with slow regenerativity, zoom in the stable region for mean duty cycle, (DC, Top) and mean duty cycle ratio, (DC ratio, Bottom) from the ten simulations (see appendix A.3 for a description of duty cycle and duty cycle ratio).

of intrinsic parameters do not cover a large parameter range (Figure 3.4, Left).

To summarize, the high robustness brought by cellular slow regenerativity allows for the modulation by both extrinsic and intrinsic parameters. In addition, the network frequency and duty cycle can be modulated independently and in the presence of physiological variability in the network.

3.3 Robustness of network oscillations requires PIR with slow regenerativity

There exists extensive experimental evidence that the rhythmic activity of neuronal circuits is robust against variability in intrinsic parameters, extrinsic parameters, and exogenous noise (such as synaptic currents external to the circuit) [61, 99, 103, 104, 155]. We tested the robustness of HCOs in a sixteen-neuron network, with PIR without slow regenerativity against with PIR with slow regenerativity (see appendix A for network description and details of the simulations). The results show the drastic influence of cellular slow regenerativity in the robustness of the network.

Intrinsic variability of the network was studied by introducing variability (see appendix A.3 for a description of variability) in the maximal conductance of the PIR current, $\overline{g}_{PIR}$. Variability in the cellular properties dramatically impacts the rhythmic activity of the network without slow regenerativity (Figure 3.5, Left). The network rhythm becomes unstable beyond 75% of variability and is significantly perturbed for smaller values. In sharp contrast, the network oscillations with slow regenerativity are robust against intrinsic variability up to 200% (Figure 3.5, Right). Remarkably, the network frequency is almost unaffected by the intrinsic variability, a consequence of the positive feedback brought by slow regenerative currents.

The robustness of the network oscillations against variability in extrinsic parameters was studied by introducing variability (see appendix A.3 for a description of variability) in the maximal synaptic conductance parameters, $\overline{g}_{syn}$. Without slow regenerativity, a small variability in the synaptic conductances affects dramatically the network activity (Figure 3.6, Left, to compare to Figure 3.5, Left, for the case without variability): identical maximal synaptic conductances generate oscillations but oscillations become unstable when the maximal synaptic conductances differ between the two populations. Oscillations with a PIR without slow regenerativity are fragile to network variability. In sharp contrast, variability in the synaptic conductances is possible for a much larger range with slow regenerativity and the network frequency is also almost independent of the synaptic variability (Figure 3.6, Right, to compare to Figure 3.5, Right, for the case without variability). Oscillations persist up to a variability of 200%. A source of slow positive feedback in the PIR mecha-

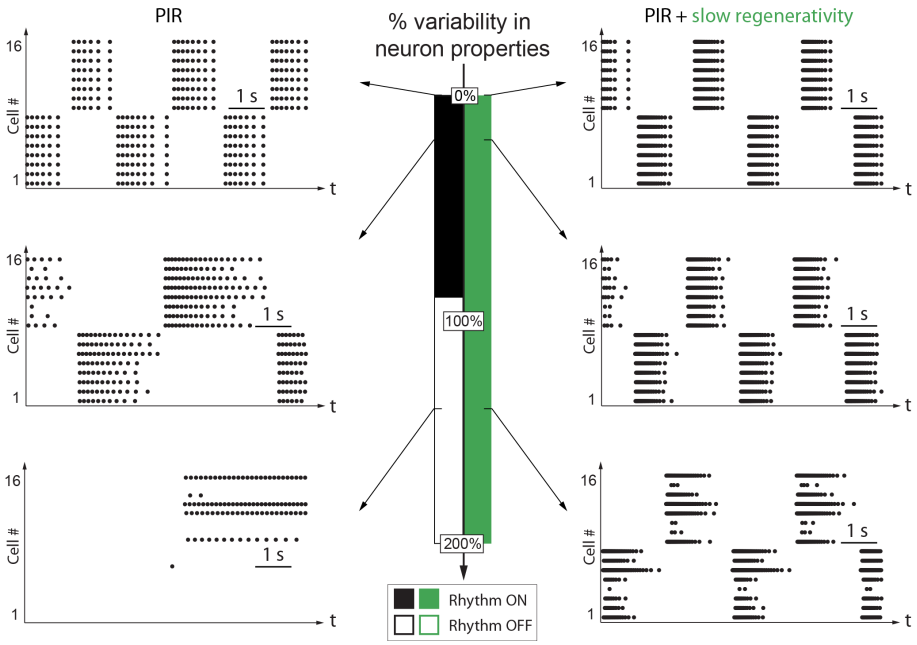

Figure 3.5 – Slow regenerativity makes network oscillations insensitive to intrinsic variability. Network oscillations are robust towards intrinsic variability only with slow regenerativity (see appendix A.3 for a description of variability). (Left) PIR only. (Right) PIR + slow regenerativity. Variability (level: 0% to 200%) in the maximal conductance of the PIR current, $\overline{g}_{PIR}$. Filled colors indicate presence of rhythmic activity and blanks indicate no rhythmic activity (see appendix A.3 for detection of rhythm). Raster plots with 0%, 20%, and 140% variability, respectively.

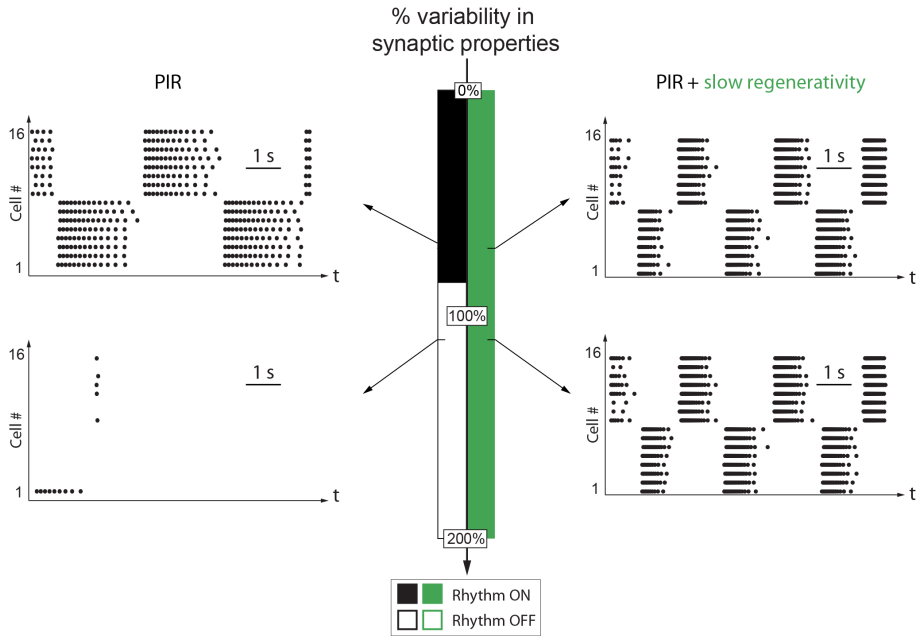

Figure 3.6 – Slow regenerativity makes network oscillations insensitive to extrinsic variability. Network oscillations are robust towards synaptic variability only with slow regenerativity (see appendix A.3 for a description of variability). (Left) PIR only. (Right) PIR + slow regenerativity. Variability (level: 0% to 200%) in the maximal conductance of the synaptic connection, $\overline{g}_{syn}$. Filled colors indicate presence of rhythmic activity and blanks indicate no rhythmic activity (see appendix A.3 for detection of rhythm). Raster plots with 80% and 110% variability, respectively.

nism is therefore essential to robustness of network oscillations against network variability.

The robustness of the network oscillations against exogenous disturbances was investigated by adding a Gaussian white noise in the equation that models membrane potential variations (see appendix A.3 for a description of noise). This emulates the external perturbations—spike train inputs from surrounding neurons—received by a network when studied in a noisy environment rather than in isolation [153]. We simulated a sixteen-neuron network with two populations, with a different noise source for each neuron (Figure 3.7).

The results are consistent with the robustness against parameter variability. Without slow regenerativity, oscillations are sensitive to noise and completely disappear with a noise level greater than $0.10mV^2$. With slow regenerativity, oscillations are robust to noise up to a level of $0.25mV^2$. Similarly to the introduction of variability in intrinsic and extrinsic parameters, the network

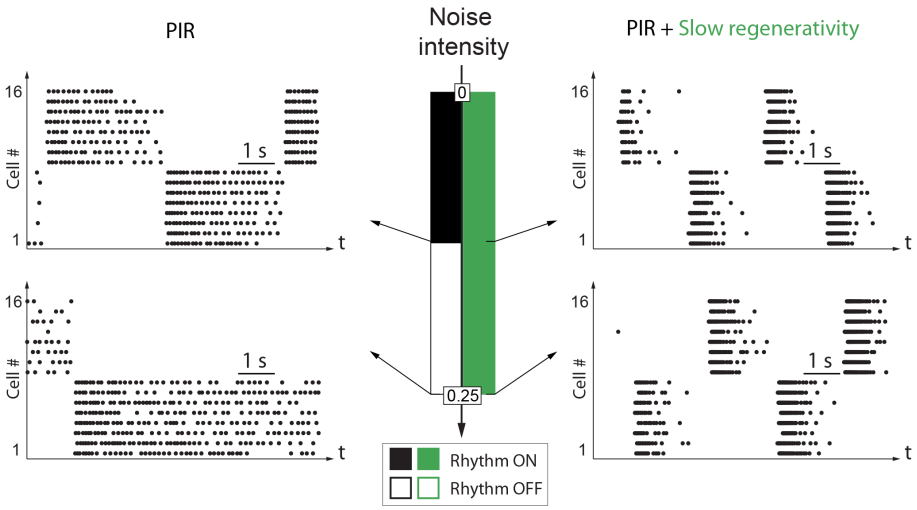

Figure 3.7 – Slow regenerativity makes network oscillations robust against exogenous noise. Network oscillations are robust towards exogenous noise only with slow regenerativity (see appendix A.3 for a description of variability). (Left) PIR only. (Right) PIR + slow regenerativity. Gaussian white noise (noise intensity D ranges from 0 to 0.25 (in $[mV^2]$)) is added to the neurons (see appendix A.3 for a description of noise). Filled colors indicate presence of rhythmic activity and blanks indicate no rhythmic activity (see appendix A.3 for detection of rhythm). Raster plots with noise intensity D of $0.10mV^2$ and $0.25mV^2$, respectively.

frequency is also less affected in the presence of slow regenerativity.

3.4 Discussion

3.4.1 Complementarity between the two types of PIR currents

In the context of HCOs, many neurons possess both I_H and $I_{Ca,T}$, the two main currents that contribute to PIR [33, 46, 50, 74, 185, 194, 228]. When those two currents are present, both I_H and $I_{Ca,T}$ can be a source of modulation. In this case, the presence of T-type calcium currents as a source of slow regenerativity is sufficient to guarantee network oscillation robustness. On the other hand, the hyperpolarization-activated cation current can modulate drastically the network frequency and duty cycle [46, 228]. However, our computational model suggests that this is only the case if a slow-regenerative current is supplied by another mechanism. It is noteworthy that slow restorativity can be provided by other means, such as the presence of high-threshold calcium channels. This requirement for slow regenerativity reveals a somewhat fundamental complementarity, distinct from the release or escape view, between the two channels: $I_{Ca,T}$ allows for stable rhythmic oscillations to emerge and I_H enlarges the modulation possibilities.

3.4.2 Positive feedback as a source of endogenous activity

Slow regenerativity is nothing but a source of positive feedback in the slow timescale of repolarization. It is a slow analog of the positive feedback brought by sodium activation in the fast timescale of spike upstroke. In previous work [89], it was shown that this positive feedback is essential for the robust coexistence of hyperpolarized and spiking states at the cellular level. It was subsequently shown in [88] that this positive feedback is essential for modulation and robustness of bursting activities. Here we show that the same positive feedback at the cellular level is also essential for robustness and modulation at the network level.

The common feature of the positive feedback in those three phenomena is that it makes the neuronal excitability in the slow timescale an endogenous property, robust to intrinsic and extrinsic variability. Making an activity endogenous is the very nature of positive feedback and has been emphasized in a number of contexts.

The results presented in this chapter are in line with the discussion of the role of positive feedback in other biological models, such as for instance the biochemical mechanisms underlying the mitotic oscillator [192, 204, 248]: the oscillator is endogenous and robust in the presence of positive feedback, whereas

it becomes exogenous and entrainable when the source of positive feedback disappears. The importance at the network level of positive feedback at the cellular level is thought to be general and not specific to the case study of HCOs chosen in this dissertation for its simplicity and physiological relevance.

3.4.3 Slow regenerativity in half-center oscillator models

There is a rich literature on computational models of oscillations generated by reciprocal inhibition. HCOs have been used to model rhythmic motor outputs in many invertebrates and vertebrates [26, 33, 117, 169, 200, 214]. In a different context, models of thalamocortical spindle oscillations suggest that the rhythm originates from the thalamic reticular nucleus, which consists in interacting inhibitory nonoscillatory neurons [56, 101, 255, 256].

It is of interest to observe the varying degree of cellular regenerativity in published models of HCOs. Early models are conductance-based and usually include at the cellular level both I_H and $I_{Ca,T}$, the two main physiological currents eliciting the PIR [33, 50, 56, 123, 185]. However, network computational studies often lead to subsequent mathematical simplifications of the cellular details and the cellular slow positive feedback is often lost in this reduction process. A frequent simplification in the literature (see e.g., [47, 100, 211, 255, 256]) is to resort to a steady-state approximation of the calcium activation in the same way as it is normally done for sodium activation. But this approximation rests on neglecting *fast* dynamics, which amounts to consider calcium channels as a source of *fast* rather than *slow* positive feedback. The resulting reduced models have therefore lost their source of slow regenerativity, which makes them unsuitable for robustness and modulation studies at the network level.

The alternative model reduction consists of modeling the cellular level as Morris-Lecar type of neurons, retaining the slow calcium currents but neglecting the fast sodium currents [223,224]. Those models do retain the slow positive feedback source necessary for robustness but they lose the modulation capabilities illustrated in the present chapter because the network interconnection properties are spike-dependent. This prevents exogenous modulation of the rhythm. In addition, if sodium spikes were added to a Morris-Lecar neuron with the addition of the spike currents (as suggested in [143]) while keeping the calcium activation at steady-state, the slow regenerativity would be destroyed.

It should be highlighted that it is possible to derive reduced neuronal models that do retain the balance of slow positive and negative feedbacks as an explicit parameter, see e.g., the recent models in [77, 88]. The results of the present chapter suggest that it is an important feature to retain in a simplified model aimed at network computational studies.

3.5 Summary

We highlighted the role of *slow regenerativity*, a cellular excitability property, in endowing network oscillations with modulation and robustness properties that seem ubiquitous in physiological neuronal networks. An ionic current is slowly regenerative if it provides a source of positive feedback around resting potential in the slow timescale of repolarization [89]. The importance of this cellular property was assessed in one of the simplest and best understood network oscillation mechanisms, the anti-phase rhythm observed between two populations of neurons reciprocally connected by inhibitory synaptic connections. Many earlier studies have emphasized the role of post-inhibitory rebound (PIR) at the cellular level as a core mechanism for the network oscillation, and have identified I_H and $I_{Ca,T}$ as two distinct ionic currents that can participate in the PIR. Our novel contribution is to observe that the cellular PIR will enable a robust and subject to modulation network oscillation only in the presence of a slow regenerative ionic current. Because both I_H and $I_{Ca,T}$ are sources of PIR currents but only $I_{Ca,T}$ is slow regenerative, our results suggest a novel and somewhat fundamental complementarity between T-type calcium and I_H channels in PIR mechanisms.

As a source of positive feedback, regenerative currents make the PIR endogenous, that is, robust to intrinsic and extrinsic sources of variability. As a consequence, a PIR with slow-regenerative currents allows for robust network oscillations and enable robust modulation. The network oscillation is robust because it can sustain large variability across the neuronal population both in intrinsic (cellular) and extrinsic (synaptic) parameters. It is also subject to modulation because the frequency and phase properties of the oscillation can be controlled over a broad range by a relative modulation of extrinsic or intrinsic conductances. Our computational investigation illustrated that this robustness and modulation properties are lost when the PIR is purely ultraslow restorative.

Our results also predict that PIR *per se* is not a sufficient cellular excitability property to ensure modulation and robustness of network oscillations. Determining the dynamics of the PIR current is also primordial. At the cellular level, this suggests an experimental essay to detect the presence or absence of a slow positive feedback source. Slow regenerativity can be detected by the neuron specific response, single spike or burst, to a transient excitatory pulse, when the neuron is under the influence of an hyperpolarization current. The triggering of a burst indicates the existence of a slow regenerative source and predicts modulation and robustness properties at the network level.

Chapter 4

Cellular feedback for transient oscillations in networks

Rhythmic activities are ubiquitous in the brain and play a major role in neuronal processing. These rhythms are very robust and can undergo modulation to adapt to changing environmental conditions [28]. The underlying physiological mechanisms are diverse—e.g., single-cell pacemaker properties or population synchronization—but display unifying principles [253]. The driving physiological application in this chapter lies in the basal ganglia, a group of subcortical nuclei involved in movement initiation and learning [2, 107, 187]. The rhythm of interest is the beta-band rhythm (oscillations between 12 and 30 hertz) involved in physiological and pathological oscillatory activities. This beta rhythm is associated with motor commands and is prominent in Parkinson's disease [20, 116, 187]. We focus on the particular subthalamic nucleus - globus pallidus pars externa (STN-GPe) network, a mutually-connected excitatory-inhibitory (E-I) network, and its potential function as a central pattern generator for beta oscillations [18].

In this chapter, we investigate, the role hyperpolarized-induced bursting, a particular cellular property which is responsible for an excitability switch from single-spike discharge to burst-firing mode, plays in the control of the transient network oscillations.

Through a computational study, we highlight the importance of a positive feedback loop for the cellular excitability switch and the distinction between this excitability switch and post-inhibitory rebounds. A reduced model captures the functional signature of the excitability switch. The cellular feedback endows E-I networks with cellular-based network switch capabilities and

procures robustness, modulation, and localization properties to network oscillations. We consider the physiological implications of such a cellular-based network switch.

The chapter is structured as follows. The excitability switch is presented in a conductance-based model in Section 4.1 and its characteristics are described in Section 4.2. Section 4.3 captures the functional signature of the excitability switch in a reduced model. Section 4.4 explores the impact at the network level, the network activity switch, in a general E-I network. Sections 4.5 and 4.6 study, in this general framework, the network properties, i.e., robustness, modulation, localization, and gating. In Section 4.7, the general framework is particularized to the STN-GPe network and the physiological relevance is investigated. The proposed mechanism is compared to previous models of basal ganglia oscillations.

Contributions. The main contributions of this chapter are (i) the identification of the peculiar role played by a cellular feedback loop for network switches, (ii) the distinction between post-inhibitory rebound and hyperpolarized-induced bursting, both at the cellular level and for network oscillations, (iii) the study of the impact of the hyperpolarized-induced bursting property on network oscillation robustness, modulation, and localization properties, (iv) the suggestion of a causal link between a transient increase in neuromodulator level and network state, (v) a network-switch model independent from synaptic changes, and (vi) a model applicable in both healthy conditions associated to movement control and persistent pathological parkinsonian oscillations.

The material of this chapter is greatly inspired from the publication in preparation [63].

4.1 The role of T-type calcium channels in underlying a cellular excitability switch

In this section, we investigate a specific intrinsic property of STN neurons: the *hyperpolarized-induced bursting* (HIB) property, i.e., the ability to switch between a single-spike discharge mode to a burst-firing mode when the membrane is hyperpolarized (Figure 4.1, Bottom). This property has been studied both experimentally [12, 15, 16, 72, 261] and computationally [95, 124]. The switch is due to the deinactivation of $I_{Ca,T}$, the low-threshold T-type calcium current introduced in section 3.1 [14, 16, 95, 115, 124, 197, 227, 261].

This T-type calcium current is the only candidate to be able to fulfill this role because the switch between the two modes is induced by a change in the sign of the slow dynamical feedback loop on membrane potential variations [88]: the slow feedback loop goes from a negative sign in the single-spike mode to a positive sign in the burst-firing mode (Figure 4.1, Top), or from *slow*

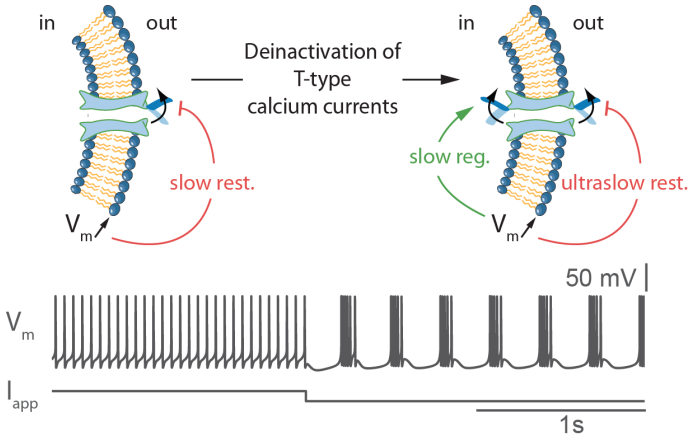

Figure 4.1 – Deinactivation of T-type calcium currents underlies an excitability switch. (Top) Schemes representing ion channel gating and transitions induced in the slow and ultraslow feedback loops by the deinactivation of T-type calcium currents. (Bottom) Switch in the firing mode, from single-spike to burst-firing, of the membrane potential (V_m) induced by a transition in the external applied current (I_{app}), from depolarizing to hyperpolarizing.

restorativity to *slow regenerativity* in the terminology of [89]. In the single-spike mode, the active currents are the two currents responsible for the generation of action potentials, I_{Na} and I_K (see section 2.2.1) [89]. Upon deinactivation by hyperpolarization, $I_{Ca,T}$ provides a slow *positive* feedback on membrane potential variations via its slow activation variable (Figure 4.1, Top, green arrow - see section 3.1). Therefore, the neurons shifts from a slow restorative excitability to a slow regenerative excitability, a necessity for burst-firing since regenerative channels provide the neuron with short-term memory [167], a key source of the hysteretic nature of burst-firing patterns (see section 2.5.1).

To develop a sustained endogenous burst-firing mode, the neuron also requires the action of an ultraslow current to terminate the bursts, e.g., the calcium-activated potassium currents I_{KCa}. I_{KCa} generates an ultraslow outward potassium current which acts as a source of negative feedback on membrane potential variations, or ultraslow restorativity (Figure 4.1, Top, red arrow). The activation of the I_{KCa} current must be faster than the inactivation of the $I_{Ca,T}$ current for endogenous burst-firing to develop in the neuron. For the neuronal activity to ressemble the one in the STN experimental literature literature [12,15,16,72,261], an hyperpolarization-activated cation current (I_H) is also added to the model. The cellular model is given explicitly in appendix A.4.2.

The burst properties are not only function of this T-type calcium current

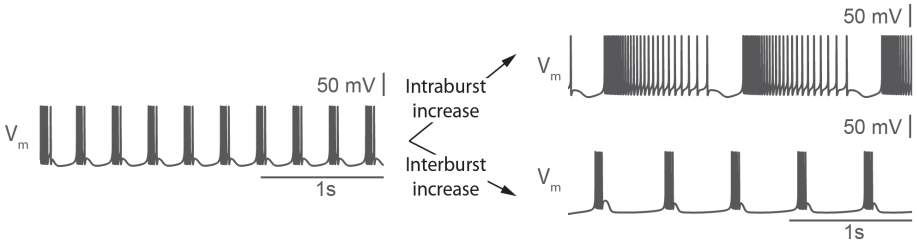

Figure 4.2 – Modulation of endogenous bursting properties independently of $I_{Ca,T}$. Both intraburst and interburst characteristics can be modulated by varying ionic conductances other than $\overline{g}_{Ca,T}$ (Intraburst increase: $\overline{g}_{KCa} * 0.2$ - Interburst increase: $\overline{g}_{H} * 0.45$).

but depend on the interactions with other currents, such as the L-type calcium currents, the persistent sodium current, the hyperpolarization-activated cation current, and the calcium-activated potassium currents [14, 16, 72, 95, 115, 124, 146, 196, 197, 227, 240, 261]. The T-type calcium current is responsible for the switch to the burst-firing mode but modulation of both the intraburst and interburst characteristics can be achieved with variations of other ionic current conductances as shown in Figure 4.2. The burst dynamics is therefore not fixed by the T-type calcium current dynamics but rather function of many parameters.

4.2 Hyperpolarized-induced bursting relies on slow activation and ultraslow inactivation

In contrast to the PIR property developed in the previous chapter, HIB requires specific timescales for both activation and inactivation of the $I_{Ca,T}$ current. Similarly to PIR, the slow activation provides slow regenerativity to the neuron, a necessity for burst-firing (see section 3.1). In addition, the ultraslow inactivation allows for *permanent* burst-firing activity: the burst-firing pattern is present while the hyperpolarization is maintained.

A faster activation prevents the neuron to switch from slow restorativity to slow regenerativity and the neuron remains slow restorative even after deinactivation of the T-type calcium channels. This precludes the neuron from transitioning to a burst-firing mode (Figure 4.3, Left). One instance of faster activation lies in the frequent modeling simplification which consists in neglecting the slow activation kinetics of T-type calcium channels and to consider the activation at steady-state, i.e., instantaneous (see section 3.1). Similarly, a faster inactivation produces a switch which is only transient rather than permanent (Figure 4.3, Right). This corresponds to a PIR, i.e., a transient source

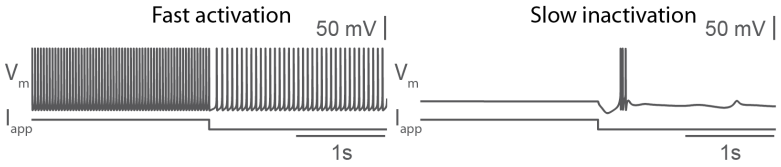

Figure 4.3 – HIB requires slow activation and ultraslow inactivation of $I_{Ca,T}$. (Left) Faster activation ($\tau_m/10$) keeps the excitability in the slow restorative regime and prevents burst-firing. The cellular excitability switch disappears. (Right) Faster inactivation ($\tau_h/10$) produces a transient switch and gives rise to a PIR rather than HIB.

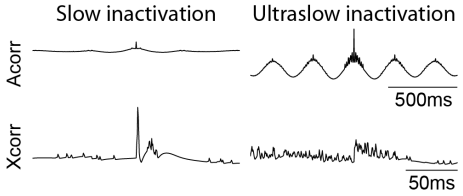

Figure 4.4 – Exogenous and endogenous behaviors in the ultraslow timescale. Auto-correlation and cross-correlation graphs reveal the exogenous and endogenous behaviors. (Left) Slow inactivation bears PIR and exogenous behavior. (Right) Ultraslow inactivation bears HIB and endogenous behavior. For a detailed description of correlation graphs, see section 5.1.

of slow regenerativity.

For this reason, the timescale of endogenous behavior is drastically distinct between PIR and HIB. With PIR, the behavior is endogenous in the fast and slow timescales (see section 3.1) but exogenous in the ultraslow timescale. In contrast, with HIB the behavior is endogenous in every timescale: the source of endogenous behavior is slowly activated and is almost permanent. This distinction in endogenous behavior is highlighted with auto-correlation (Acorr) and cross-correlation (Xcorr) graphs in Figure 4.4 (see appendix A.4.2 for details). With slow activation, the auto-correlation graph reveals no intrinsic activity and the sharp peak in the cross-correlation graph reveals that the output of the system primarily reflects the input, i.e., the system has an exogenous behavior. With ultraslow inactivation, the auto-correlation graph shows strong rhythmic intrinsic activity and the absence of sharp peak in the cross-correlation graph shows that the output primarily reflects memory of the past, i.e., the system has an endogenous behavior. This distinction at the cellular level has major impacts on network oscillatory behavior.

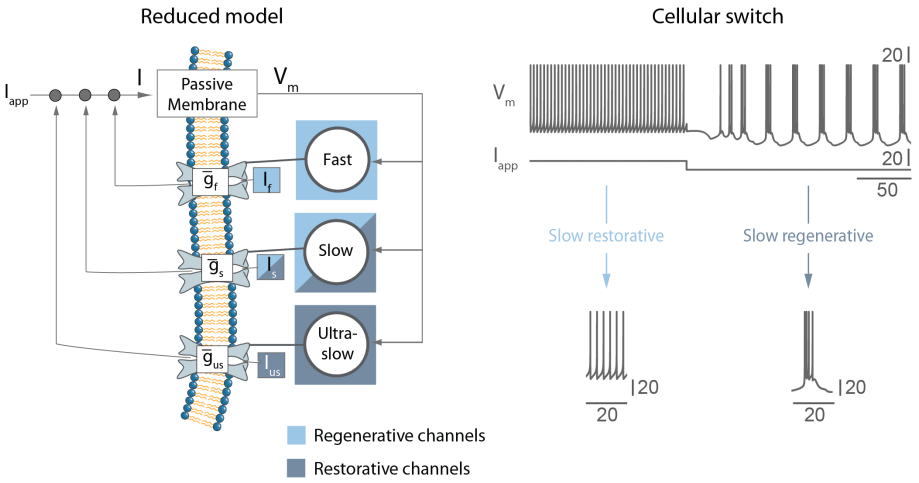

Figure 4.5 – The three-timescale bursting model captures the functional signature of the excitability switch with the modulation parameter $\overline{g}_s$. (Left) The reduced model is composed of three feedback loops, one fast, one slow, and one ultraslow, corresponding to three currents active in the respective timescales, I_f, I_s, and I_{us}, multiplied by their respective feedback gains. The $\overline{g}_s$ parameter captures the balance between slow restorative and slow regenerative ion channels. (Right) The neuron polarization level, controlled via I_{app}, sets the modulation parameter $\overline{g}_s$ and smoothly shifts the neuron excitability between slow restorative (single-spike mode) and slow regenerative (burst-firing mode).

4.3 The three-timescale bursting model captures the cellular switch

To study the impact of the cellular switch at the network level, we use the three-timescale bursting model presented in section 2.5.2 (Figure 4.5, Left). This reduced model captures the functional signature of the excitability switch. As mentioned in section 2.5.2, the model is composed of three feedback loops: one fast, one slow, and one ultraslow, corresponding to three currents active in the respective timescales, I_f, I_s, and I_{us}, multiplied by their respective feedback gains. The balance switch between the two firing modes is controlled by the physiologically meaningful modulation parameter $\overline{g}_s$.

Variations of the modulation parameter $\overline{g}_s$ by the neuron polarization level—accounted for by a voltage dependence of the modulation parameter, which reflects the ultraslow deinactivation of T-type calcium channels at low threshold (see appendix A.2.1)—bear smooth and reversible transitions from single-spike discharge mode to burst-firing mode, or transitions from slow restorativity to slow regenerativity (Figure 4.5, Right). One should notice that, due to the

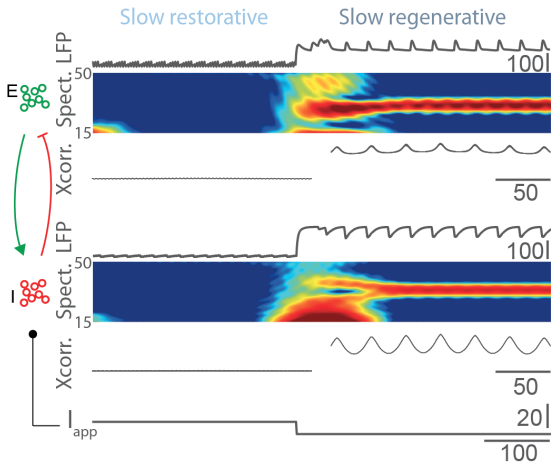

Figure 4.6 – The cellular switch translates into a network switch in an E-I network. The transition between modes is controlled by the applied current I_{app} (excitatory connection) on the I population (see appendix A.2.2). LFP, spectrogram analysis (Spect.), and intra-population cross-correlations between every cell pair (Xcorr.) for both the E and I populations (see appendix A.3). Slow restorative excitability corresponds to a nonoscillatory LFP and asynchronous single-cell firing patterns. Slow regenerative excitability corresponds to a strongly oscillatory LFP and synchronous single-cell firing patterns.

model definition by the three timescales of neuronal bursting [88], the model uses dimensionless units. The three-timescale bursting model is sufficient to capture the cellular switch in a population model. In the next section, we investigate the effect of a cellular switch on the behavior of a general E-I network.

4.4 The cellular switch induces a network switch

We use a general E-I network inspired from the STN-GPe network configuration (see section 4.7.1). Each population is composed of sixteen neurons in order to develop a population activity, captured by the local field potential (LFP), which reflects the global activity of the population (see appendix A.3). All the neurons in the E population connect with excitatory synapses to all the neurons in the I population and, reciprocally, all the neurons in the I population connect via inhibitory synapses to all the neurons in the E population (see appendix A.2.2). The applied current, I_{app}, acts on the I population (Figure 4.6).

The applied current switches the I population from the slow restorative (single-spike) mode to the slow regenerative (burst-firing) mode by hyperpolarization. As a result, the inhibitory action of the I population on the E

population switches the E population to the slow regenerative (burst-firing) mode. In contrast to the network rhythm in the previous chapter which develops from resonance between rebound bursts via the network connections, endogenous rhythms develop at the cellular level and the network rhythm results from the interplay between the two cellular endogenous rhythms. This distinction bears drastic differences for the robustness of the network rhythm between the mechanism with PIR in the previous chapter and the mechanism with HIB in this chapter.

The network bursting is not a mere reflection of the unicellular bursting, but a combination of two concomitant effects: the endogenous effect—HIB—and the network effect—the synaptic connections. The network rhythm depends on both the cellular and synaptic properties, respectively function of *intrinsic* and *extrinsic* parameters (see section 4.5).

The cellular switch corresponds to a switch in the population activity as reflected in the LFP traces and spectrogram analysis (Spect.) of Figure 4.6: each population switches from a nonoscillatory LFP when slow restorative (no specific power band in the spectrogram analysis) to a strongly oscillatory LFP when slow regenerative, confirmed by a high spectral power in a confined frequency band in the spectrogram analysis, due to the action of I_{app}.

This population switch is also visible in the cross-correlation analysis between the firing pattern of the cells within each population (Figure 4.6, Xcorr.). In the slow restorative mode, the cross-correlations are weak and show no oscillatory activity. In the slow regenerative mode, the cross-correlations reach higher values and exhibit a clear oscillatory activity. In summary, the cellular switch triggers a switch at the network level, from asynchronous single-spike discharge to synchronous burst-firing.

4.5 Robustness and modulation of the network rhythmic activity

In this section, we investigate the network rhythm robustness and modulation properties. In the restorative mode, the neurons fire asynchronously and no specific activity is present in the population LFPs. For this reason, we focus on the network robustness and modulation properties solely in the slow regenerative mode.

The network rhythmic activity that emerges in the slow regenerative mode is highly robust (Figure 4.7). The slow regenerativity at the cellular level provides robustness towards heterogeneity in intrinsic parameters (relative to the cell), extrinsic parameters (relative to the synaptic connections), and noise. We simulated the network with 20% variability in intrinsic parameters (the slow timescale τ_s, the ultraslow timescale τ_{us}, and the ultraslow feedback gain

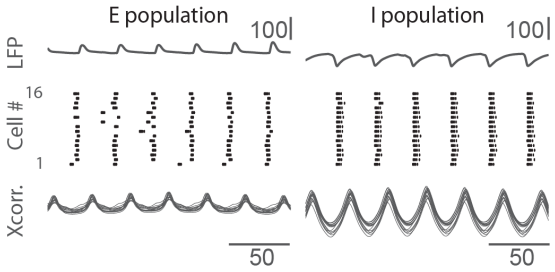

Figure 4.7 – Robust oscillations despite heterogeneity and noise. The network rhythmic activity survives despite 20% variability in intrinsic and extrinsic parameters and noise sources. LFP, spike rasters (Cell #) and intra-population cross-correlations between every cell pair (Xcorr.) for both the E and I populations (see appendix A.3). The LFPs are strongly oscillatory, the spikes rasters show diversity in the individual cell firing patterns, and the cross-correlations show a close-to-synchronous activity.

$\overline{g}_{us}$), with 20% variability in extrinsic parameters (the synaptic gain $\overline{g}_{syn}$), and with gaussian white noise sources of intensity 1 (see appendix A.3 for variability and noise intensity definitions). The network rhythmic activity survives despite heterogeneity and noise, and the population LFPs remain strongly oscillatory (Figure 4.7, LFP). The raster plots show diversity in the firing pattern of the individual neurons and the intra-population cross-correlations highlight that the neurons do not fire in perfect synchrony but still develop an overall burst synchrony that generate the LFP oscillatory activity. The robustness extends to the cellular switch in control of the network switch: the switch can be achieved through a switch of only a fraction of the population provided that the heterogeneity in the cellular switch is compensated for by a sufficient level of connectivity within the population.

The network rhythmic activity that emerges in the slow regenerative mode can be robustly modulated (Figure 4.8). The rhythmic activity is function of both the intrinsic and extrinsic parameters. As a result, modulation can be achieved by a variation of both parameter types. We look at two simple measures to quantify the rhythmic activity: T_{osc}, the oscillation period or the duration between two burst onsets, and T_{burst}, the duration of the burst, from the burst onset to the last spike, distinct for the two populations. Starting from a set of parameters and a given rhythmic activity (Figure 4.8 A), the rhythm can be slowed down (T_{osc} increases) by both intrinsic (Figure 4.8 B, variation of τ_{us}) and extrinsic (Figure 4.8 C, variation of τ_{syn}) parameters. Similarly, the rhythm can be accelerated (T_{osc} decreases) by both intrinsic (Figure 4.8 D, variation of $\overline{g}_s$) and extrinsic (Figure 4.8 E, variation of $\overline{g}_{syn}$) parameters. Concomitant variation of a combination of parameters allows to cover a wide modulation range for both T_{osc} and T_{burst} and to emulate characteristics of

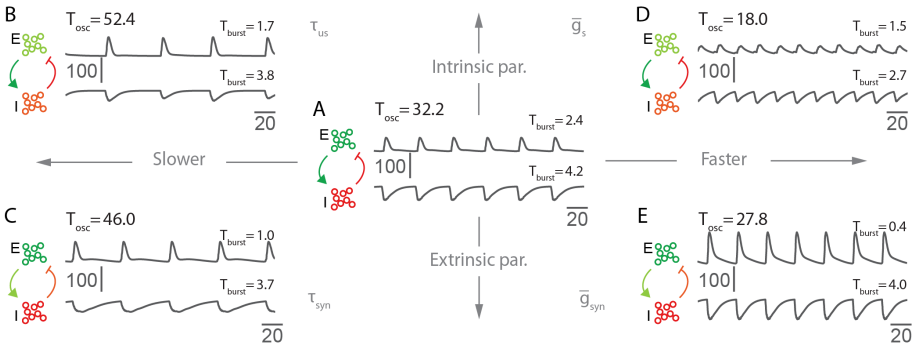

Figure 4.8 – Robust modulation via both extrinsic and intrinsic parameters. Color-code in schemes represents the variations introduced in parameter values (see appendix A.4.2). LFPs for both the E and the I populations show the rhythmic pattern. T_{osc} for the network and T_{burst} for each population quantify the properties of the rhythmic activity. A: Initial configuration. B: T_{osc} increases with variation of the intrinsic parameter τ_{us}. C: T_{osc} increases with variation of the extrinsic parameter τ_{syn}. D: T_{osc} decreases with variation of the intrinsic parameter $\overline{g}_s$. E: T_{osc} decreases with variation of the extrinsic parameter $\overline{g}_{syn}$.

physiological networks.

4.6 Temporal and spatial localization of the network switch

In this section, we investigate both temporal and spatial localization properties of the network activity switch. Inspired from the STN-GPe network architecture (see section 4.7.1), we explore how an external nucleus controls the switch by its action on the I population and how spike inputs on the E population are processed (Figure 4.9). The external nucleus connects to all the I neurons with inhibitory synapses and the neuron model includes the effect of a neuromodulator via a scaling coefficient (see appendix A.2.2). The spike train I_{spike} on the E population are spikes with time intervals selected from a Poisson distribution with an enforced minimum interval and acting via excitatory synapses (see appendix A.2.2). To study the spatial localization property, we use the same network but with four distinct currents, each one targeting a different subpopulation, and with exponential decay in the synaptic conductances, emulating a decrease in the reciprocal connection strength between two neurons with an increase in spatial distance along a one-dimensional axis (Figure 4.9, Right - see appendix A.2.2).

Figure 4.9 (Left) shows the temporal localization of the switch: a transient

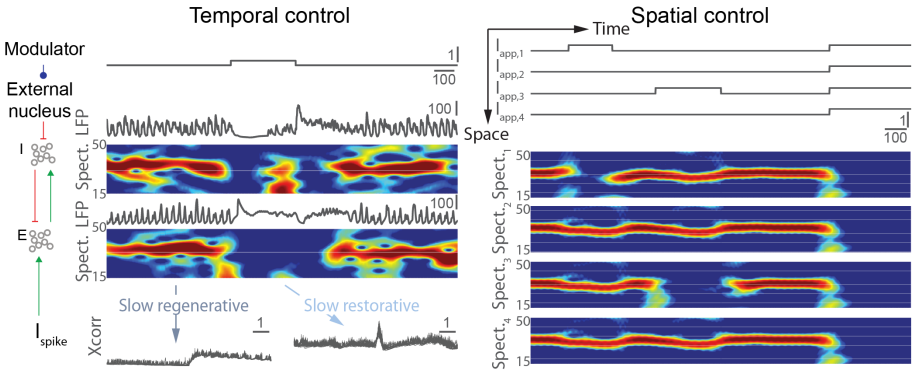

Figure 4.9 – Control of transient network oscillations and spatial localization of the network switch. (Left) The neuromodulator controls an external nucleus which switches the E-I network between oscillatory and nonoscillatory activity patterns by its action on the I population. The spike train I_{spike} acts via excitatory synapses on the E population. Neuromodulator level (Modulator), LFP, and spectrogram analysis (Spect.) for both the I and E populations. Cross-correlations (Xcorr) between the neuron membrane potentials and the input spike train in the slow regenerative (weak Xcorr - oscillatory OFF mode) and slow restorative mode (strong Xcorr - transfer ON mode). (Right) Four distinct applied currents and exponential decaying synapses along a one-dimensional spatial axis (Space) highlights the spatial localization of the switch. Spectrogram analysis (Spect.) for the four subpopulations in the E population.

change in the modulator level triggers an external nucleus-mediated switch in the E-I network. The LFPs switch between oscillatory and nonoscillatory and the spectrogram analyses highlight this transition. The switch is transient in both directions and solely the modulator level controls the network oscillatory activity.

In addition to this network activity switch, Figure 4.9 (Left) uncovers a network state switch: in the slow regenerative mode, the neurons exhibit an endogenous burst-firing pattern which carries little information about the input spike train. This is in sharp contrast with the slow restorative mode, where the neurons fire exogenous single spikes which are mainly function of the intensity, duration, and frequency of depolarizing inputs. At the network level, this translates into two distinct network states: when the network is prone to oscillations (slow regenerative), the cross-correlations between the individual cell firing patterns and input spike train are low and do not possess a sharp transition, reflecting an *oscillatory* mode where spikes are filtered (OFF state). When the network is nonoscillatory (slow restorative), the cross-correlations are high and a sharp transition indicates the direct link between incoming spikes and action potentials, underlining a *transfer* mode (ON state).

The cellular-based network switch is endowed with spatial localization property (Figure 4.9, Right). Different subpopulations, spatially spread on a one-dimension axis (Space), can be controlled and switched individually. The I population is controlled by four distinct applied currents, each one targeting one-fourth of the population along the axis (see appendix A.2.2). As a results, only the targeted I subpopulation undergoes the population switch and switches the respective E subpopulation. The LFPs for the E subpopulations—the LFPs regroup the activity of the neurons that are spatially close—are therefore orchestrated individually and the rhythmic activity patterns differ along the spatial axis: the transient increase in $I_{app,1}$ transiently turns off the rhythm in LFP_1, the transient increase in $I_{app,2}$ acts similarly on LFP_2, and the transient increase in all I_{app} turns off any rhythm in the entire network (Figure 4.9, Right).

4.7 Discussion

4.7.1 The cellular-based network switch yields physiologically relevant applications

A large amount of recent experimental evidence demonstrates that the basal ganglia include all the required ingredients to provide a robust instance of the proposed mechanistic link and to support the role of T-type calcium channels as key ionic mediators between the molecular action of a transient depolarization source and rhythmic pattern modulation. The basal ganglia act as one of

the fundamental processing units of the brain and play a major role in the planning and initiation of voluntary movements [2, 20, 22, 52, 181, 187]. In this dissertation, we focus on the role of the proposed mechanistic link in the control of transient oscillations in the STN-GPe network.

At the cellular level, experimental evidence shows that both STN and GPe neurons possess the ionic currents to undergo an excitability switch. The prominent role of low-threshold voltage-gated calcium channels in the burst-firing of STN neurons has been identified [14–16, 115, 197, 227, 261]. STN neurons possess the HIB property: sustained hyperpolarization of STN neurons induces endogenous burst-firing [12, 15, 16, 72, 261]. T-type calcium channels are necessary for subthalamic burst-firing and inhibitors of T-type calcium currents dramatically decrease STN burst-firing activity in vivo [238]. In parallel, subgroups of GPe neurons exhibit the two firing modes, single-spike discharge and burst-firing [43, 188]. Although no experimental recording has shown the switch in isolation, many GPe neurons do possess the regenerative T-type calcium channels required for the excitability switch [43, 188]. As a result, STN and GPe neurons can be modeled with the same reduced model and the balance between restorative and regenerative ion channels in the slow timescale plays a fundamental role as it acts as a modulation parameter.

At the network level, oscillations have been recorded in the STN-GPe network in vitro [202] and in vivo [18, 24, 97, 165, 191, 237]. Reciprocal STN-GPe interconnections are primordial for the generation and amplification of the oscillatory activity of STN neurons [237]. These considerations led to the STN-GPe pacemaker hypothesis: the STN-GPe network is a central pattern generator for beta oscillations (oscillations between 12 and 30 hertz) in the basal ganglia [18]. Other origins are attributed to the beta oscillations, such as other parts of the basal ganglia—e.g., the striatum [174]—or of the brain—e.g., the cortex [113, 149]. While it is likely that the rhythmic pattern stems from the emergent properties of the interconnected networks, in this dissertation we focus on the STN-GPe origin of the network switch.

The STN-GPe network fits the general mechanism of the previous section (Figure 4.9, Left), with the GPe as the I population and the STN as the E population. In this network, the oscillatory state is controlled by the input on the GPe neuron, via an external nucleus. The firing rate of this external nucleus can be modulated by an external modulator, similarly to the phasic modulation of the striatal firing rate by dopamine via its D2-type receptors [80, 125, 225, 236, 257]. It is noteworthy that dopamine acts also via extra-striatal pathways directly on GPe and STN [1, 17, 36, 225] and it is the combined action on all sites that determines the STN-GPe network oscillatory state.

The gating mechanism proposed by analogy to the thalamocortical network could be at play in the processing of the hyperdirect pathway, i.e., the excitatory inputs from the cortex directly on the STN. In the restorative mode,

the STN neurons acts as linear transformers by relaying the strength of inputs [196]. An excessive synchrony in the network reduces the capacity of STN neurons to encode the information, which may have an impact on the treatment of motor information [165]. The spatial control of the switch could also be a necessary feature in view of the basal ganglia organization in segregated functional loops [210]: the possibility for independent control of each loop could reveal to be necessary.

We advance two specific situations of movement-related beta-band activity in the basal ganglia where the cellular-based network switch could be at play: (i) the event-related desynchronization (ERD) and synchronization (ERS) of the beta-band oscillations in relation to movement initiation and (ii) the switch between the healthy nonoscillatory state and strongly oscillatory state in the case of Parkinson's disease. The specificity of our approach lies in that the same model applies in both situations, considering the parkinsonian state as an exaggerated version of an healthy phenomenon (this approach is for example proposed in [22, 133]). The transient property of the model is primordial for movement initiation whereas its robustness ensures strong and robust oscillations under parkinsonian conditions.

Movement initiation: a transient network-switch

The basal ganglia play a major role in the planning and initiation of voluntary movements. In particular, the coherence and strength of basal ganglia beta oscillations are associated with voluntary movements initiation, both in animals [82, 150] and in humans [6, 25, 82, 147, 148, 151]. Experimental studies show a reduction or abolishment of oscillatory activity at the single-cell level during movements [6]. At the population level, there is a prospective increase in beta synchrony prior to voluntary movements [133] and an ERD in the beta band during movement [147, 151]. Additionally, the increase and decrease in beta oscillations strongly correlates with behavioral performances [133, 148].

Initiation of voluntary movements is also linked to an increase in dopamine and, in particular, to a transient increase in the activity of nigrostriatal circuits (phasic dopamine release) in response to cues in reaction-time tasks or prior to voluntary movements [133, 136, 187]. The increase in the firing rate of dopaminergic neurons in the substantia nigra pars compacta lasts on the order of hundreds of milliseconds and happens prior to the movement execution [133, 136]. Striatal neurons with D2-type dopamine receptors follow the inverse trend and decrease their firing rate. This dopamine transient increase triggers the decrease of the beta-band activity coherence and power [22, 133], as predicted by our model with a transient increase in modulator. The potential functional role of beta-band oscillations could therefore be to maintain the current sensorimotor state during movement preparation [82], until dopamine signals the onset of movement execution, opening the gate for motor informa-

tion transfer via the hyperdirect pathway [133].

Parkinson's disease: a robust network-switch

As mentioned in section 2.6.2, the hallmark of Parkinson's disease is a dopaminergic denervation of the striatum, altering information patterns along movement-related ganglia-mediated pathways in the brain. Severe motor symptoms result [116, 258].

In Parkinson's disease, the baseline level of synchrony within and between basal ganglia nuclei in the beta band is high: increased beta-band activity has been reported in the STN, GPe, and GPi nuclei in both single-unit activity and LFPs [20]. Similarly, animal models of the disease have shown increases in basal ganglia structures in burst discharge, oscillatory firing, and synchronous firing patterns [212]. The excessive synchrony in the beta-frequency band correlates with the motor symptoms and is thought to limit the information coding of neurons, the neurons being locked to the population rhythm [25, 116].

Beta synchrony diminution under dopaminergic therapies (the administration of the dopamine prodrug levodopa (L-DOPA), a precursor to dopamine in the brain [92, 215]), following ablative surgeries, or during deep brain stimulation (DBS corresponds to a high-frequency stimulation, through chronically implanted macroelectrodes, of a specific brain area [75, 92, 145]) is associated with an amelioration of the motor impairments [116, 257, 258]. It has been suggested that the degree of suppression of beta oscillations in the STN by dopaminergic medications can predict the level of improvement in bradykinesia and rigidity [258].

Parkinson's disease corresponds to a pathological depleted dopaminergic state (tonic dopamine release), an exaggerated version of the healthy case [22, 133]. Normally, at the onset and during movement, the synchronization in basal ganglia structures is drastically reduced. But under parkinsonian conditions, baseline levels of synchrony are higher and more resistant to suppression [116]. In this configuration, the phasic increase in dopamine is not sufficient to trigger a network switch and strong beta oscillations remain [133], impairing cortical spikes transfer through the basal ganglia and thereafter motor movements. Our model is fully consistent with these observations.

Furthermore, experimental evidence shows that T-type calcium channels, as employed in our model, are strongly involved in the disease. Indeed, pharmacological blockade of T-type calcium channels decreases burst activity in STN neurons both in vitro and in vivo and reduces motor deficits in animal models [238, 267]. In addition, low-frequency DBS, with long depolarization pulses, improve motor impairments in parkinsonian rats presumably by inactivating T-type channels [238].

4.7.2 Comparison with experimental data

It is of course of prime interest to investigate to what extent a proposed mechanism is consistent with available experimental data. When making such comparisons, one should keep in mind, however, the difference between the experimental and modeling setups. In the case of excitability studies such as the one presented in this chapter, it is essential to compare models and experiments on the same spatial and temporal scales. In addition, in vivo experiments involve many interconnected networks not taken into account in the simplified model representations.

As an illustration, we test our model predictions against the experimental paper of Tachibana et al. [237]. In this paper, the authors study parkinsonian monkeys and observe how abnormally synchronized oscillations are affected by blocking currents in different basal nuclei. It should be noted that the study of Tachibana et al. presents so many constraints that none of the currently published models is fully consistent with the data. Moreover, the results of the study have not yet been independently replicated.

Many of the reported experiments in [237] provide results consistent with the mechanism described in our model: decrease in abnormal neuronal oscillations (8-15 Hz) in the GPe and STN after administration of L-DOPA (Figures 6 and 7), suppression of parkinsonian signs by silencing of the STN (Figure 8), decrease in the 8-15-Hz oscillatory power in the GPe by blocking of glutamatergic neurotransmission on GPe (Figure 9), reduction of STN oscillations by blocking GABAergic inputs from the GPe (Figure 12). We are not aware of other models in the literature consistent with those data.

Other experimental data in [237] might be inconsistent with our model prediction: the authors observe that blocking of GABAergic transmission increases the power of beta oscillations (Figure 10). Likewise, they observe that blocking glutamatergic inputs to STN increases burst patterns but decreases the power of beta oscillations (Figure 11).

Those observations conflict our model predictions if we interpret blocking GABAergic transmission as an inhibitory input on the GPe and blocking glutamatergic inputs to STN as an excitatory input on the STN. One should be cautious, however, that blocking transmissions affects a whole network away from its normal behavior. We speculate that our isolated model of the GPe-STN network cannot account for such perturbations. This observation highlights the precaution required for interpretation of experimental data in excitability studies. Considering the exogenous and endogenous character of the behavior as well as the global versus local aspect is critical.

4.7.3 Comparison with previous models

In this section, we highlight the key novelties our model has compared to the other computational models published in the literature. The key features of our model lie in (i) the presence of a slow positive feedback at the cellular level, which ensures modulation, robustness, and localization properties, (ii) the role of the HIB property, distinct from the PIR property, and amenable to oscillations in a wide frequency range, (iii) the independence on synaptic changes for network oscillatory state transition, which results in the transient and local aspects of the switch, and (iv) the validity of the model for both healthy oscillations associated to movement control and persistent pathological parkinsonian oscillations.

To our knowledge, this is the first network model to investigate the impact of cellular HIB for network robustness, modulation, and localization properties. The closest study to our model uses the same cellular HIB property but with a neuron model based on an extension of the functionality of spiking neurons and does not investigate the network switch [124].

Several models have investigated oscillations in the basal ganglia within the STN-GPe pacemaker hypothesis framework [42, 96, 126, 190, 199, 240] and some of them have highlighted the importance of calcium channels in the genesis of the oscillations [126, 240]. However, the cellular property at play is PIR, a property closely related to HIB but exogenous in the ultraslow timescale (see section 4.2). Rebound bursting constrains the oscillation frequency to the lower frequency bands due to the resonance between rebound bursts. This is for example the mechanism at play in the thalamic relay (TC)-thalamic reticular (RE) network as described in section 5.6.2 [60, 101, 102, 226, 239, 254]. Among the computational models, many approximates the activation of T-type calcium channels by its steady-state value (e.g [53, 54, 58, 59, 101, 102, 239, 240, 254]), suppressing the source of slow regenerativity. As discussed in chapter 3, the deletion of the source of slow cellular feedback might have drastic impacts on network robustness and modulation properties.

In addition, all the models with the STN-GPe pacemaker hypothesis study the network switch in relation to Parkinson's disease and we are not aware of any other computational model that presents healthy movement initiation and parkinsonian conditions in a synergetic approach. For this reason, the modulation of oscillatory activity in the E-I network involves changes in the synaptic connections, which cannot be of application in movement-related transient oscillations due to the rapid timescales in play. Other models study the genesis of basal ganglia oscillations from other nuclei in the basal ganglia [149, 174] or from other parts of the brain [113, 189].

4.8 Summary

We evaluated the impact of a cellular feedback loop on transient oscillations in an E-I network. The proposed mechanism is simple, generic, and robust, and suggests the orchestration of network oscillations via a cellular switch mediated by neurotransmitters. We illustrated the mechanism on the modulation of beta oscillations in the basal ganglia in relation to movement initiation and Parkinson's disease.

At the cellular level, slow-regenerative currents endow the neuron with an excitability switch capability, between single-spike discharge and burst-firing mode, controlled by polarizing sources. T-type calcium channels are a prominent example of such slow-regenerative currents because of their slow activation and ultraslow inactivation. At the network level, an E-I network robustly switches, via a cellular-based network switch, from an exogenous asynchronous mode to an endogenous synchronous mode under the modulation of its external drive.

The network rhythmic activity emerges from the interplay of the endogenous cellular rhythms. The network rhythm is highly robust and amenable to modulation due to the presence of a slow-regenerative ionic current at the cellular level. The network rhythmic activity is robust because it can sustain large variability across the neuronal population both in intrinsic (cellular) and extrinsic (synaptic) parameters, and noise disturbances. It is also amenable to modulation because the oscillation period and the burst duration characteristics can be both increased or decreased by a relative modulation of intrinsic or extrinsic parameters.

Because it is controlled at the cellular level, the network switch possesses both temporal and spatial localization properties. As such, it is a wonderful candidate to explain transient physiological oscillations associated, for instance, to movement control or attention shift. The timescales involved in movement planing and initiation are such that network-level modifications cannot be the cause of the phenomenon [35, 173]. On the contrary, a rapid change in neuron excitability due to activation or inactivation of ion channels is fast enough to be responsible for the observed network dynamical changes. The spatial localization of the switch allows to exert an independent control of the different subnetworks involved and to target specific pathways while maintaining other pathways unaffected.

Finally, the network-switch mechanism provides a causal link between a transient increase in neuromodulator level and network state: an oscillatory OFF state where incoming spikes are filtered and a transfer ON state where incoming spikes are transmitted. This *gating* function is a strict analog to the one described in the thalamocortical network [176, 177, 217].

Chapter 5

Localized transfer properties of excitable behaviors

In the two previous chapters, we have studied examples of the interplay of motifs at different resolution levels and how basic cellular properties might impact network level properties.

This approach can be generalized to investigate the excitability motif properties and especially how these properties are maintained and interact across scales in *multiresolution excitability*.

We show that excitable systems possess two types of behaviors, exogenous and endogenous, with distinct transfer properties. In addition, excitable systems are endowed with localization properties, limiting their action to specific excitability windows, or resolution levels. We argue that, thanks to this localization property, excitability obeys a superposition principle and that excitability windows at distinct resolutions can interact to generate multiresolution systems which are amenable to multiplex signaling. We investigate these properties and the input-output behavior in three resolution levels in neuroscience: i) *spike excitability*, or cellular fast spike, e.g., the Hodgkin-Huxley neuron (section 2.2.1), ii) *burst excitability*, or cellular slow spike, in bursting neurons (section 2.5.2), and iii) *circuit excitability*, or spike in the local field potential (LFP), in excitable neuronal circuits similar to the network model of Wilson-Cowan (section 2.4.2).

The chapter is structured as follows. Section 5.1 describes how traditional correlation measures can be exploited to quantify the behavior of excitable systems. Section 5.2 considers the excitability input-output behavior in a monoresolution motif for spike excitability and introduces the conceptual underpinnings

for multiresolution excitability: localization properties. Section 5.3 studies excitability properties in a multiresolution motif in the temporal dimension with burst excitability. Section 5.4 adds the spatial dimension in multiresolution motifs with circuit excitability. Section 5.5 suggests the capability for multiplex signaling in multiresolution objects. In section 5.6, we emphasize the importance of the hierarchy in feedback loops, in addition to the sign, in order to get the localization properties and physiological implications of this hierarchy are presented.

Contributions. The main contributions of this chapter are (i) the quantification of the behavior of excitable systems with correlation measures, (ii) the association of input-output behavior characteristics to the excitability motif, (iii) the identification of localization properties in excitable systems, (iv) the application of a superposition principle to form multiresolution excitable systems, (v) the exploration of multiplex signaling in objects with multiresolution excitability, and (vi) the identification of the importance of hierarchical feedback loops.

The material of this chapter has not yet been published.

5.1 Excitable systems have an exogenous and an endogenous behavior

In section 2.3.3, we described the +FB then –FB excitability motif. This motif is composed of a fast positive feedback loop (+FB) and a slower negative feedback loop (–FB). The two feedback loops are responsible for distinct aspects of the behavior (see section 2.3.1): the positive feedback introduces bistability in the system (the robust coexistence of two stable attractors), i.e., it generates a two-state automaton, whereas the negative feedback is responsible for the exogenous behavior. The static level sets the balance between the two extremes: the positive feedback—switch-like characteristics—and the negative feedback—sigmoidal-like characteristics.

Excitability has been extensively studied, both in biological and chemical systems with motifs and threshold behaviors [11, 73, 140], and in dynamical system theory with phase-planes and bifurcation analyses [83, 128, 129]. We propose to adopt a novel approach to study excitability by investigating the input-output behavior and transfer properties of excitable systems. This approach comes from signal processing theory and is complimentary to what is found in the neurodynamics literature.

The input-output behavior of excitable systems is studied by considering the system input I, state X, and output O (5.1, Left). From these three signals, we extract the auto-correlation (Acorr) and the cross-correlation (Xcorr) relations (5.1, Right). Correlations are classic measures of the similarity between

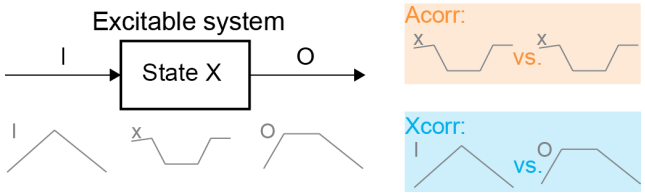

Figure 5.1 – Input-output behavior of excitable systems. (Left) Block diagram for an excitable system with input I, state X and output O. Illustration of I, X, and O signals. (Right) Auto-correlation and cross-correlation representations.

two signals as a function of the lag of one relative to the other [28, 195] (see appendix A.3.6). The auto-correlation measures the similarity of the state signal with itself and reveals the endogenous rhythmic activity in the system. In contrast, the cross-correlation measures the similarity between the input and the output signals and quantifies the transfer properties of the system. Auto-correlation and cross-correlations analyses have been used in neurophysiology previously [28]. The novelty resides in using these traditional techniques to quantify the behavior of excitable systems.

The auto-correlation and the cross-correlation reveal two distinct states in excitable systems: an *exogenous state* and an *endogenous state*. These states differ in their transfer properties and intrinsic behavior. In the exogenous state, the output of the system primarily reflects the input and the cross-correlation is composed of a sharp peak; there is no intrinsic behavior and the auto-correlation shows no autonomous activity. In the endogenous state, the output primarily reflects memory of the past and there is no peak in the cross-correlation; there is a strong intrinsic behavior and the auto-correlation shows rhythmic autonomous activity.

In this chapter, we distinguish between the exogenous and the endogenous state in three excitable systems encountered previously: i) the Hodgkin-Huxley neuron (section 2.2.1), ii) the bursting neuron (section 2.5.2), and iii) the E-I network (section 2.4.2). The auto-correlations and cross-correlations are computed with a random impulse train as an input on the system. The width of the impulses and the minimum time interval between two impulses is function of the excitability timescale (see appendix A.4.3 for details).

5.2 Monoresolution excitability motif

One of the seminal work about monoresolution excitability is the description, by Hodgkin and Huxley, of spike excitability—or *cellular fast spike*—in a conductance-based model [120]. Conductance-based models describe the dynamic interactions between the membrane potential V_m and gating variables

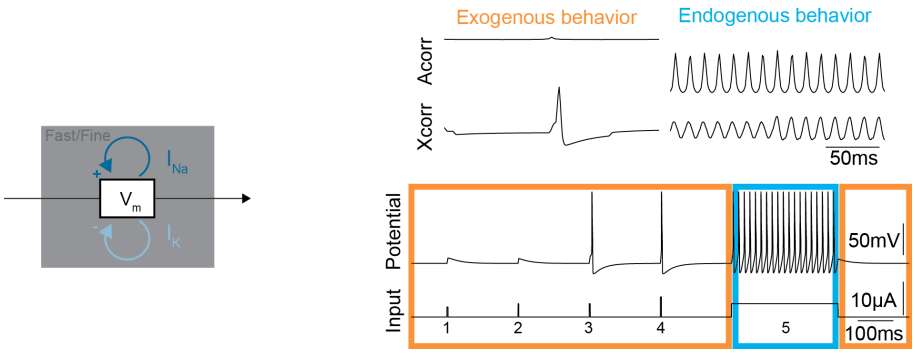

Figure 5.2 – Properties of the monoresolution excitability motif with the Hodgkin-Huxley neuron. (Left) Motif and resolution: the fast sodium current I_{Na} and the slow delayed-rectifier potassium current I_K generate a fast- and fine-resolution excitability motif (see appendix A.1.1 for the neuron model). (Right) Properties. The auto-correlation (Acorr) and the cross-correlation (Xcorr) graphs show the transfer properties and reveal a two-state automaton: a resting exogenous state responsive to inputs (orange) and an excited endogenous state with rhythmic intrinsic activity (blue). Membrane potential and input traces show the localization properties in amplitude and in time.

that control the ionic flow through the membrane (section 2.2.1). The Hodgkin-Huxley model and reduced versions focus on the two currents responsible for the generation of action potentials, the fast sodium current I_{Na} and the slow delayed-rectifier potassium current I_K, and give the motif representation in Figure 5.2, Left (section 2.4.1).

For the monoresolution excitability motif, the input I consists in a spike train, the state X and the output O are similar and correspond to the neuron membrane potential (see appendix A.4.3). The auto-correlation and cross-correlations graphs show that this system possesses two distinct states (Figure 5.2, Right): a resting exogenous state (in orange) and an excited endogenous state (in blue). The resting exogenous state possesses a sharp peak in the cross-correlation and no autonomous activity in the auto-correlation. In contrast, the excited endogenous state possesses no peak in the cross-correlation and rhythmic autonomous activity in the auto-correlation.

In the input-output behavior perspective, the monoresolution excitability motif can be abstracted as a two-state automaton, the state of which is controlled by the system input: a static depolarizing input switches the system from the exogenous state to the endogenous state and vice versa (Figure 5.2, Right, Potential and Input traces).

In addition, the excitability motif is endowed with localization properties, both in amplitude and in time (Figure 5.2, Right, Potential and Input traces).

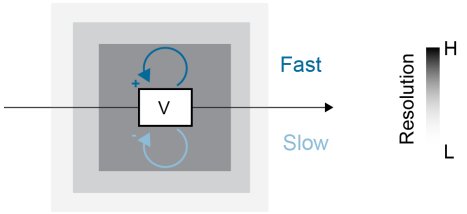

Figure 5.3 – The +FB then –FB excitability motif. The excitability motif is composed of a fast positive feedback loop (+FB)—or auto-catalysis—and a slower negative feedback loop (–FB). The motif can be repeated in different excitability windows, or at different resolution levels (defined by a spatiotemporal scale), as indicated by the shade of grey. The different excitability windows interact, generating multiresolution excitability.

Localization in amplitude means that a subthreshold input does not trigger a fast spike in the neuron (input 1 is subthreshold and results in no fast spike) while superthreshold inputs trigger a fast spike in an all-or-none manner (inputs 3 and 4 are superthreshold and the fast spike amplitude is the same in both cases). For a depolarizing step of current, the amplitude of the stimulation must remain below a certain level to avoid depolarization blocks during which action potentials are absent. Localization in time imposes a minimum time duration for the input to trigger a fast spike (input 2 is of short time duration and results in no fast spike) and explains why a longer input produces fast spikes of similar time length (input 5 is a long depolarizing step; however, the resulting fast spikes possess a similar timescale as fast spikes triggered by impulses, for instance with inputs 3 and 4).

These localization properties are a consequence of the interaction of the feedback loops, which set the behavior of the system in an *excitability window*. The timescales of the feedback loops set the excitability window in a specific time dimension, which produces localization in time. In addition, the spatial scale—neuron or network level—at which the feedback loops act sets the excitability window in a specific spatial dimension, which produces localization in space. The spatiotemporal scale establishes the *resolution level* of the excitability window (Figure 5.3).

We argue that, thanks to these localization properties, excitability, although a non-linear phenomenon, approximately obeys a superposition principle. We study the superposition of different resolution levels and how the different excitability windows interact to form multiresolution excitability. We focus on two multiresolution systems in neuroscience: burst excitability—or cellular slow spike—in a bursting neuron and circuit excitability—or spike in the local field potential (LFP)—in a two-neuron circuit.

5.3 Bursting as coexisting fast and slow excitability

The burst-firing pattern has been described in section 2.5 and the peculiar role played by the low-threshold T-type calcium channel $I_{Ca,T}$ has been emphasized in previous chapters. Section 4.1 details the action of two ionic currents, the slow regenerative $I_{Ca,T}$ and the ultraslow restorative I_{KCa}, for the *hyperpolarized-induced bursting* property, i.e., the ability to switch between a single-spike discharge mode and a burst-firing mode when the membrane is hyperpolarized: $I_{Ca,T}$ provides a slow positive feedback on membrane potential variations and I_{KCa} an ultraslow negative feedback.

In the motif formalism, bursting corresponds to the superposition of the excitability motif in two temporal resolution windows (Section 2.5.3). In the fast excitability window, the excitability motif is identical to the one described in the previous section (dark grey window in Figure 5.4, Left). Similarly to what is done in the previous section, the input I consists in a spike train, the state X and the output O correspond to the neuron membrane potential. In the slow excitability window, the excitability motif results from the interaction of the slow $I_{Ca,T}$ and ultraslow I_{KCa} feedback loops (light grey window in Figure 5.4, Left). In this slow excitability window, the system output is averaged over time to reflect the lower resolution and a burst is referred to as a *cellular slow spike*. For the system in the slow excitability window, the input I consists in a train of hyperpolarizing steps, the state X and the output O are similar and correspond to the time-average of the neuron membrane potential (see appendix A.4.3).

The multiresolution excitability of the bursting neuron possesses four distinct states and can be abstracted as a four-state automaton: to the fast exogenous state (which is now defined as slow tonic firing) and fast endogenous state (fast tonic firing) of the fast excitability motif, are added the slow resting exogenous state (in orange) and slow excited endogenous state (in blue) of Figure 5.4. The auto-correlation graphs of Figure 5.4 (Left) show no intrinsic activity in the exogenous state and a rhythmic intrinsic activity in the endogenous state. In the slow excitability window, the state of the automaton is controlled by the system input: a static hyperpolarizing input switches the system from the exogenous state to the endogenous state and vice versa (Figure 5.4, Right, Average and Input traces).

Transfer properties in both excitability windows are function of the slow excitability state (Figure 5.4, Right): in the fast excitability window, fast depolarizing inputs are transmitted in the slow exogenous state but filtered in the slow endogenous state (cross-correlation graphs in the fast excitability window); in the slow excitability window, slow hyperpolarizing inputs are transmitted in the slow exogenous state but filtered in the slow endogenous state (cross-correlation graphs in the slow excitability window).

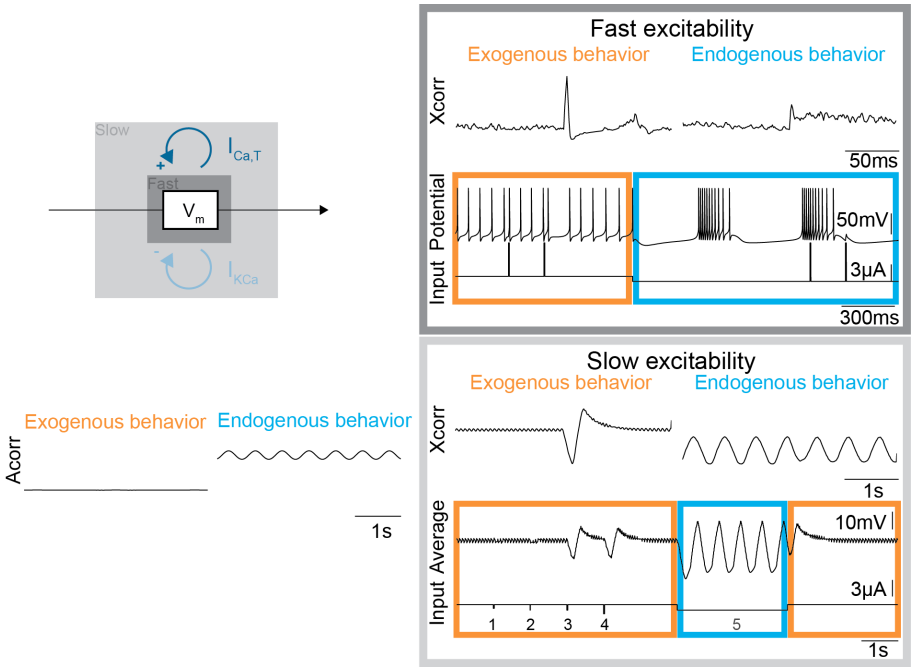

Figure 5.4 – Coexisting fast and slow excitability motifs in the bursting neuron. (Left) Motif and resolution: the slow T-type calcium current $I_{Ca,T}$ and the ultraslow calcium-activated potassium current I_{KCa} generate a slow excitability motif on top of the fast excitability motif of the I_{Na} and I_K currents (see appendix A.1.1 for the neuron model). Endogenous and exogenous behaviors in the slow excitability window: the auto-correlation (Acorr) graphs reveal a resting exogenous state (orange) and an excited endogenous state with rhythmic intrinsic activity (blue). (Right) Membrane potential or time-averaged voltage (Average), input, and cross-correlation graphs (Xcorr) for fast excitability and slow excitability in the slow exogenous and slow endogenous states.

The coexistence of fast and slow excitability ensures excitability properties in each resolution level. On top of the localization properties in the fast excitability window, both amplitude and time localization properties develop in the slow excitability window (Figure 5.4, Right, Average, and Input traces). Localization in amplitude means that a subthreshold input does not trigger a slow spike in the neuron (input 1 is subthreshold and results in no slow spike) while superthreshold inputs trigger a slow spike in an all-or-none manner (inputs 3 and 4 are superthreshold and the slow spike amplitude is the same in both cases). For an hyperpolarizing step of current, the amplitude of the stimulation must remain below a certain level to avoid suppressing all activity in the neuron. Localization in time imposes a minimum time duration for the input to trigger a slow spike (input 2 is of short time duration and results in no slow spike) and explains why a longer input produces slow spikes of similar time length (input 5 is a long hyperpolarizing step; however, the resulting slow spikes possess a similar timescale as slow spikes triggered by impulses, for instance with inputs 3 and 4).

5.4 Circuit spike as coexisting fine and coarse excitability

Transient network oscillations and the peculiar role played by the low-threshold T-type calcium channel $I_{Ca,T}$ have been described for an E-I circuit in section 4.6. This E-I circuit, represented in Figure 5.5 (Left), is excitable and is highly similar to the one presented in the work of Wilson-Cowan detailed in section 2.4.2. The major difference lies in the fact that we keep the description of the circuit at the cellular level rather than averaging in a population model (mean-field E-I network). In this circuit, the source of the positive feedback on neuron E is cellular in the form of the slow regenerative $I_{Ca,T}$ current (instead of the recurrent connections in the E population of the Wilson-Cowan model). The source of negative feedback is the ultraslow synaptic connection via neuron I (I_{syn}).

In the motif formalism, transient network oscillations can be described with the superposition of the excitability motif in two spatiotemporal resolution windows: in the fine (fast cellular scale) excitability window, the excitability motif is identical to the one described in the previous section (dark grey window in Figure 5.5, Left) and the input, output and system state are similar as well. In the coarse (slow circuit scale) excitability window, the excitability motif results from the interaction of the slow $I_{Ca,T}$ and the ultraslow I_{syn} feedback loops (light grey window in Figure 5.5, Left). In this coarse excitability window, the system input I consists in a train of hyperpolarizing steps on neuron I, the state X and the output O are the LFP (see appendix A.4.3), and an excursion

of the LFP following a superthreshold input is referred to as a *circuit spike*. The analysis is similar to the previous section except that we add the spatial dimension in the circuit analysis.

The multiresolution excitability of the excitable circuit possesses four distinct states and can be abstracted as a four-state automaton: to the fine exogenous state and fine endogenous state of the fine excitability motif, are added the coarse resting exogenous state (in orange) and coarse excited endogenous state (in blue) of Figure 5.5. The auto-correlation graphs of Figure 5.5 (Left) show no intrinsic activity in the exogenous state and a rhythmic intrinsic activity in the endogenous state. In the coarse excitability window, the state of the automaton is controlled by the system input: a static hyperpolarizing input on neuron I switches the system from the exogenous state to the endogenous state and vice versa (Figure 5.5, Right, LFP and Inputs traces).

Transfer properties in both excitability windows are function of the coarse excitability state (Figure 5.5, Right): in the fine excitability window, fast depolarizing inputs on neuron E are transmitted in the coarse exogenous state but filtered in the coarse endogenous state (cross-correlation graphs in the fine excitability window); in the coarse excitability window, slow hyperpolarizing inputs on neuron I are transmitted in the coarse exogenous state but filtered in the coarse endogenous state (cross-correlation graphs in the coarse excitability window).

The coexistence of fine and coarse excitability ensures excitability properties in each resolution level. On top of the localization properties in the fine excitability window, both amplitude and time localization properties develop in the coarse excitability window (Figure 5.5, Right, LFP, and Inputs traces). Localization in amplitude means that a subthreshold input does not trigger a circuit spike (input 1 is subthreshold and results in no circuit spike) while superthreshold inputs trigger a circuit spike in an all-or-none manner (inputs 3 and 4 are superthreshold and the circuit spike amplitude is the same in both cases). For an hyperpolarizing step of current, the amplitude of the stimulation must remain below a certain level to avoid suppressing all activity in the circuit. Localization in time imposes a minimum time duration for the input to trigger a circuit spike (input 2 is of short time duration and results in no circuit spike) and explains why a longer input produces circuit spikes of similar time length (input 5 is a long hyperpolarizing step; however, the resulting circuit spikes possess a similar timescale as circuit spikes triggered by impulses, for instance with inputs 3 and 4).

5.5 Multiplex signaling

The multiresolution excitability introduced in sections 5.3 and 5.4 allows for *multiplex signaling* (Figure 5.6): a single physical object—a bursting neuron

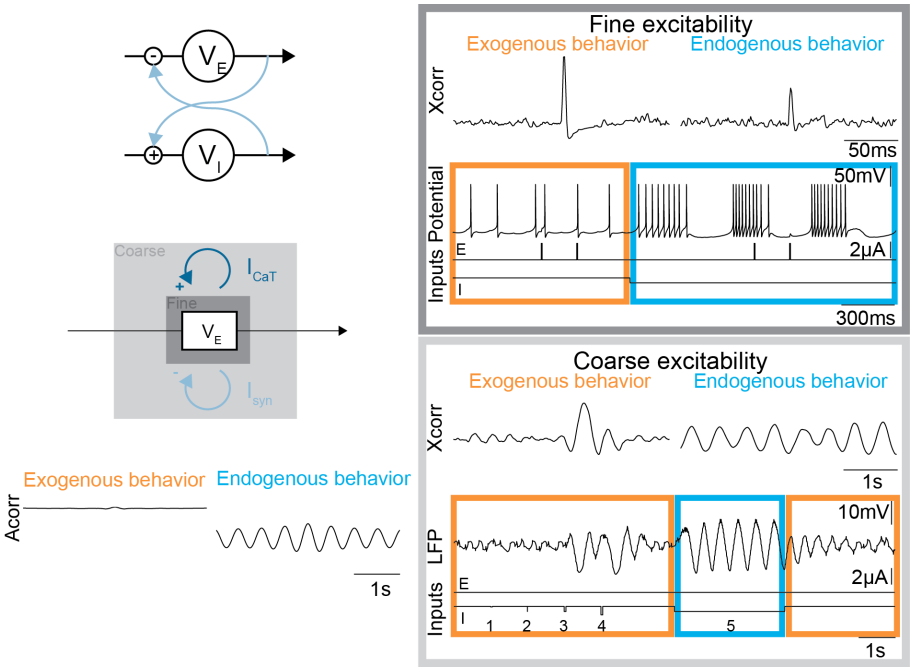

Figure 5.5 – Coexisting fine and coarse excitability motifs in the excitable E-I circuit. (Left) Architecture for the E-I circuit (see appendix A.1.2 for the network model). Motif and resolution: the slow T-type calcium current $I_{Ca,T}$ and the ultraslow synaptic current I_{syn} generate a coarse excitability motif on top of the fine excitability motif of the I_{Na} and I_K currents. Endogenous and exogenous behaviors in the coarse resolution: the auto-correlation (Acorr) graphs reveal a resting exogenous state (orange) and an excited endogenous state with rhythmic intrinsic activity (blue). (Right) Membrane potential or LFP, inputs, and cross-correlation graphs (Xcorr) for fine excitability and coarse excitability in the coarse exogenous and coarse endogenous states.

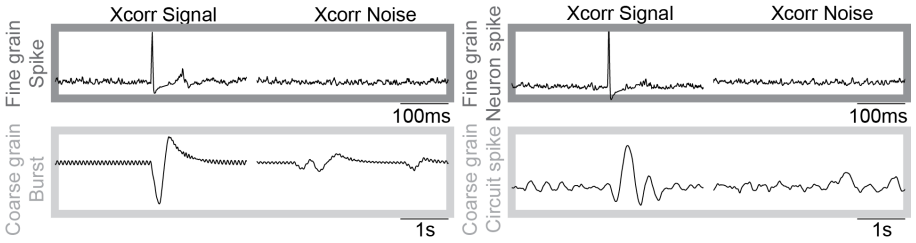

Figure 5.6 – Multiresolution objects are endowed with multiplex signaling capabilities. A single physical object allows for a two-resolution level communication. (Left) Bursting neuron multiplexing. (Right) Two-neuron circuit multiplexing. Top row: fine grain communication via spikes with fast depolarizing inputs. Cross-correlation graphs of the system output (the membrane potential) with the system input (a train of fast depolarizing inputs (Xcorr Signal)) and with a random input (Xcorr Noise). Bottom row: coarse grain communication via bursts (resp. circuit spikes) with slow hyperpolarizing inputs. Cross-correlation graphs of the system output (neuron time-averaged membrane potential and LFP, respectively) with the system input (a train of slow hyperpolarizing inputs (Xcorr Signal)) and with a random input (Xcorr Noise).

or a two-neuron circuit, respectively—bears a two-resolution level communication. With the monoresolution motif of section 5.2, signaling is only possible in the fast timescale of action potential and at the cellular spatial scale. Multiresolution motifs introduce multiplex signaling, i.e., the input controls the spatiotemporal scale in which the communication takes place.

In the bursting neuron model, the input controls the excitability window selected for the signaling (Figure 5.6, Left): a fast depolarizing input sets the cursor on the fast excitability window and allows for fine grain communication via cellular fast spikes. By contrast, a slow hyperpolarizing input sets the cursor on the slow excitability window and the communication is coarse grain via bursts, or cellular slow spikes. Figure 5.6 (Left) shows the cross-correlation graphs in each excitability window with an input signal (Xcorr Signal) and with a random input (Xcorr Noise). The peaks in the cross-correlation graphs with an input signal indicates that both types of input are processed in their corresponding excitability window.

Similarly, the two-neuron circuit is also a two-resolution object but in the spatial and temporal dimensions (Figure 5.6, Right): a fast depolarizing input on neuron E sets the cursor on the fine excitability window and allows for fine grain communication via neuron spikes, or cellular fast spikes. A slow hyperpolarizing input on neuron I sets the cursor on the coarse excitability window and the communication is coarse grain via circuit spikes. The peaks in the cross-correlation graphs of Figure 5.6 (Right) also highlight that each input signal type is processed in its corresponding excitability window.

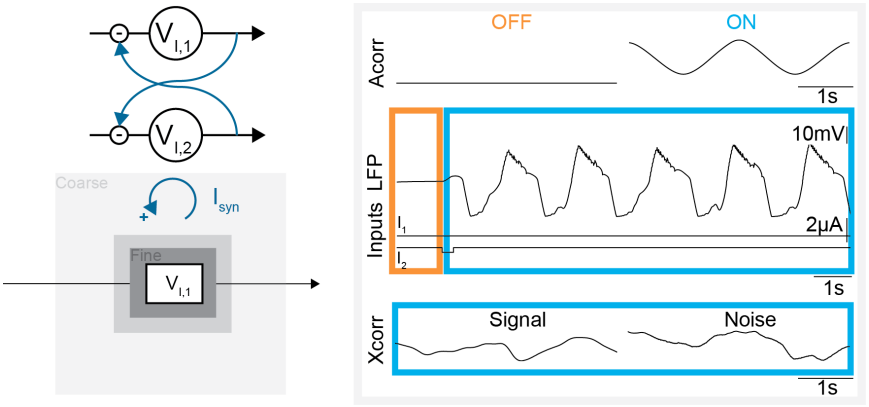

Figure 5.7 – Positive feedback from synaptic connections prevents hierarchy in feedback loops. (Left) Architecture for the I-I circuit. Motif and resolution: the ultraslow synaptic current I_{syn} generates a positive feedback on top of the motifs in the lower resolution windows. (Right) Properties: LFP and input traces show the lack of localization properties. The auto-correlation (Acorr) and the cross-correlation (Xcorr) graphs reveal a bistable behavior: a resting OFF state with no intrinsic activity (orange) and an excited ON state with rhythmic intrinsic activity (blue). Once the circuit is switched to the ON state, it remains excited and the system output is similar with a train of slow hyperpolarizing inputs (Signal) and a random input (Noise).

5.6 Discussion

5.6.1 Localization and hierarchical sources of feedback

In networks, positive feedback can also be provided at the network level, via synaptic connections. One instance of such positive feedback is provided by the I-I two-neuron circuit studied in chapter 3 and given in Figure 5.7 (Left). The synaptic connections via two inhibitions provide a positive feedback on neuron 1 (Figure 5.7, Left).

With this architecture, the motif representation lacks hierarchy between the positive and negative feedback loops: the positive feedback is ultraslow and spatially spread (Figure 5.7, Left). In order to get the excitability motif, a negative feedback in a slower and coarser dimension is required. This highlights the importance of the spatiotemporal dimension, in addition to the sign, of the feedback loops.

This lack of hierarchy destroys localization properties (Figure 5.7, Right). There is no localization in time because a transient hyperpolarizing input on neuron 2 triggers a switch and induces continuous oscillations in the circuit as shown in the oscillatory activity of the LFP. Transient inputs do not result in transient outputs but rather in a permanent switch between an OFF (no

intrinsic activity - orange) or ON (rhythmic intrinsic activity - blue) mode (Figure 5.7, Right, Acorr). Once the ON mode is triggered, any type of transfer capability disappears and a train of slow hyperpolarizing inputs or a random input give rise to the same circuit behavior (Figure 5.7, Right, Xcorr).

Regarding the spatial localization, the coarse circuit excitability in the E-I network is studied in Figure 4.9 (Right) of chapter 4: the spatial dimension of the input directly impacts the spatial dimension of the output. A similar analysis is performed here with exponential decay in the synaptic maximal conductances, emulating a decrease in the reciprocal connection strength between two neurons with an increase in spatial distance along a one-dimensional axis (Figure 5.8, Left). In addition, the cellular positive feedback source is removed in neuron 9, 10 and 13. As expected, an input on neuron 1 and 5 results in no activity in the LFP for the E population whereas an input on neuron 3 and 6 results in LFP oscillatory activity. For the positive feedback from network connections in the I-I network with exponential decay in the synaptic maximal conductances (Figure 5.8, Right), there is no localization property in space: in the network, an input on one neuron results in the switch of the entire population.

This observation highlights a major difference between the source of positive feedback provided by a cellular mechanism—in this case the $I_{Ca,T}$ current—and by a network mechanism, the I_{syn} current. Both sources provide a feedback loop of positive sign but solely the cellular mechanism respects the hierarchy, in time and space, in the feedback loops to get the excitability motif and the corresponding localization properties.

5.6.2 Physiological implications

The role of T-type calcium currents in brain oscillations has been extensively studied in the literature [32, 216, 232, 233, 243]. However, their peculiar role for spatial and temporal localization properties had never been highlighted before. In this section, we give several physiological examples where multiresolution excitability and multiplex signaling are at play.

The prime example of physiological system where T-type calcium currents generate multiresolution properties lies the thalamus. The thalamus acts as a relay between different subcortical areas and the cerebral cortex, by gating and modulating the information flow [218]. Different thalamic circuits process information from different sensory modalities, e.g., vision, audition and touch. An archetype of thalamic circuits is provided by the lateral geniculate nucleus, which relays the visual information from the retina and connects to the thalamic reticular nucleus [176]. The neurons in these two nuclei, the thalamocortical (TC) and thalamic reticular (RE) neurons, respectively, exhibit a dense distribution of T-type calcium channels and possess two distinct response modes, single-spike discharge and burst-firing [176, 217]. The TC and RE neurons form

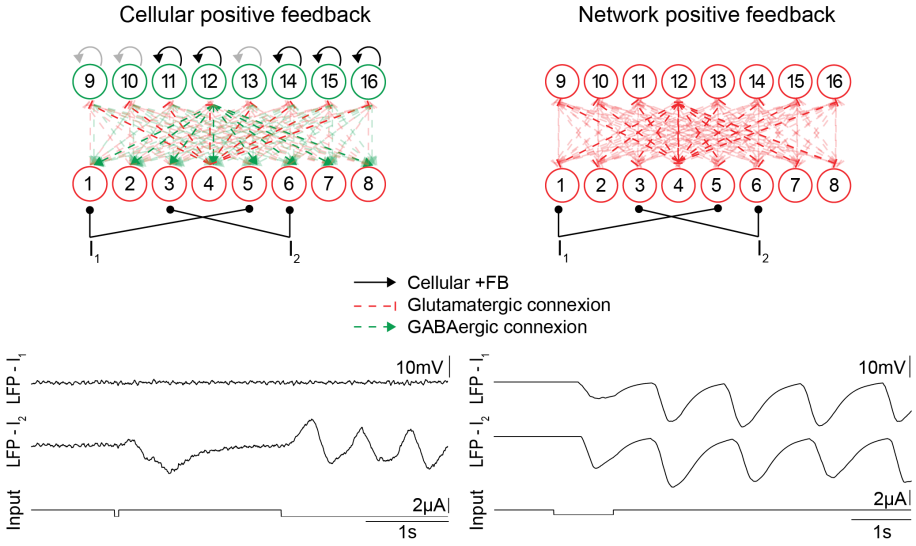

Figure 5.8 – The lack of hierarchy prevents spatial localization property. Architecture for the network, LFPs and input traces. The grey color represents the absence of cellular positive feedback. The light green and light red colors represent existing connections and are used to lighten the scheme. (Left) The cellular positive feedback of the E-I network brings spatial localization property. (Right) The network positive feedback of the I-I network prevents spatial localization property and the switch is global.

an E-I circuit from which various oscillatory rhythms emerge, mediated by both intrinsic and extrinsic (or network) mechanisms [176, 220, 232, 243].

The *wake-up call* mechanism instantiates a rhythm emerging from cellular properties [216]. Experimental evidences suggest that the geniculate relay cells can fire arrhythmically in burst mode during waking behavior, maximizing initial stimulus detection [208,216,217,221]. The wake-up call triggers arrhythmic bursts, localized in both time and space, similarly to the burst excitability, or cellular slow spike model. The two-resolution system that emerges allows to multiplex between the two firing modes depending on the contextual environment: single-spike discharge for high linearity or burst-firing for signal detection [62, 158, 217]. The spatial localization property constrains the bursts on restricted territories and allows for discrete and segregated patterns to develop in the network [231].

Sleep spindles (waxing-and-waning field potentials at 7–14 hertz) correspond to an illustration of cellular and network mechanisms working in combination [54, 176]. Spindles arise during periods of drowsiness and synchronized sleep, and take the form of rhythmic, synchronized bursting waves [175, 217]. Under sleep spindles, the responsiveness to stimulation of peripheral receptive fields is greatly reduced [175, 217, 231]. The rhythm develops from the interaction of the inhibitory RE neurons, amongst themselves and with the TC neurons [10, 57, 176, 178]. This circuit has a positive feedback at the network level with no localization properties and therefore gives rise to an ON or OFF behavior: a global oscillatory mode unresponsive to external perturbations and a transfer mode in which the ability to respond to barrages of phasic excitatory inputs is greatly enhanced [177,217]. Highly synchronized sleep oscillations may develop into absence epilepsy, a behavioral state that can be viewed as a brain disconnection from the external world [31, 222, 232].

Another example of thalamic multiplexing has been highlighted in recent papers: Sherman et *al.* propose to differentiate the action of *drivers* from the one of *modulators* [219]. The drivers carry the message from the receptive fields, defining the activity pattern, and are localized in both time and space; the modulators can alter transmission properties and are spatially and temporally more spread [217, 219, 220].

One illustration of spatial localization property in another network can be found in the layer V of the cortex involved in vision. Models of this layer V of the cortex include an E-I circuit and T-type calcium currents [138] and could therefore represent an instance of the circuit spike described earlier. In this brain region, oscillatory activity in the alpha band (8–12 hertz) gates information by inhibiting task-irrelevant regions, thus routing information to task-relevant regions [135,137]: alpha oscillations provide a functional inhibition and reduce the processing capabilities. Attention modulates the alpha activity for a functionally relevant sensory gating mechanism: attention increases alpha-band

activity in the hemisphere ipsilateral to, and decreases alpha-band activity in the hemisphere contralateral to the attended site in visual tasks [137, 266].

Another potential candidate for localization properties and superposition of excitability motifs is the resurgent sodium current present in the Purkinje neurons of the cerebellum [45, 206]: this current is also a slow regenerative current dynamically modulated. The cerebellum is involved in the regulation of complex movements and in cognitive tasks, e.g., language, memory, and attention [201]. The Purkinje cells form the sole output of the cerebellar cortex which innervates the deep cerebellar nuclei, the main output of the cerebellum [51, 201]. Purkinje cells provide an essential timing signal to the cerebellar nuclei and are primordial for the orchestration of motor behaviors. Purkinje cells can fire both simple spikes and complex spikes [51]. Complex spikes consist in small bursts of action potentials elicited upon stimulation of climbing fibers [51, 206]. The resurgent sodium current is believed to play an essential role in these complex spikes as it activates immediately following action potentials and elicits the firing of multiple spikes in an all-or-none manner [141, 206, 207]. Multiplexing is exploited in the spatiotemporal activity pattern of Purkinje cells, in the form of the selection between complex-spike activity and simple-spike activity in each spatially segregated populations of Purkinje cell [51]. In addition, Purkinje neurons are known to be intrinsically bistable and complex spikes are thought to switch Purkinje neurons between their two states: the hyperpolarized quiescent state and the depolarized high-frequency spiking state [156, 157, 159, 260, 268]. From these observations, the pictures that emerges is more complex than a simple slow cellular spiking abstraction and requires further investigations.

Multiplex signaling has also been proposed for the electro-sensory system of the weakly electric fish [144]. The transition from a single-spike to a burst-firing code is correlated with feature extraction, i.e., the presence of a communication or prey signal [144]. Spatiotemporally varying stimuli features are encoded in the spatiotemporal property of neural activity [91]. In addition, bursts can improve the reliability of information transmission across unreliable synapses and provide an effective mechanism for *selective communication* among neurons by increasing the reliability of synaptic transmission to specific intraburst frequencies [130, 144, 154]. In this view, the single-spike and burst-firing modes form a continuum of sensory responses [144].

5.7 Summary

In this chapter, we characterized the excitability motif with its input-output behavior. We used classic correlations measures to reveal the two distinct states in excitable systems, the exogenous and the endogenous states. We showed that excitability, although a non-linear phenomenon, obeys a superposition princi-

ple: thanks to localization properties, different excitability resolution windows can be superposed and interact, generating multiresolution objects. We investigated transfer characteristics in multiresolution excitability motifs.

Excitability is described by its motif, the +FB then –FB motif, and the excitability window resolution is set by the spatial and temporal scales of the feedback loops that compose the motif. The three types of excitability studied in this dissertation are spike excitability, burst excitability, and circuit excitability.

In each resolution window, the excitable system is endowed with localization properties—in amplitude, time and space—and a duality between exogenous and endogenous states. With these multiresolution objects, spike excitability properties are still at play at slower or coarser resolution levels.

We also showed that multiresolution objects are endowed with multiplexing capabilities: the input controls the resolution in which the communication takes place.

Finally, we emphasized the necessary hierarchy in the feedback loops for localization and we differentiated two sources of positive feedback in networks: (i) a fast and fine cellular positive feedback which gives rise to localization properties and therefore allows for spatial modulation, and (ii) a slow and coarse network positive feedback which produces a general and permanent switch. In physiology, both sources are probably present and are at play for different types of activity pattern.

We anticipate that this superposition principle extends to other resolution levels and is not limited to neuroscience: at higher resolution levels, ion channel opening and closing could instantiate such +FB then –FB motifs; at lower resolution levels, circuits, or combination of circuits, could provide an example of the +FB then –FB motif. Such systems are legion in systems biology (e.g., the toggle switch [247]).

Chapter 6

Conclusion

This dissertation emphasizes the importance of investigating the interplay between different resolution levels by extracting elements at high resolution levels for their role and impact at lower resolution levels. The simplification of systems to the description of solely their coarser elements results in the suppression of finer resolution levels and the destruction of intrinsic multiresolution characteristics. At the other side of the spectrum, highly detailed models at very high resolution levels are not computationally tractable and analyzable for large systems. The interplay between resolution levels was studied in neuroscience in the hope of a better understanding of brain functions and diseases.

Starting from two examples, this dissertation stresses the significance of the interplay between resolution levels: it suggests to identify fundamental mechanisms, in the form of feedback loops, from high resolution levels for the activity at lower resolutions. In this dissertation, this approach is used to tackle system-level questions and to study the role of feedback in maintaining robustness and modulation across scales, from the neuron to the network resolution levels. The approach is applied to two neurophysiological examples, the mutual-inhibition network of the HCOs and the E-I network of the basal ganglia, and extended to the general concept of multiresolution excitability motif.

The conclusion is organized as follows. The first section summarizes the main contributions of this dissertation and their implications. The second section enlarges the view with further perspectives.

6.1 Summary

Interplay between resolutions

The brain is a complex system made of many components, each shaping the brain activity and functioning at distinct resolution levels. Mathematical mod-

els capture the activity of these components in their respective resolution. The interplay between the different resolution levels, and more precisely the impact of lower resolutions on the activity at higher resolutions levels is still unclear. To narrow this gap, we propose to investigate the interactions between resolution levels by extracting the important elements, in the form of feedback loops, from one resolution to the next.

Motifs have been largely exploited in systems biology to identify shared design principles and simplify systems. The novelty lies in the exploitation of the motif approach to study the modeling of the brain across scales, i.e., to capture, in models, the mechanisms at different resolution levels in order to tackle system-level questions, mainly robustness and modulation. The approach is particularized to study of the role of feedbacks in maintaining robustness and modulation across scales, from the neuron to the network resolution levels.

A cellular positive feedback loop for network robustness and modulation

The cellular post-inhibitory rebound (PIR) property is well-known to play a key role in underlying neural network oscillations. PIR is an intrinsic cellular property that elicits transient membrane depolarization when released from hyperpolarization. Two ionic currents have been identified for the generation of PIR: the hyperpolarization-activated cation current and the low-threshold T-type calcium current. Our novel contribution is to predict that PIR per se is not a sufficient cellular excitability property to ensure modulation and robustness of network oscillations. In addition, the current dynamics, i.e., its slow positive feedback (regenerative) nature, is an important parameter.

Because both currents are sources of PIR currents but only the calcium current acts, through its slow activation, as a source of positive feedback in the slow timescale, our results propose a novel and somewhat fundamental complementarity between calcium and cation channels in PIR mechanisms.

This observation also suggests that the network modulation and robustness properties can be investigated by looking at single-cell experiments: slow regenerativity can be detected in the neuron response to a transient excitatory pulse, when the neuron is under the influence of a hyperpolarizing current. The triggering of a burst indicates a bistable behavior due to a slow regenerative source and predicts modulation and robustness properties at the network level.

A cellular positive feedback loop for localization properties of network oscillations

Cellular positive feedback can also underlie hyperpolarized-induced bursting (HIB), a cellular excitability switch property, from single-spike discharge to burst-firing mode. In contrast to PIR, HIB is a permanent source of endoge-

nous behavior. HIB endows E-I networks with cellular-based network switch capabilities and procures robustness, modulation, and localization properties to network oscillations. The proposed mechanism is simple, generic, and robust and suggests the orchestration of network oscillations via a cellular switch mediated by neurotransmitters.

Because it is controlled at the cellular level, the network switch possesses both temporal and spatial localization properties. As such, it is a wonderful candidate to explain transient physiological oscillations associated, for instance, to movement control or attention shift. To our knowledge, this is the first attempt to model the modulation of beta oscillations in the basal ganglia both in healthy conditions (in relation to movement initiation) and in Parkinson's disease.

Localized transfer properties of multiresolution excitable systems

The basic building blocks of excitability, the fast positive and slow negative feedback loops, endow the system with localization properties. As such, we claim that excitability obeys a superposition principle and that excitability windows at distinct resolutions can interact to generate multiresolution excitable systems.

We propose to study the excitability motif, in each resolution level, with its input-output characteristics and investigate its transfer properties in the two opposite states, resting exogenous and excited endogenous, as well as the transition between those states. We use classic correlation measures to quantify the behavior of excitable systems.

We introduce the concept of circuit excitability, by analogy to spike and burst excitability, which denotes a circuit spike in the form of the excursion of the LFP following a superthreshold input before it resumes to its stable resting state.

We also highlight the importance of hierarchical feedback loops for localization properties and differentiate between a cellular positive feedback with localization properties and a network positive feedback leading to global permanent switches. Physiological systems probably emphasize one or the other mechanism depending on the situation as illustrated in the thalamus.

The emergence of gating properties and multiplexing

Signal processing aspects are also tackled in the dissertation. The transient network oscillations in the E-I network are suggested to provide a gating mechanism, similar to the one described in the thalamocortical network. This gating function mechanism provides a causal link between a transient increase in neuromodulator level and network state: an oscillatory OFF state where incoming spikes are filtered and a transfer ON state where incoming spikes are trans-

mitted. In addition, the localized aspect of the network switch enables for a spatial control of the gating function, i.e., the targeting of specific pathways while maintaining other pathways unaffected.

Multiresolution excitable systems can also benefit from multiplexing capabilities: the input controls the spatiotemporal scale in which the communication takes place. A single object, a bursting neuron or a two-neuron circuit in the present dissertation, is therefore capable of fine grain communication via neuron spike and coarse grain communication via neuron burst or circuit spike. Depending on the environmental context, one type of communication can be preferred over the other.

6.2 Prospects

6.2.1 A neuromorphic gating control mechanism for information transfer

In section 4.6, we proposed that the cellular-based network switch underlies a gating function mechanism. This functional mechanism opens (transfer ON state where spikes are transmitted) or closes (oscillatory OFF state where spikes are filtered) the gate to incoming spikes. The gating mechanism can be temporally and spatially controlled and provides a causal link between a transient increase in neuromodulator level and network state.

In this section, we suggest to exploit this physiological concept in engineered applications: in a biologically inspired manner, it could be used in artificial neural networks as a routing mechanism to control the information flow along many divergent routes, just as it is done in brain circuits. This routing capacity could be one of the novel features of spiking neural networks compared to threshold and sigmoidal nets and could bring new information processing capabilities to artificial neural networks.

The gating function corresponds to the switch, at the cellular level, between single-spike discharge and burst-firing (see section 4.1). Numerous previous works have highlighted the functional implication of the discharge mode on the relationship between incoming excitatory inputs and action potential generation (e.g., [177]): in the single-spike discharge mode, the pattern of action potentials generated is an almost faithful representation of the characteristics of incoming depolarizing inputs; by contrast, in the burst-firing mode, the pattern of action potentials is not a trustful reflection of the input spike train and the amplitude of the burst discharge carries little information about the depolarizing inputs (it is rather an endogenous function of internal variables, i.e., the membrane potential before the burst and the time interval since the last burst occurred).

In the reduced-model used in chapter 4, the cellular switch is controlled by

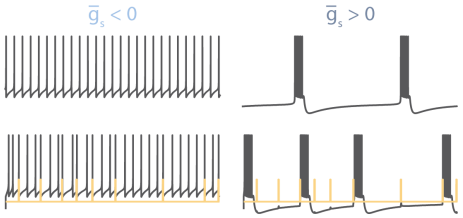

Figure 6.1 – The modulation parameter $\overline{g}_s$ controls the information processing mode. (Left) Single-spike discharge 'transferring' mode ($\overline{g}_s < 0$): membrane potential without and with incoming depolarizing inputs (in yellow) reveals that the pattern of action potential represents the incoming depolarizing inputs. (Right) Burst discharge 'blocking' mode ($\overline{g}_s > 0$): membrane potential without and with incoming depolarizing inputs (in yellow) reveals that the pattern of action potentials carries little information about the incoming depolarizing inputs.

the modulation parameter $\overline{g}_s$. Therefore, this parameter controls the switch between two distinct information processing modes (see Figure 6.1): a single-spike 'transferring' mode—action potentials are generated in relative independence of one another and the neuron has the ability to respond to excitatory inputs—and a burst 'blocking' oscillatory mode with a strong endogenous rhythm prone to synchronization—the neuron's responsiveness to stimulation of peripheral receptive fields is greatly reduced.

The cellular switch has the remarkable ability to quickly and easily spread from the unicellular level to the network level (see section 4.4). This is because the endogenous bursting rhythm is much more prone to synchronization than the exogenous single-spike rhythm. As a consequence, a heterogeneous population of neurons is likely to act as a parallel population of disconnected integrators when the neurons are in their single-spike mode. But the same population can generate a synchronous endogenous oscillation at the network level when the neurons switch to their bursting mode (see Figure 4.9). As a consequence, the 'transferring' and 'blocking' capabilities of two-mode spiking neurons are naturally enhanced at the network level and define a global exogenous state, or 'ON' state (the input spikes are transmitted through the spiking neural network and the global activity of the network reflects the depolarizing inputs), and a global endogenous neural state, or 'OFF' state (the input spikes are filtered and are not reflected in the global network activity).

The functional switch can be used in artificial (spiking) neural network applications. Spiking neural networks are called the third generation of neural network models [160] (see section 2.1.3). The first generation of neural networks used the McCulloch Pitts neurons, also called perceptrons or threshold gates, as computational units. Examples of such neural networks are the Hopfield nets and the Boltzmann machines [160]. Their particularity is to be universal for

digital computations, i.e., computations with digital inputs and outputs. The second generation of neural networks was based on neurons with an activation function, in general the sigmoid function. Typical neural networks of this generation are sigmoidal neural nets and multilayer perceptrons [160]. These neural networks are universal for analog computations, i.e., computations with analog inputs and outputs.

In recent years, the growing recognition that neural information is coded in spike timings and not only in firing rates [252], gave rise to the third generation of artificial neural networks [160]. Spiking neuron models are more biophysiologically realist and code the information in single spikes rather than in the rate of firing. Spiking neuron models have been widely used in computational neuroscience [93] as well as in artificial intelligence and neuromorphic applications [139]. However, the computational gain of spiking neurons compared to threshold and sigmoidal gates is still under investigation [139, 160]. We propose that the functional gating properties could be one of the novel features of spiking neural networks and suggest three applications.

Reservoir Computing

Reservoir Computing has many different implementations, liquid state machines (LSMs) [162] being one of them, of the same conceptual framework: a reservoir—a fully connected one-hidden-layer recurrent neural network—exhibits dynamics at the 'edge of chaos' and is read out by simple external linear functions [251]. Computational units can consist of a broad range of node types: perceptrons, sigmoidal gates, or spiking neurons [161]. The reservoir is not trained, only the weights to the output layer are [205]. Under some conditions on the reservoir and the class of possible readout functions, the LSMs have universal computational power with regard to computational operations on analog functions of time [161].

The main appeal of Reservoir Computing is its ease of training: the recurrent neural network is sparsely connected with most of its weights fixed a priori to randomly chosen values. Only the readout layer is trained. The training can be performed with any suitable statistical learning method, e.g., least-mean-square error solutions or margin-maximization criteria known from training support vector machines, in a single pass through the training set [162, 205]. But this simplicity of training comes with one big challenge: creating a highly enough dimensional dynamical state for the reservoir, particularly if the same network is used in parallel to perform multiple computations [205].

Inputs are integrated temporally and the complex network dynamics are explicitly used as means to integrate information [55]. However, no network information sensitivity state is exploited due to the use of the simple integrate-and-fire neuron model. Other behaviors of spiking neurons have been studied and have shown an increase in the computational power of the spiking neu-

ral networks [161] but no new capability has been introduced in LSMs and neuromorphic applications.

We propose that the cellular-based network switch controlled by modulators can introduce the network state as a computational tool. The network state, governed by intrinsic properties of neurons, could be determined for specific information transfer requirements. On top of the parallel multicomputational capacity of the LSMs, modulatory inputs would introduce temporal and spatial control over a single network to produce different functional outputs. Modulators could turn ON and OFF specific spiking neural subnetworks, enlarging the computational possibilities.

Computational routing

The new feature described above could be used for routing the information flow in computational applications. Distinct subnetworks could be activated or inactivated through specific modulatory action on the functionally distinct circuits, blocking-off the task-irrelevant pathways (similarly as described in section 5.6.2 for the alpha-band oscillations in the visual cortex). The switch mechanism provides spiking neural networks with a top-down control to enable certain processes and integration of only some subsets of the available information.

Feedback with learning

By integrating synaptic plasticity in the computational framework, spiking neural networks can learn to generate spatiotemporal spiking patterns [21]. The use of a biologically-inspired Spike-Timing Dependent Plasticity (STDP) rule—a presynaptic spike followed by a postsynaptic spike leads to an increase of the synaptic connection strength and vice versa—for the synaptic weights towards reservoir and outputs neurons leads to optimal learning [21].

Synchronization plays a key role in this STDP learning rule by promoting neural plasticity and can produce profound effects on learning and task implementation [37]. A control of subnetwork synchronization can strengthen the synaptic connections for a specific information flow and reinforce this route for future tasks. This allows for learning of more complex spatiotemporal patterns.

6.2.2 Hardware implementation

Living organisms are able to successfully perform challenging tasks such as perception, classification, association, and control. In hope for similar successes in artificial systems, neuromorphic engineering uses neurophysiological models of perception and information processing in biological systems to emulate their functions but also resemble their structure [179]. In this perspective, engineers

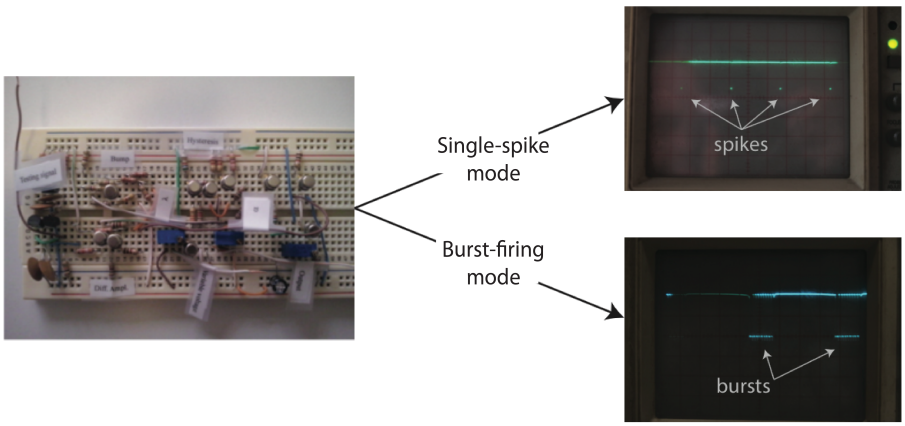

Figure 6.2 – Hardware implementation of the three-timescale bursting neuron model. (Left) Hardware. (Right) Oscilloscope recordings show the two modes of discharge: single-spike or burst-firing. Courtesy of Alessio Franci.

'morphe' the structure of neural connections into silicon circuits, creating neuromorphic microchips [19]. These hardware implementations of spiking neurons can also be effective to emulate in real-time large-scale neural networks [9,127]: silicon neurons are hybrid analog/digital very large scale integration (VLSI) circuits and the simulation speed is independent on the numbers of neurons in the network.

Hardware implementation of the cellular-based network switch described in this dissertation could lead to useful applications. For instance, the signal processing properties—gating and multiplexing—endowed in the network can be exploited in engineered applications. A first step in this direction has been carried out by Alessio Franci (Department of Mathematics, Universidad Nacional Autónoma de Mèxico, Mexico) and Fernando Castaños (Automatic Control Department, Cinvestav, Mexico). Similarly to the approach used in [9], they designed a hardware implementation of a spiking neuron based on dynamical systems theory. From the three-timescale bursting neuron model described in section 2.5.2, one can isolate the essential building blocks to realize the winged-cusp singularity and its universal unfolding that organize three timescale bursters [88]. The winged-cusp singularity and its universal unfolding can be realized by a feedback interconnection of an hysteresis and a bump nonlinearities (the interconnection laws are parametrized by the unfolding parameters) [90]. By adding simple first-order filters in the static feedback interconnections, the circuit can implement rest-spike bistability organized by the winged-cusp and, with the addition of an ultraslow negative feedback, bursting neurons [90]. With simple electronic components, Alessio Franci and Fernando

Castaños designed a hardware implementation of such a circuit (Figure 6.2). The next step should be the implementation of an E-I network with gating properties.

6.2.3 Multiresolution excitability in technology

In this dissertation, we highlight the importance, for system-level questions, of studying a system by the interplay of its different resolutions rather than each resolution individually. The *multiresolution approach* emerges in order to gain some insights on how elements at high resolution levels impact lower resolution levels. The simplification of systems to the description of solely their coarser elements results in the suppression of finer resolution levels and the destruction of intrinsic multiresolution characteristics. At the other side of the spectrum, highly detailed models at very high resolution levels are not computationally tractable and analyzable for large systems. The multiresolution approach aims at narrowing the gap between those two extremes and at extracting essential elements, in the form of feedback loops, to be maintained from one resolution to the next.

The multiresolution approach has been widely used in other fields, such as in signal processing [152, 163, 164]. In computer vision for instance, the multiresolution approach analyzes images at several resolutions simultaneously. The original image is decomposed into a sum of signals, each is a specific scale (both in space and in frequency). Different types of representation have been proposed, such as the scale-space theory and the wavelet theory. The multiresolution approach provides a simple hierarchical framework to represent images, at the interface of the spatial and the Fourier domains [163].

The multiresolution excitability described in chapter 5 is very specific to biological and chemical systems. By contrast, technology uses both positive (switches, e.g., transistors in microprocessors) and negative (regulators, e.g., thermostats in heating systems) feedback loops but not in a mixed configuration such as in the +FB then –FB motif (on this matter, the interested reader can watch the TEDxLiège talk of Prof. Sepulchre).

However, the interplay of the +FB and –FB loops gives rise to localization properties (in amplitude, time, and space) and the multiresolution characteristics of natural systems. Engineers could take advantage from what is observed in nature and design new technologies with mixed feedback loops. Potential applications could take the form of multiresolution sensors (much alike the electro-sensory system of the weakly electric fish described in section 5.6.2) or multiresolution memories (multiplexing for storage and recall as a function of the scales of the input signal). The power of the +FB then –FB motif could potentially endow technologies with new capabilities.

Appendix A

Numerical tools

All the numerical simulations and analyses were performed with MATLAB, MathWorks. The models were implemented in a MATLAB code and simulated using a forward Euler method with a time step of $0.005ms$.

A.1 Conductance-based model

A.1.1 Neuron model

The conductance-based model is inspired from the crab stomatogastric ganglion (STG) conductance-based neuron model [155, 244]. The model contains the standard Hodgkin-Huxley currents (see section 2.2.1): the transient sodium current, I_{Na}, a fast depolarizing current, and the delayed-rectifier potassium current, I_K, a slower hyperpolarizing current, plus a leak current, I_L. In addition, there are three ionic currents; the low-threshold T-type calcium current, $I_{Ca,T}$, the hyperpolarization-activated cation current, I_H, and the calcium-activated potassium currents, I_{KCa}. The membrane potential dynamics writes as follows:

$$C\dot{V}_m = -I_{Na} - I_K - I_L - I_{Ca,T} - I_H - I_{KCa} + I_{app},$$

where $C = 1\mu F/cm^2$ is the membrane capacitance and I_{app} is the applied current in $\mu A/cm^2$.

Each ionic current i, except for I_{KCa}, takes the standard Hodgkin-Huxley form:

$$I_i = \overline{g}_i m_i^{p_i} h_i^{q_i} \left(V_m - E_i\right),$$

where $\overline{g}_i$ is the maximal conductance for current i, p_i and q_i are integers, and E_i is the reversal potential of the ion i. Table A.1 lists the values of $\overline{g}_i$, p_i, q_i, and E_i for the different currents.

Table A.1 – **Parameters for the membrane currents of the neuron model.**

I_i	$\overline{g}_i$	p_i	q_i	E_i
I_{Na}	60	3	1	50
I_K	40	4	0	-80
I_L	0.035	0	0	-49
$I_{Ca,T}$	0.3	3	1	120
I_H	0.12	1	0	-20

Notation is explained in the text. All conductances are in mS/cm^2 and membrane potentials in mV.

Activation and inactivation variable dynamics follow the classical formalism:

$$\tau_{m,i}(V_m)\dot{m}_i = m_{\infty,i}(V_m) - m_i,$$
$$\tau_{h,i}(V_m)\dot{h}_i = h_{\infty,i}(V_m) - h_i,$$

where the functions for $\tau_{m,i}$, $m_{\infty,i}$, $\tau_{h,i}$, and $h_{\infty,i}$ are given in Table A.2. Note that, if $p_i = 0$ and/or $q_i = 0$, $\tau_{m,i}$ and $m_{\infty,i}$ and/or $\tau_{h,i}$ and $h_{\infty,i}$ are not listed, respectively.

Table A.2 – **Functions for the membrane currents of the neuron model.**

I_i	$m_{\infty,i}(V_m)$	$h_{\infty,i}(V_m)$	$\tau_{m,i}(V_m)$	$\tau_{h,i}(V_m)$
I_{Na}	$\frac{1}{1+e^{\left(\frac{V_m+35.5}{-5.29}\right)}}$	$\frac{1}{1+e^{\left(\frac{V_m+48.9}{5.18}\right)}}$	$1.32 - \frac{1.26}{1+e^{\left(\frac{V_m+120}{-25.0}\right)}}$	$\frac{0.67}{1+e^{\left(\frac{V_m+62.9}{-10.0}\right)}} * \left(1.5 + \frac{1}{1+e^{\left(\frac{V_m+34.9}{3.6}\right)}}\right)$
I_K	$\frac{1}{1+e^{\left(\frac{V_m+12.3}{-11.8}\right)}}$		$7.2 - \frac{6.4}{1+e^{\left(\frac{V_m+28.3}{-19.2}\right)}}$	
$I_{Ca,T}$	$\frac{1}{1+e^{\left(\frac{V_m+57.1}{-7.2}\right)}}$	$\frac{1}{1+e^{\left(\frac{V_m+82.1}{5.5}\right)}}$	$43.4 - \frac{42.6}{1+e^{\left(\frac{V_m+68.1}{-20.5}\right)}}$	$840 - \frac{718.4}{1+e^{\left(\frac{V_m+55}{-16.9}\right)}}$
I_H	$\frac{1}{1+e^{\left(\frac{V_m+80}{6}\right)}}$		$272 + \frac{1149}{1+e^{\left(\frac{V_m+42.2}{-8.73}\right)}}$	

Notation is explained in the text. All time constants are in ms.

The ionic current I_{KCa} takes a similar form to the one described in [78]:

$$I_{KCa} = \overline{g}_{KCa} \left(\frac{[Ca^{2+}]_{in}}{[Ca^{2+}]_{in} + Kd} \right)^2 (V_m - E_K),$$

where $\overline{g}_{KCa} = 3.4$, $\frac{d[Ca^{2+}]_{in}}{dt} = -k_1 I_{Ca,T} - k_2 [Ca^{2+}]_{in}$, $K_D = 170$, $k_1 = 0.1$, and $k_2 = 0.01$.

A.1.2 Network model

There are two types of network studied: the I-I network of chapter 3 and the E-I network of chapter 5. Excitatory synapses are α-Amino-3-hydroxy-5-methyl-4-isoxazolepropionic acid (AMPA) synapses and inhibitory synapses are gamma-aminobutyric acid (GABA) synapses. The network size varies with the simulation: two-neuron networks or sixteen-neuron networks, with two populations of eight neurons. The sixteen-neuron network is used in Figures 3.5-3.7 in order to study the impact of variability in the parameters and the effect of different noise sources and in Figure 5.8 to study spatial localization properties. For each network, the two neuronal populations (either one neuron or eight neurons) are reciprocally connected all-to-all.

The synapses are exponential synapses and the synaptic current between two neurons takes the form [101]:

$$\begin{aligned} I_{syn} &= \overline{g}_{syn} (V_m - E_{syn}) \frac{1}{N} \sum_{i=1}^{N} s_{Ai}, \\ \dot{s}_{Ai} &= k_{fA} x_\infty(V_i) (1 - s_{Ai}) - k_{rA} s_{Ai}, \\ x_\infty(V) &= [1 + exp(-(V - \Theta_s)/\sigma_s)]^{-1}, \end{aligned} \tag{A.5}$$

where V_i is the presynaptic membrane potential, N the number of presynaptic neurons (1 or 8), $k_{fA} = 2ms^{-1}$, and $k_{rA} = 0.1ms^{-1}$, $\Theta_s = -45mV$, $\sigma_s = 2mV$. For AMPA synapses, $\overline{g}_{AMPA} = 0.1mS/cm^2$ and $E_{AMPA} = 0mV$. For GABA synapses, $\overline{g}_{GABA} = 0.3mS/cm^2$ and $E_{GABA} = -80mV$.

To introduce the spatial dimension in Figure 5.8, the synaptic strength from neuron i to neuron j decays with distance in the form of a Gaussian function:

$$\overline{g}_{SD} = \overline{g}_{syn} e^{-\frac{(j-i)^2}{(2*c_{ij}^2)}}$$

where $\overline{g}_{syn}$ is the synaptic strength defined previously, c_{ij} is the space constant controlling the spread of connectivity (0.75 in this dissertation), and i, j are the positions of the neuron in the populations E and I. $\overline{g}_{SD}$ is normalized over the presynaptic population to get the same overall connection strength for each neuron in the postsynaptic population.

A.2 Reduced model

A.2.1 Neuron model

The reduced model is the three-timescale bursting model of section 2.5.2. It is a modified version of the model described previously [77, 87–89]:

$$\begin{aligned} \dot{v} = v^2 + bvx_s - x_s^2 \pm \overline{g}_s x_s - \overline{g}_{us} x_{us} + I_{app} + I_{static} \quad & \text{if } v \geq v_{th}, \text{then} \\ \tau_s \dot{x}_s = a_s v - x_s \quad & v \leftarrow c, x_s \leftarrow d_s, \\ \tau_{us} \dot{x}_{us} = a_{us} v - x_{us}, \quad & x_{us} \leftarrow x_{us} + d_{us}. \end{aligned}$$

where v merges the membrane potential and fast variables, x_s merges all slow recovery variables, and x_{us} all ultraslow adaptation variables.

I_{app} represents the applied current. I_{static} is the static current that determines the resting potential. This current depends on the value of the slow equivalent gain, $\bar{g}_s$, in the form: $I_{static} = 50 * |\bar{g}_s| + \bar{g}_s^2$. The neuron model is submitted to a geometrical modification such that the currents, I_{static} and I_{app}, are null at the transcritical bifurcation [87]. Otherwise stated, the parameters are fixed to physiological appropriate values: $b = -3$, $\overline{g}_{us} = -1$, $\tau_s = 1$, $\tau_{us} = 10$, $a_s = 0.1$, $a_{us} = 0$, $v_{th} = 80$, $c = 15$, $d_s = 15$, and $d_{us} = 40$.

The effect of T-type calcium channels on the neuron excitability is accounted for by a voltage dependence of the slow equivalent gain, $\overline{g}_s$, which reflects the ultraslow deinactivation of T-type calcium channels at low threshold ($g_s = \pm\overline{g}_s$):

$$\tau_{g_s} \dot{g}_s = a_{g_s} \left(v - v_{\frac{1}{2}} \right) - g_s + g_{s,min}$$

where $v_{\frac{1}{2}}$ is the inactivation threshold and $g_{s,min}$ the minimal value of g_s reached when all virtual T-type calcium channels are inactivated. g_s is also restricted to a maximal value $g_{s,max}$ through the saturation rule

$$\text{if } g_s \geq g_{s,max}, \text{then } g_s = g_{s,max}.$$

This results in a piecewise linear inactivation function centered at $v_{\frac{1}{2}} \geq 0$ and whose minimal and maximal values are $g_{s,min}$ and $g_{s,max}$, respectively. The values of the parameters are: $\tau_{g_s} = 22$, $a_{g_s} = 0.89$, $v_{1/2} = -2.5$, $g_{s,min} = -8$, and $g_{s,max} = 16$.

A.2.2 Network model

The E-I network of chapter 4 is composed of sixteen neurons in each of the two populations. The model parameters τ_s and τ_{us} slightly differ between the two populations to introduce heterogeneity between the two populations. For population E, $\tau_s = 0.66$ and $\tau_{us} = 10$; for population I, $\tau_s = 1.25$ and $\tau_{us} = 20$.

The applied current I_{app} is constant for the E population ($I_{app,E} = 50$) and takes value 0 for the depolarized state and -100 for the hyperpolarized state for the I population.

The two populations are reciprocally connected all-to-all with GABA inhibitory synapses and AMPA excitatory synapses. The synaptic current from neuron i to neuron j takes the form [131]:

$$I_{syn,ij} = -\, g_{k,i}\,(v_j - E_k)\,,$$

where v_j is the post-synaptic membrane potential, and the subscript k indicates the receptor type, GABA or AMPA. Each synaptic gain satisfies the equation $\dot{g}_{k,i} = -g_{k,i}/\tau_k$ and gets incremented by the synaptic strength $\overline{g}_k$ at each spike of the presynaptic neuron i. The synaptic current to neuron j is: $I_{syn,j} = \frac{1}{N}\sum_{i=1}^{N} I_{syn,ij}$, where N is the number of presynaptic neurons. The synaptic parameters are: $\tau_{AMPA} = 5$, $E_{AMPA} = 40$, $\overline{g}_{AMPA} = 0.5$, $\tau_{GABA} = 6$, $E_{GABA} = -30$, and $\overline{g}_{GABA} = 2$.

In Figure 4.9 (Left) the model equations for the external nucleus neurons (sixteen-neuron population) are [125]:

$$\begin{aligned} C\dot{v} &= k\,(v - v_r)\,(v - v_t) - u + I && \text{if } v \geq v_{th}, \text{then} \\ \dot{u} &= a\,[b\,(v - v_r) - u]\,, && v \leftarrow c, u \leftarrow u + d, \end{aligned}$$

with $C = 50$, $k = 1$, $v_r = -80$, $v_t = -25$, $v_{th} = 40$, $a = 0.01$, $b = -20$, $c = -55$, and $d = 150$. The effect of a neuromodulator is accounted for in a scaling coefficient, β_2, which determines the relationship between the neuromodulator occupancy and the effect magnitude on the applied current: $I = I_{app} * (1 - \beta_2\phi_2)$ with $\phi_2 = 1$, expressing the proportion of active modulator receptors, $\beta_2 = 0.2$ for the basal level of modulator, and $\beta_2 = 0.6$ during the transient increase in modulator. Heterogeneity is introduced in the external nucleus drive by varying the applied current on the external nucleus neurons: one-half of the external nucleus neurons received the average current ($I_{app} = 1400$), one-quarter an I_{app} 10% above the average, and one-quarter an I_{app} 10% below the average. The neurons in each group result from a random distribution of all the external nucleus neurons. The inhibitory connections from the external nucleus to the I population are of the GABA type with $\overline{g}_{GABA} = 10$.

The spike train on population E are spikes with time intervals selected from a Poisson distribution with an enforced minimum interval of 2. Each time interval is computed via $2 - log(rand(1))/.03$ where $rand(1)$ is a pseudo-random number selected from a uniform distribution on $[0, 1]$. The synapses are AMPA synapses with $\overline{g}_{AMPA} = 2$.

Similarly, to introduce the spatial dimension in Figure 4.9 (Right), the synaptic strength from neuron i to neuron j decays with distance in the form of a Gaussian function. A representation of the decaying connection strength is given in Figure A.1.

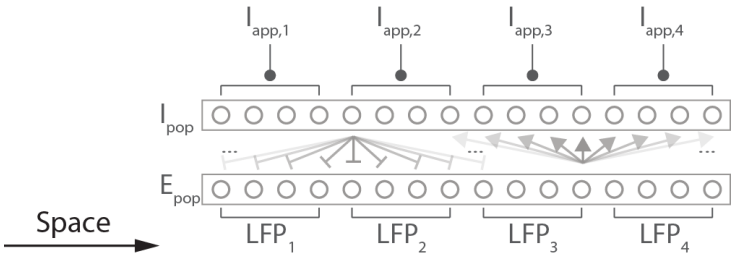

Figure A.1 – Spatial aspect of the network configuration. The synaptic strength from neuron i to neuron j, $\overline{g}_{SD}$, is a monotonically decaying distance function, as represented by the different shades of grey. The I population I_{pop} is controlled by four distinct applied currents $I_{app,1-4}$. Four different LFPs, LFP_{1-4}, are recorded from the four subpopulations in the E population E_{pop}.

A.3 Tools for simulation analysis

A.3.1 Variability

Physiological variability is modeled by randomly selecting (by generation of uniformly distributed pseudorandom numbers with the MATLAB function *rand*) the values for the parameter subjected to variability in an interval, called *variation range*, centered on a given parameter value. The *variability level* quantifies the width of this interval, in percentage of the given value. For instance, a 200% variability in $\overline{g}_{PIR}$ means that, for a given parameter value of $0.3mS/cm^2$, the variation range has a width of $200\% * 0.3 = 0.6$ and is centered on 0.3. The parameters are therefore randomly selected out of the interval $[0mS/cm^2, 0.6mS/cm^2]$.

A.3.2 Network rhythm

A network is categorized as having a stable rhythmic activity (rhythm ON) if all the neurons in the network are still bursting in the stationary state (after the transient initiation phase). Due to the specific network structure—connection all-to-all from one population to the other, and vice versa—all the neurons in one population receive the same input (coming from all the neurons in the other population). Therefore, if all the neurons are bursting, the bursts have been elicited by the same transient hyperpolarizing input—bursting cannot happen without this hyperpolarization—and the bursts are synchronous, i.e., all the bursts overlap but not necessarily the spikes. This provokes HCO anti-phase oscillations. Bursting in neurons is detected by having two consecutive spikes less than $100ms$ apart.

In chapter 3, the frequency is the inverse of the time duration between the

beginning of two bursts, or period, averaged over the two neurons of the two-neuron network. The duty cycle is the ratio between the burst duration and the period, averaged over the two neurons. The duty cycle ratio is the ratio between the duty cycle in neuron 1 (the neuron upon which acts the external hyperpolarization) and in neuron 2 (the other neuron). Each value for the mean frequency, mean duty cycle and mean duty cycle ratio was computed from ten simulations with the same set of parameter but with 40% variability in $\overline{g}_{syn}$ and 20% variability in $\overline{g}_{PIR}$. Only simulations endowed with rhythmic activity in the sense defined previously were considered to compute the means and standard deviations. If no rhythmic activity was detected, the computed means and standard deviations were set to 0. The proportion of oscillatory HCO quantifies the percentage of simulations that showed rhythmic activity out of the ten simulations with the same set of parameter.

In chapter 4, the quantities T_{osc} and T_{burst} of Figure 4.8 are, respectively, the duration between two burst onsets, and the duration of the burst, from the burst onset to the last spike. The parameters are identical to the ones given previously. Modulation is introduced by varying a single parameter, different for each panel.

A.3.3 Noise

A Gaussian white noise is added in the voltage equation to model the typical spike train input received from the many other unmodeled neurons [153]. The noise is modeled by $\sqrt{2D}\xi(t)$, where D is the noise intensity and $\xi(t)$ is drawn from a normal distribution with zero mean and unitary standard deviation and is different for each neuron.

A.3.4 Local field potential and time-average

The local field potential (LFP) is the mean field measure of the average behavior of large numbers of interacting neurons and it reflects the linear sum of numerous overlapping fields generated by current sources and sinks [28]. Therefore, the LFP dynamics results from the collective synaptic activity of the neuronal population and can be modeled by the normalized sum of the postsynaptic currents $I_{syn,j}$: $LFP = \sum_{j=1}^{M} I_{syn,j}/M$, where M is the number of postsynaptic neurons in the population. The LFPs are low-pass filtered at 100 hertz via a one-dimensional digital filter to reflect the use of macro-electrodes in LFP acquisition.

In the slow excitability window of Figures 5.4 and 5.6, the membrane potential is averaged to reflect the slower timescale. This is performed with a smoothing of the membrane potential signal with a moving-average filter with a window size of 200ms.

A.3.5 Spectrogram

The spectrogram analyses (Spect.), or time-frequency plots, result from a logarithmic representation of the spectrogram (using the Goertzel algorithm) of the short-time Fourier transform of the LFP. For the short-time Fourier transform, we consider a sampling frequency $F_s = 1000$ and a window of $F_s/4 = 250$. This sets the Rayleigh frequency at 4. The time step between two consecutive windows is 5. The frequencies of interest cover the $[15, 50]$ frequency range with a step of 0.1.

A.3.6 Correlations

In chapters 4 and 5, the auto-correlations (Acorr.) and cross-correlations (Xcorr.) are computed for a random input current by using the MATLAB cross-correlation function estimate. The random input current takes the form of a train of impulses with time intervals selected from a Poisson distribution with an enforced minimum interval and fixed impulse width and amplitude. For the cross-correlations against noise in Figure 5.6, a similar function is used but with a different Poisson distribution for the time intervals.

For the reduced model in chapter 4, the cross-correlations (Xcorr.) are computed over a 1000 period for a given I_{app} (depolarizing or hyperpolarizing) from the MATLAB cross-correlation function estimate. In Figures 4.6 and 4.7, the cross-correlations are given by pairing two-by-two all the neurons in each population. In Figure 4.9, the cross-correlations are given for each neuron in the E population with respect to the input spike train.

A.4 Simulation details

A.4.1 Chapter 3

In this chapter, the two currents responsible for PIR are: a low threshold T-type calcium current, $I_{Ca,T}$, and a hyperpolarization activated cation current, I_H. The calcium-activated potassium current is null ($g_{KCa} = 0$). The maximal synaptic conductance takes value $\overline{g}_{syn} = 4mS/cm^2$.

To capture the cellular dynamics at the network level (Figures 3.3-3.7), we use a reduced cellular model with three ionic currents: the two Hodgkin-Huxley currents responsible for action potentials, I_{Na} and I_K, and a single "PIR current", I_{PIR}, responsible for the PIR. Based on the observation (Figure 3.2) that the excitability properties of a restorative model are similar with an instantaneously activated T-type calcium current and with an I_H current, we model the I_{PIR} current with the T-type calcium channel parameters and functions of Tables A.1 and A.2, but with an instantaneous activation when considering a restorative current and with a slow activation when considering a regenerative

current. In this way, the two PIR currents only differ in the nature of their slow feedback, but they possess identical I/V curves. Our reduced model does not capture the physiological sag brought by an I_H current but the results of the paper do not depend on that cellular property. We insist that the variation of the activation time constant in our reduced model is not physiological but only meant to capture the restorative or regenerative nature of the PIR in an otherwise identical reduced model. Our PIR current can be thought as the aggregated current resulting from all physiological currents contributing to the PIR.

The simulations of Figure 3.1, are performed using the conductance-based neuron model described above, with $\overline{g}_{Ca,T} = 0mS/cm^2$ for Mechanism A and $\overline{g}_H = 0mS/cm^2$ for Mechanism B. The applied current, I_{app}, takes values of $-0.8\mu A/cm^2$ and $-3.8\mu A/cm^2$ for Mechanism A and values of $-0.55\mu A/cm^2$ and $-1.95\mu A/cm^2$ for Mechanism B. Simulations in Figure 3.1 (Center) do not present any parameter variability, the two neurons and synaptic connections are identical. Physiological variability is simulated in Figure 3.1 (Bottom) with 40% variability in $\overline{g}_{syn}$ and 20% variability in $\overline{g}_H$ and $\overline{g}_{Ca,T}$.

The cell models in Figure 3.2 were performed using the conductance-based neuron model described above, with $\overline{g}_{Ca,T} = 0mS/cm^2$ (Figure 3.2, Left), $\overline{g}_H = 0mS/cm^2$ and instantaneous activation (Figure 3.2, Center), and $\overline{g}_H = 0mS/cm^2$ and slow activation (Figure 3.2, Right). The applied current is identical as to Figure 3.1 but takes a value of $10\mu A/cm^2$ for $10ms$ for the fast depolarizing input.

In Figure 3.3, the maximal synaptic conductance, $\overline{g}_{syn}$ (from $0mS/cm^2$ to $10mS/cm^2$), and the synaptic time constant ($1/k_{rA}$, k_{rA} varies from $0ms^{-1}$ to $1ms^{-1}$), vary simultaneously for the two neurons. The variability level is 40% for $\overline{g}_{syn}$ and 20% for $\overline{g}_{PIR}$. Membrane potential plots ($\overline{g}_{syn}[mS/cm^2]$, $k_{rA}[ms^{-1}]$): top left panel–(1.5, 0.1) and (4.5, 0.05); top right panel–(8.5, 0.75) and (4.5, 0.05); bottom panel–(6, 0.15) with variability. In Figure 3.4, the maximal PIR conductances, $\overline{g}_{PIR,1}$ for neuron 1 and $\overline{g}_{PIR,2}$ for neuron 2 (from $0.25mS/cm^2$ to $0.75mS/cm^2$), vary independently for the two neurons. The variability level is 40% for $\overline{g}_{syn}$ and 20% for $\overline{g}_{PIR}$. The zoom for the duty cycle and duty cycle ratio covers a range from $0.25mS/cm^2$ to $0.50mS/cm^2$.

For Figure 3.5, the intrinsic neuron parameter is $\overline{g}_{PIR} = 0.3mS/cm^2$ with a variability level from 0% to 200%. For Figure 3.6, the extrinsic neuron parameter is $\overline{g}_{syn} = 2mS/cm^2$ with a variability level from 0% to 200%. In Figure 3.7, D, the noise intensity, varies from 0 to 0.25.

A.4.2 Chapter 4

For the conductance-based neuron model of this chapter (Figures 4.1-4.4), $\overline{g}_{Ca,T} = 0.48$, $\overline{g}_H = 0.06$, and $\overline{g}_{KCa} = 3.4$. The kinetics of the gating variables for the $I_{Ca,T}$ are slightly modified to give rise to hyperpolarized-induced

bursting (see Table A.3). The other figures use the reduced model described above.

Table A.3 – **Functions for the $I_{Ca,T}$ current.**

	$m_{\infty,Ca,T}(V_m)$	$h_{\infty,Ca,T}(V_m)$	$\tau_{m,Ca,T}(V_m)$	$\tau_{h,Ca,T}(V_m)$
$I_{Ca,T}$	$\frac{1}{1+exp\left(\frac{V_m+67.1}{-7.2}\right)}$	$\frac{1}{1+exp\left(\frac{V_m+80.1}{5.5}\right)}$	$21.7 - \frac{21.3}{1+exp\left(\frac{V_m+68.1}{-20.5}\right)}$	$205 - \frac{89.8}{1+exp\left(\frac{V_m+55}{-16.9}\right)}$

Notation is explained in the text. All time constants are in ms.

For the simulations of Figures 4.1 and 4.3, the applied current, I_{app}, takes values of $-1.2\mu A/cm^2$ for the depolarized state and $-1.9\mu A/cm^2$ for the hyperpolarized state. For Figure 4.2 intraburst increase is achieved with $\overline{g}_{KCa} * 0.2$ and interburst increase with $\overline{g}_H * 0.45$, all other parameters being constant. The applied current takes value $-1.9\mu A/cm^2$. For Figure 4.3, the fast activation is set by $\tau_m/10$ and the slow inactivation is set by $\tau_h/10$. Auto-correlations and cross-correlations of Figure 4.4 are computed over a 20s period, with a static signal of $-1.9\mu A/cm^2$. A random impulse train—100ms minimum interval, 5ms impulse-width and $4\mu A/cm^2$ impulse-amplitude—is superposed to this static signal.

For the simulations of Figures 4.5 and 4.6, the applied current, I_{app}, takes values 0 for the depolarized state and -150 for the hyperpolarized state.

In Figure 4.7, there is a 20% variability in the intrinsic parameters τ_s, τ_{us}, and $\overline{g}_{us}$, and a 20% variability in the extrinsic parameters $\overline{g}_{AMPA}$ and $\overline{g}_{GABA}$.

Figure 4.8 B: $\tau_{us,E} = 20$; Figure 4.8 C: $\tau_{AMPA} = 15$ and $\tau_{GABA} = 18$; Figure 4.8 D: $g_{s,max} = 12$; Figure 4.8 E: $\overline{g}_{AMPA} = 2$ and $\overline{g}_{GABA} = 5$.

In Figures 4.7 and 4.9, a Gaussian white noise is added with noise intensity $D = 1$.

A.4.3 Chapter 5

For the conductance-based neuron model of this chapter, $\overline{g}_{Na} = 120$, $\overline{g}_{Ca,T} = 0.4$, $\overline{g}_H = 0.04$, and $\overline{g}_{KCa} = 2$. The kinetics of the gating variables for the $I_{Ca,T}$ are slightly modified to give rise to hyperpolarized-induced bursting (see Table A.3).

The simulations of Figure 5.2 are performed using the conductance-based neuron model described above, with $\overline{g}_{Ca,T} = \overline{g}_H = \overline{g}_{KCa} = 0mS/cm^2$. The applied current, I_{app}, takes values of $-0.5\mu A/cm^2$ for the static signal, $-1.8\mu A/cm^2$ for $I_{app,1}$, $3.5\mu A/cm^2$ for $I_{app,2,3,5}$, and $5.5\mu A/cm^2$ for $I_{app,4}$. Auto-correlations and cross-correlations are computed over a 5s period, with a static signal of $-0.5\mu A/cm^2$ for the exogenous behavior and of $3.5\mu A/cm^2$ for the endogenous

behavior. A random impulse train—100ms minimum interval, 5ms impulse-width and $4\mu A/cm^2$ impulse-amplitude—is superposed to this static signal.

The simulations of Figure 5.4 are performed using the conductance-based neuron model described above. For the fast excitability window, the applied current, I_{app}, takes values of $-1.4\mu A/cm^2$ for the exogenous behavior and $-2\mu A/cm^2$ for the endogenous behavior. The impulses have a 5ms impulse-width and $2.6\mu A/cm^2$ impulse-amplitude. Cross-correlations are computed over a 15s period with a random impulse train—100ms minimum interval, 5ms impulse-width and $4\mu A/cm^2$ impulse-amplitude—superposed to the static signal. For the slow excitability window, the applied current, I_{app}, takes values of $-1.4\mu A/cm^2$ for the static signal, $-1.8\mu A/cm^2$ for $I_{app,1}$, $-2\mu A/cm^2$ for $I_{app,2,3,5}$, and $-2.4\mu A/cm^2$ for $I_{app,4}$. Auto-correlations and cross-correlations are computed over a 50s period from the averaged potential, with a static signal of $-1.4\mu A/cm^2$ for the exogenous behavior and of $-2\mu A/cm^2$ for the endogenous behavior. A random impulse train—3s minimum interval, 25ms impulse-width and $-0.6\mu A/cm^2$ impulse-amplitude—is superposed to this static signal.

The simulations of Figure 5.5 are performed using the conductance-based neuron model described above and an E-I circuit connectivity. For the fine excitability window, the applied current, $I_{app,I}$, takes values of $-1.4\mu A/cm^2$ for the exogenous behavior and $-2\mu A/cm^2$ for the endogenous behavior. The $I_{app,E}$ static current takes value of $-0.2\mu A/cm^2$ and the impulses have a 5ms impulse-width and $1.8\mu A/cm^2$ impulse-amplitude. Cross-correlations are computed over a 15s period with a random impulse train—100ms minimum interval, 5ms impulse-width and $4\mu A/cm^2$ impulse-amplitude—superposed to the static signal $I_{app,E}$. For the coarse excitability window, the applied current, $I_{app,I}$, takes values of $-1.4\mu A/cm^2$ for the static signal, $-1.5\mu A/cm^2$ for $I_{app,1}$, $-2\mu A/cm^2$ for $I_{app,2,3,5}$, and $-2.4\mu A/cm^2$ for $I_{app,4}$, and $I_{app,E}$ takes value of $-0.2\mu A/cm^2$. Auto-correlations and cross-correlations are computed over a 50s period from the LFP, with a static signal of $-1.4\mu A/cm^2$ for the exogenous behavior and of $-2\mu A/cm^2$ for the endogenous behavior. A random impulse train—3s minimum interval, 40ms impulse-width and $-0.6\mu A/cm^2$ impulse-amplitude—is superposed to this static signal.

For Figure 5.6, the signals are the ones for the cross-correlations in Figures. 5.4 and 5.5 and are cross-correlated with the input signal (Xcorr Signal) or with a signal with the same characteristics but another Poisson distribution for the time intervals (Xcorr Noise).

The cell model of Figure 5.7 is slightly different with $\overline{g}_{Na} = 60mS/cm^2$, $\overline{g}_{Ca,T} = 0.3mS/cm^2$, $\overline{g}_H = \overline{g}_{KCa} = 0mS/cm^2$, and $K_D = 120$. The circuit is an I-I circuit with $\overline{g}_{GABA} = 4mS/cm^2$. The applied currents, $I_{app,I1}$ and $I_{app,I2}$, take values of $-0.55\mu A/cm^2$ for the static signal, and $-1.1\mu A/cm^2$ for the step input. Auto-correlations and cross-correlations are computed over a 50s period from the LFP, with static signals of $-0.55\mu A/cm^2$. For the OFF

mode, no step has been presented to the circuit whereas a step has switched the circuit for the ON mode. A random impulse train—3s minimum interval, 40ms impulse-width and $-0.6\mu A/cm^2$ impulse-amplitude—is superposed to the static signal $I_{app,I1}$. A signal with the same characteristics but different Poisson distribution for the time intervals is used for the cross-correlation against noise.

Figure 5.8 uses the network models of Figure 5.5 (Left) and Figure 5.7 (Right) but with eight neurons in each population. The stimulation currents take the same value as $I_{app,I}$ and $I_{app,I2}$, respectively. Synaptic decay affects the synaptic connections to incorporate the spatial dimension.

Appendix B

Omitted derivations

In this appendix, we propose a state-space model for the E-I network of chapter 4 with the neurons in the burst-firing mode. The model possesses an hybrid formulation and can be used, under some assumptions, to compute T_{osc}, the oscillation period or the duration between two burst onsets, and T_{burst}, the duration of the burst, from the burst onset to the last spike. The mathematical derivations are based on considerations for bursting oscillators in Chapter 6 of Pierre Sacré's dissertation [213].

B.1 State-space model

Starting from the three-timescale bursting model of section 2.5.2, we reduce the set of equations to the study of the dynamics of the ultraslow variable $x_{us}(t)$ (see Figure B.1). The $x_{us}(t)$ dynamics is approximated by the dynamics of the variable $z(t)$, described by two equations, f_B and f_R—equation for the bursting state and equation for the resting state, respectively—and with two boundary conditions, z_{SN} and z_{SH} which represent the saddle-node and saddle-homoclinic bifurcation boundaries, respectively.

The state-space model for a single neuron writes in the hybrid formalism:

$$\begin{array}{c|c} \text{While } p = 1 \text{ and } z \leq z_{SH}\,(I) & \text{While } p = -1 \text{ and } z \geq z_{SN}\,(I) \\ \left\{ \begin{array}{l} \dot{p} = 0 \\ \dot{z} = f_B(z) \end{array} \right. & \left\{ \begin{array}{l} \dot{p} = 0 \\ \dot{z} = f_R(z) \end{array} \right. \end{array}$$

With reset conditions: if $z \geq z_{SH}\,(I)$ and $p = 1$ or $z \leq z_{SN}\,(I)$ and $p = -1$

$$\begin{aligned} p^+ &= -p \\ z^+ &= z \end{aligned}$$

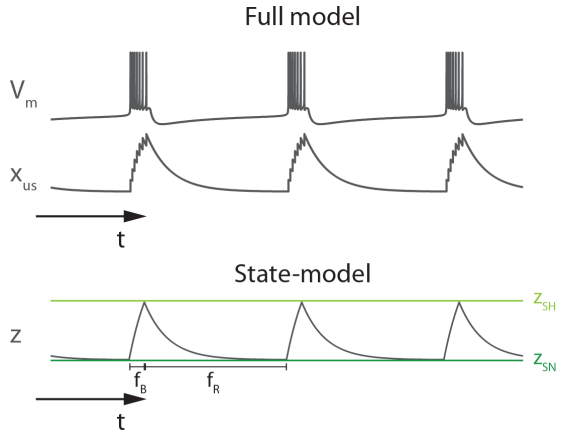

Figure B.1 – State-space model. The dynamics of the three-timescale model (V_m) is characterized by the dynamics of its ultraslow variable x_{us} and approximated by the variable z, with two set of equations, f_B and f_R, and two boundary conditions, z_{SN} and z_{SH}.

with

$$\begin{aligned} f_B &= 1/\tau_{us}\left(-z + \frac{\tau_{us} d_{us}}{T_f}\right) \\ f_R &= 1/\tau_{us}\,(-z) \\ T_f &= f(z, I) \approx c^{st} \\ z_{SH} &= I/\overline{g}_{us} \\ z_{SN} &= \frac{F(v_{SN}) + I}{\overline{g}_{us}} \\ F(v_{SN}) &= v_{SN}^2 + b v_{SN} w_{SN} - w_{SN}^2, v_{SN} = \frac{-b\overline{g}_s}{2+ab}, w_{SN} = \frac{-2v_{SN}}{b} \end{aligned}$$

T_f represents the intraburst firing period and is considered constant, and I is the external applied current. Numerical validation of the model was performed and the monotonic increase of f_B and monotonic decrease of f_R between the boundary conditions was verified numerically.

Two neurons i and j are connected via the external applied current with:

$$I_i = f(z_i, z_j, p_i, p_j, I_i, I_j) = -u_i * (v_i - v_u)$$

where v_u is the reversal synaptic potential E_k.

v_i represents the membrane potential of neuron i:

$$v_i = f(z_i, p_i, I_i) = \begin{cases} \overline{V}_{LC}(z_i, I_i) & \text{if } p_i = 1 \\ V_{eq}(z_i, I_i) & \text{if } p_i = -1 \end{cases}$$

where $\overline{V}_{LC}$ is an approximation of the value of v_i on the limit circle during the bursting state and V_{eq} is the value of v_i during the resting state (stationary fixed point):

$$\begin{aligned}
\overline{V}_{LC}(z,I) &= \frac{1}{T_f}\int_0^{T_f} V_{LC}(s,z)ds \approx c^{st} \\
V_{eq}(z,I) &= -\left(\overline{g}_s - \frac{2\overline{g}_s - a\sqrt{R} + ab\overline{g}_s}{2\left(-a^2+ba+1\right)}\right)/a \\
R &= 4\overline{g}_{us}z - 4I + 4Ia^2 + 4\overline{g}_s + b^2\overline{g}_s^2 - 4a^2\overline{g}_{us}z - 4Iab + 4ab\overline{g}_{us}z
\end{aligned}$$

u_i is function of the state of the other neuron j (see [40] for analytical details):

$$\begin{aligned}
u_i &= f(z_j,p_j,I_j) = \frac{\overline{g}}{T_f}Q\left(t_j, \min(t_j,\Delta_j)\right) \\
&= \begin{cases} \frac{\overline{g}}{T_f}Q\left(t_j,t_j\right) & \text{if } p_j = 1 \\ \frac{\overline{g}}{T_f}Q\left(t_j,\Delta_j\right) & \text{if } p_j = -1 \end{cases} \\
t_j &= f(z_j,p_j,I_j) \\
&= \begin{cases} -\tau_{us} * ln\frac{z_j - \frac{d_{us}\tau_{us}}{T_f}}{C_{up} - \frac{d_{us}\tau_{us}}{T_f}} & \text{if } p_j = 1 \\ -\tau_{us} * ln\frac{z_j}{C_{down}} & \text{if } p_j = -1 \end{cases} \\
C_{up} &= z_{SN} \\
C_{down} &= z_{SH}/e^{(-\Delta_j/\tau_{us})} \\
\Delta_j &= t(z_{SH}, p_j = 1) \\
Q(t,a) &= e^{-\alpha(t-a)}\left(1+\alpha(t-a)\right) - e^{-\alpha t}\left(1+\alpha t\right)
\end{aligned}$$

where $\overline{g}$ the maximal synaptic conductance.

B.2 Linear state-space model

The system is linearized to have $I_i = f(z_i, z_j, p_i, p_j)$ by approximating $v_i = f(z_i, p_i, I_i) \approx f(z_i, p_i)$ and $u_i = f(z_j, p_j, I_j) \approx f(z_j, p_j)$ (see Figure B.2).

The hybrid system writes as follows:

$$\begin{aligned}
(p_i,z_i) &\in \{p_i = 1, z_i \le z_{SH}(I_i)\} \begin{cases} \dot{p_i} = 0 \\ \dot{z_i} = z_i/\bar{\tau}_{us} + \bar{d}_{us} \end{cases} \\
(p_i,z_i) &\in \{p_i = -1, z_i \ge z_{SN}(I_i)\} \begin{cases} \dot{p_i} = 0 \\ \dot{z_i} = z_i/\bar{\tau}_{us} \end{cases} \\
(p_i,z_i) &\in \{p_i = 1, z_i \ge z_{SH}(I_i)\} \cup \{p_i = -1, z_i \le z_{SN}(I_i)\} \begin{cases} p_i^+ = -p_i \\ z_i^+ = z_i \end{cases}
\end{aligned}$$

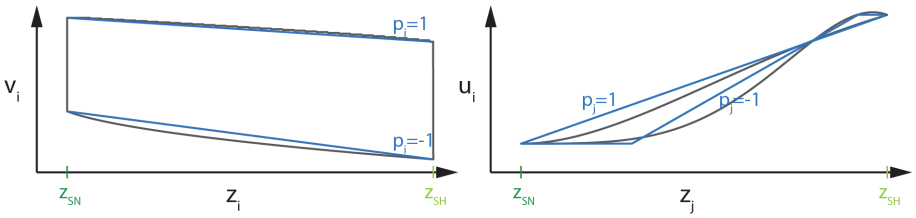

Figure B.2 – Linearization of state-space model. Approximation in blue of $v_i = f(z_i, p_i, I_i)$ and $u_i = f(z_j, p_j, I_j)$ by $v_i \approx f(z_i, p_i)$ and $u_i \approx f(z_j, p_j)$, respectively.

with:

$$\begin{aligned} z_{SH} &= \bar{K}_z I_i \\ z_{SN} &= \bar{K}_z I_i + \bar{V}_{SN} \\ I_i &= f(z_i, z_j, p_i, p_j) = -u_i(v_i - \bar{v}_u) \\ v_i &= f(z_i, p_i) = \begin{cases} \bar{h}_1 z_i + \bar{l}_1 & \text{if } p_i = 1 \\ \bar{h}_2 z_i + \bar{l}_2 & \text{if } p_i = -1 \end{cases} \\ u_i &= f(z_j, p_j) = \begin{cases} \bar{g}_1 z_j + \bar{q}_1 & \text{if } p_j = 1 \\ \bar{g}_2 z_j + \bar{q}_2 & \text{if } p_j = -1 \end{cases} \end{aligned}$$

where the upper bar denotes that the quantity is fixed for a given set of simulation parameters.

B.3 System of equations for T_{osc} and T_{burst}

Under some assumptions, there exist a set of 11 equations with 10 unknowns to determine T_{osc} and T_{burst}. Assumptions:

- i is an excitatory neuron (E) and j is an inhibitory neuron (I);
- the two neurons burst in synchrony;
- the activity patten goes as follows: (i) the neuron i starts its burst, (ii) the neuron j starts its burst, (iii) the neuron i ends its burst, and (iv) the neuron j ends its burst;
- the influence of the inhibitory burst is over when the excitatory burst begins.

The unknowns are represented on Figure B.3. There are two equations for the dynamics of $z(t)$:

$$\begin{aligned} \text{Neuron in bursting phase :} \quad & z(t) = z_{min} e^{-t/\bar{\tau}_{us}} + \bar{d}_{us} \left(1 - e^{-t/\bar{\tau}_{us}}\right) \\ \text{Neuron in resting phase :} \quad & z(t) = z_{max} e^{-t/\bar{\tau}_{us}} \end{aligned}$$

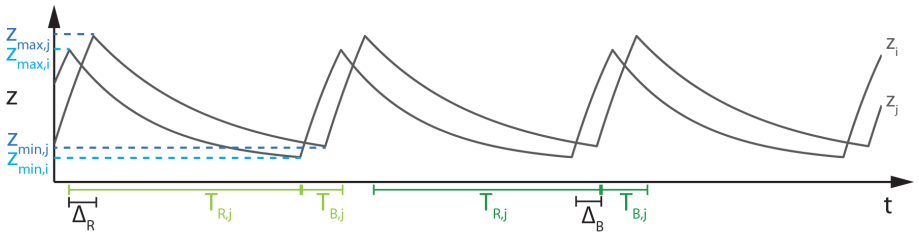

Figure B.3 – Set of equations to compute T_{osc} and T_{burst}. Excitatory neuron i and inhibitory neuron j burst in synchrony. The unknowns are introduced for the set of equations.

From there, we draw the set of equations:

$$
\begin{aligned}
z_{min,i} &= z_{SN,i} = \bar{K}_z I_i + \bar{V}_{SN} = \bar{K}_z(I_{app,i} + I_{min,i}) + \bar{V}_{SN} \\
z_{min,i} &= z_{max,i} e^{-T_{R,i}/\bar{\tau}_{us}} \\
z_{min,j} &= z_{SN,j} = \bar{K}_z I_j + \bar{V}_{SN} = \bar{K}_z(I_{app,j} + I_{min,j}) + \bar{V}_{SN} \\
z_{min,j} &= z_{max,j} e^{-T_{R,j}/\bar{\tau}_{us}} \\
z_{max,i} &= z_{SH,i} = \bar{K}_z I_i = \bar{K}_z(I_{app,i} + I_{max,i}) \\
z_{max,i} &= z_{min,i} e^{-T_{B,i}/\bar{\tau}_{us}} + \bar{d}_{us}(1 - e^{-T_{B,i}/\bar{\tau}_{us}}) \\
z_{max,j} &= z_{SH,j} = \bar{K}_z I_j = \bar{K}_z(I_{app,j} + I_{max,j}) \\
z_{max,j} &= z_{min,j} e^{-T_{B,j}/\bar{\tau}_{us}} + \bar{d}_{us}(1 - e^{-T_{B,j}/\bar{\tau}_{us}}) \\
T_{B,i} + T_{R,i} &= T_{B,j} + T_{R,j} \\
T_{R,i} &= \Delta_R + T_{R,j} - \Delta_B \\
T_{B,i} &= \Delta_B + T_{B,j} - \Delta_R \\
&\text{with} \\
I_{min,i} &= -u_i(v_i - \bar{v}_{u,i}) = -(\bar{g}_2 z_{m,j} + \bar{q}_2)((\bar{h}_2 z_{min,i} + \bar{l}_2) - \bar{v}_{u,i}) \\
z_{m,j} &= z_{max,j} e^{-(T_{R,j} - \Delta_B)/\bar{\tau}_{us}} \\
I_{min,j} &= -u_j(v_j - \bar{v}_{u,j}) = -(\bar{g}_1 z_{m,i} + \bar{q}_1)((\bar{h}_2 z_{min,j} + \bar{l}_2) - \bar{v}_{u,j}) \\
z_{m,i} &= z_{min,i} e^{-\Delta_B/\bar{\tau}_{us}} + \bar{d}_{us}(1 - e^{-\Delta_B/\bar{\tau}_{us}}) \\
I_{max,i} &= -u_i(v_i - \bar{v}_{u,i}) = -(\bar{g}_1 z_{M,j} + \bar{q}_1)((\bar{h}_1 z_{min,i} + \bar{l}_1) - \bar{v}_{u,i}) \\
z_{M,j} &= z_{min,j} e^{-(T_{B,j} - \Delta_R)/\bar{\tau}_{us}} + \bar{d}_{us}(1 - e^{-(T_{B,j} - \Delta_R)/\bar{\tau}_{us}}) \\
I_{max,j} &= -u_j(v_j - \bar{v}_{u,j}) = -(\bar{g}_2 z_{M,i} + \bar{q}_2)((\bar{h}_1 z_{min,i} + \bar{l}_1) - \bar{v}_{u,j}) \\
z_{M,i} &= z_{max,i} e^{-\Delta_R/\bar{\tau}_{us}} \\
T_{osc} &= T_{B,i} + T_{R,i} = T_{B,j} + T_{R,j} \\
T_{burst,i} &= T_{B,i} \\
T_{burst,j} &= T_{B,j}
\end{aligned}
$$

Bibliography

[1] P. M. Abedi, C. Delaville, P. De Deurwaerdère, W. Benjelloun, and A. Benazzouz. Intrapallidal administration of 6-hydroxydopamine mimics in large part the electrophysiological and behavioral consequences of major dopamine depletion in the rat. *Neuroscience*, 236:289–97, 2013.

[2] R. L. Albin, A. B. Young, and J. B. Penney. The functional anatomy of basal ganglia disorders. *Trends Neurosci*, 12(10):366–75, 1989.

[3] U. Alon. Network motifs: theory and experimental approaches. *Nat Rev Genet*, 8(6):450–61, 2007.

[4] U. Alon. Simplicity in biology. *Nature*, 446(7135):497, 2007.

[5] S. Amari. Dynamics of pattern formation in lateral-inhibition type neural fields. *Biol Cybern*, 27(2):77–87, 1977.

[6] R. Amirnovin, Z. M. Williams, G. R. Cosgrove, and E. N. Eskandar. Visually guided movements suppress subthalamic oscillations in Parkinson's disease patients. *J Neurosci*, 24(50):11302–6, 2004.

[7] A. G. Androulidakis, L. M. F. Doyle, K. Yarrow, V. Litvak, T. P. Gilbertson, and P. Brown. Anticipatory changes in beta synchrony in the human corticospinal system and associated improvements in task performance. *Eur J Neurosci*, 25(12):3758–65, 2007.

[8] J. D. Angstadt, J. L. Grassmann, K. M. Theriault, and S. M. Levasseur. Mechanisms of postinhibitory rebound and its modulation by serotonin in excitatory swim motor neurons of the medicinal leech. *J Comp Physiol A Neuroethol Sens Neural Behav Physiol*, 191(8):715–32, 2005.

[9] J. V. Arthur and K. Boahen. Silicon-neuron design: a dynamical systems approach. *IEEE Trans Circuits Syst I Regul Pap*, 58(5):1034–43, 2011.

[10] T. Bal and D. A. McCormick. Mechanisms of oscillatory activity in guinea-pig nucleus reticularis thalami in vitro: a mammalian pacemaker. *J Physiol*, 468(1):669–91, 1993.

[11] B. Ballarò, P. G. Reas, and R. Riccardi. Mathematical models for excitable systems in biology and medicine. *Riv Biol*, 100(2):247–66, 2007.

[12] J. Baufreton, M. Garret, S. Dovero, B. Dufy, B. Bioulac, and A. Taupignon. Activation of GABA(A) receptors in subthalamic neurons in vitro: properties of native receptors and inhibition mechanisms. *J Neurophysiol*, 86(1):75–85, 2001.

[13] R. L. Beurle. Properties of a mass of cells capable of regenerating pulses. *Philos Trans R Soc Lond B Biol Sci*, 240(669):55–94, 1956.

[14] C. Beurrier, B. Bioulac, J. Audin, and C. Hammond. High-frequency stimulation produces a transient blockade of voltage-gated currents in subthalamic neurons. *J Neurophysiol*, 85(4):1351–6, 2001.

[15] C. Beurrier, B. Bioulac, and C. Hammond. Slowly inactivating sodium current (INaP) underlies single-spike activity in rat subthalamic neurons. *J Neurophysiol*, 83(4):1951–7, 2000.

[16] C. Beurrier, P. Congar, B. Bioulac, and C. Hammond. Subthalamic nucleus neurons switch from single-spike activity to burst-firing mode. *J Neurosci*, 19(2):599–609, 1999.

[17] M. D. Bevan, J. F. Atherton, and J. Baufreton. Cellular principles underlying normal and pathological activity in the subthalamic nucleus. *Curr Opin Neurobiol*, 16(6):621–8, 2006.

[18] M. D. Bevan, P. J. Magill, D. Terman, J. P. Bolam, and C. J. Wilson. Move to the rhythm: oscillations in the subthalamic nucleus-external globus pallidus network. *Trends Neurosci*, 25(10):525–31, 2002.

[19] K. Boahen. Neuromorphic microchips. *Sci Am*, 292(5):56–63, 2005.

[20] T. Boraud, P. Brown, J. A. Goldberg, A. M. Graybiel, and P. J. Magill. Oscillations in the basal ganglia: the good, the bad, and the unexpected. In J. P. Bolam, C. A. Ingham, and P. J. Magill, editors, *The Basal Ganglia VIII*, volume 56 of *Advances in Behavioral Biology*, pages 1–24. Springer US, 2005.

[21] J. Brea, W. Senn, and J.-P. Pfister. Sequence learning with hidden units in spiking neural networks. In J. Shawe-Taylor, R. Zemel, P. Bartlett, F. Pereira, and K. Weinberger, editors, *Advances in Neural Information Processing Systems (NIPS) 24*, pages 1422–30. MIT Press, Cambridge, MA, 2011.

[22] J.-S. Brittain and P. Brown. Oscillations and the basal ganglia: Motor control and beyond. *Neuroimage*, 2013.

[23] P. Brown. Abnormal oscillatory synchronisation in the motor system leads to impaired movement. *Curr Opin Neurobiol*, 17(6):656–64, 2007.

[24] P. Brown, A. Oliviero, P. Mazzone, A. Insola, P. Tonali, and V. Di Lazzaro. Dopamine dependency of oscillations between subthalamic nucleus and pallidum in Parkinson's disease. *J Neurosci*, 21(3):1033–8, 2001.

[25] P. Brown and D. Williams. Basal ganglia local field potential activity: character and functional significance in the human. *Clin Neurophysiol*, 116(11):2510–9, 2005.

[26] T. G. Brown. The intrinsic factors in the act of progression in the mammal. *Proc R Soc Lond B*, 84(572):308–19, 1911.

[27] R. J. Butera, Jr, J. Rinzel, and J. C. Smith. Models of respiratory rhythm generation in the pre-Bötzinger complex. II. Populations of coupled pacemaker neurons. *J Neurophysiol*, 82(1):398–415, 1999.

[28] G. Buzsáki. *Rhythms of the Brain*. Oxford University Press, New York, 2006.

[29] G. Buzsáki, C. A. Anastassiou, and C. Koch. The origin of extracellular fields and currents–EEG, ECoG, LFP and spikes. *Nat Rev Neurosci*, 13(6):407–20, 2012.

[30] G. Buzsáki and X.-J. Wang. Mechanisms of gamma oscillations. *Annu Rev Neurosci*, 35:203–25, 2012.

[31] S. M. Cain and T. P. Snutch. Voltage-gated calcium channels in epilepsy. *Epilepsia*, 51:11, 2010.

[32] S. M. Cain and T. P. Snutch. T-type calcium channels in burst-firing, network synchrony, and epilepsy. *Biochim Biophys Acta*, 1828(7):1572–8, 2013.

[33] R. L. Calabrese and E. De Schutter. Motor-pattern-generating networks in invertebrates: modeling our way toward understanding. *Trends Neurosci*, 15(11):439–45, 1992.

[34] J. Cannon, M. M. McCarthy, S. Lee, J. Lee, C. Börgers, M. A. Whittington, and N. Kopell. Neurosystems: brain rhythms and cognitive processing. *Eur J Neurosci*, 39(5):705–19, 2014.

[35] R. T. Canolty, K. Ganguly, and J. M. Carmena. Task-dependent changes in cross-level coupling between single neurons and oscillatory activity in multiscale networks. *PLoS Comput Biol*, 8(12):e1002809, 2012.

[36] J. Chetrit, A. Taupignon, L. Froux, S. Morin, R. Bouali-Benazzouz, F. Naudet, N. Kadiri, C. E. Gross, B. Bioulac, and A. Benazzouz. Inhibiting subthalamic D5 receptor constitutive activity alleviates abnormal electrical activity and reverses motor impairment in a rat model of Parkinson's disease. *J Neurosci*, 33(37):14840–9, 2013.

[37] D. Chik. Does dynamical synchronization among neurons facilitate learning and enhance task performance? *J Comput Neurosci*, 33(1):169–77, 2012.

[38] S. Ching, A. Cimenser, P. L. Purdon, E. N. Brown, and N. J. Kopell. Thalamocortical model for a propofol-induced alpha-rhythm associated with loss of consciousness. *Proc Natl Acad Sci U S A*, 107(52):22665–70, 2010.

[39] O. Cinquin and J. Demongeot. Positive and negative feedback: striking a balance between necessary antagonists. *J Theor Biol*, 216(2):229–41, 2002.

[40] S. Coombes. Dynamics of synaptically coupled integrate-and-fire-or-burst neurons. *Phys Rev E Stat Nonlin Soft Matter Phys*, 67(4 Pt 1):041910, 2003.

[41] S. Coombes. Waves, bumps, and patterns in neural field theories. *Biol Cybern*, 93(2):91–108, 2005.

[42] S. Coombes and C. Laing. Delays in activity-based neural networks. *Philos Trans A Math Phys Eng Sci*, 367(1891):1117–29, 2009.

[43] A. J. Cooper and I. M. Stanford. Electrophysiological and morphological characteristics of three subtypes of rat globus pallidus neurone in vitro. *J Physiol*, 527(2):291–304, 2000.

[44] R. Courtemanche, N. Fujii, and A. Graybiel. Synchronous, focally modulated beta-band oscillations characterize local field potential activity in the striatum of awake behaving monkeys. *J Neurosci*, 23(37):11741–52, 2003.

[45] J. S. Cruz, D. F. Silva, L. A. Ribeiro, I. G. A. Araújo, N. Magalhães, A. Medeiros, C. Freitas, I. C. Araujo, and F. A. Oliveira. Resurgent Na+ current: a new avenue to neuronal excitability control. *Life Sci*, 89(15-16):564–9, 2011.

[46] G. S. Cymbalyuk, Q. Gaudry, M. A. Masino, and R. L. Calabrese. Bursting in leech heart interneurons: cell-autonomous and network-based mechanisms. *J Neurosci*, 22(24):10580–92, 2002.

[47] S. Daun, J. E. Rubin, and I. A. Rybak. Control of oscillation periods and phase durations in half-center central pattern generators: a comparative mechanistic analysis. *J Comput Neurosci*, 27(1):3–36, 2009.

[48] P. Dayan. Twenty-five lessons from computational neuromodulation. *Neuron*, 76(1):240–56, 2012.

[49] P. Dayan and L. F. Abbott. *Theoretical Neuroscience: Computational and Mathematical Modeling of Neural Systems*. MIT Press, 2005.

[50] E. De Schutter, J. D. Angstadt, and R. L. Calabrese. A model of graded synaptic transmission for use in dynamic network simulations. *J Neurophysiol*, 69(4):1225–35, 1993.

[51] C. I. De Zeeuw, F. E. Hoebeek, L. W. J. Bosman, M. Schonewille, L. Witter, and S. K. Koekkoek. Spatiotemporal firing patterns in the cerebellum. *Nat Rev Neurosci*, 12(6):327–44, 2011.

[52] M. R. DeLong. Primate models of movement disorders of basal ganglia origin. *Trends Neurosci*, 13(7):281–5, 1990.

[53] A. Destexhe. Spike-and-wave oscillations based on the properties of GABAB receptors. *J Neurosci*, 18(21):9099–111, 1998.

[54] A. Destexhe, T. Bal, D. A. McCormick, and T. J. Sejnowski. Ionic mechanisms underlying synchronized oscillations and propagating waves in a model of ferret thalamic slices. *J Neurophysiol*, 76(3):2049–70, 1996.

[55] A. Destexhe and D. Contreras. Neuronal computations with stochastic network states. *Science*, 314(5796):85–90, 2006.

[56] A. Destexhe, D. Contreras, T. J. Sejnowski, and M. Steriade. A model of spindle rhythmicity in the isolated thalamic reticular nucleus. *J Neurophysiol*, 72(2):803–18, 1994.

[57] A. Destexhe, D. Contreras, T. J. Sejnowski, and M. Steriade. Modeling the control of reticular thalamic oscillations by neuromodulators. *Neuroreport*, 5(17):2217–20, 1994.

[58] A. Destexhe, D. Contreras, and M. Steriade. Mechanisms underlying the synchronizing action of corticothalamic feedback through inhibition of thalamic relay cells. *J Neurophysiol*, 79(2):999–1016, 1998.

[59] A. Destexhe, D. Contreras, M. Steriade, T. J. Sejnowski, and J. R. Huguenard. In vivo, in vitro, and computational analysis of dendritic calcium currents in thalamic reticular neurons. *J Neurosci*, 16(1):169–85, 1996.

[60] A. Destexhe, D. A. McCormick, and T. J. Sejnowski. A model for 8-10 Hz spindling in interconnected thalamic relay and reticularis neurons. *Biophys J*, 65(6):2473–7, 1993.

[61] A. Destexhe and M. Rudolph-Lilith. Neuronal noise. In A. Destexhe and R. Brette, editors, *Springer Series in Computational Neuroscience*, volume 8. Springer US, 2012.

[62] A. Destexhe and T. J. Sejnowski. The initiation of bursts in thalamic neurons and the cortical control of thalamic sensitivity. *Philos Trans R Soc Lond B Biol Sci*, 357(1428):1649–57, 2002.

[63] J. Dethier, G. Drion, A. Franci, and R. Sepulchre. Cellular control of network oscillations. In preparation.

[64] J. Dethier, G. Drion, A. Franci, and R. Sepulchre. Impacts of a unicellular mechanism on network behaviors. In *Proc 32nd Benelux Meeting on Systems and Control*, Houffalize, 2013.

[65] J. Dethier, G. Drion, A. Franci, and R. Sepulchre. Modulation of beta oscillations during movement initiation: modeling the ionic basis of a functional switch. In *Proc 43rd Annual Meeting of the Society for Neuroscience*, San Diego, CA, 2013.

[66] J. Dethier, G. Drion, A. Franci, and R. Sepulchre. A positive feedback at the cellular level promotes robustness and modulation at the circuit level. *J Neurophysiol*, 2015. In Press.

[67] J. Dethier, G. Drion, and R. Sepulchre. Contrasting the role of Ih and ICaT currents in post-inhibitory rebound mechanisms in reciprocal-inhibitory networks. In *Proc 44th Annual Meeting of the Society for Neuroscience*, Washington, DC, 2014.

[68] J. Dethier, D. Ernst, and R. Sepulchre. Neuromorphic reinforcement learning. In *Proc 31st Benelux Meeting on Systems and Control*, Heijen/Nijmegen, 2012.

[69] J. Dethier, P. Nuyujukian, S. I. Ryu, K. V. Shenoy, and K. Boahen. Design and validation of a real-time spiking-neural-network decoder for brain-machine interfaces. *J Neural Eng*, 10(3):036008, 2013.

[70] P. S. Dickinson. Neuromodulation of central pattern generators in invertebrates and vertebrates. *Curr Opin Neurobiol*, 16(6):604–14, 2006.

[71] M. Dipoppa and B. S. Gutkin. Flexible frequency control of cortical oscillations enables computations required for working memory. *Proc Natl Acad Sci U S A*, 110(31):12828–33, 2013.

[72] M. T. H. Do and B. P. Bean. Subthreshold sodium currents and pacemaking of subthalamic neurons: modulation by slow inactivation. *Neuron*, 39(1):109–20, 2003.

[73] J. Dockery. Existence of standing pulse solutions for an excitable activator-inhibitory system. *J Dyn Differ Equ*, 4(2):231–57, 1992.

[74] A. Doloc-Mihu and R. L. Calabrese. A database of computational models of a half-center oscillator for analyzing how neuronal parameters influence network activity. *J Biol Phys*, 37(3):263–83, 2011.

[75] J. O. Dostrovsky and A. M. Lozano. Mechanisms of deep brain stimulation. *Mov Disord*, 17(S3):S63–S68, 2002.

[76] G. Drion, A. Franci, J. Dethier, and R. Sepulchre. Dynamic input conductances shape neuronal spiking. *eneuro*, 2015.

[77] G. Drion, A. Franci, V. Seutin, and R. Sepulchre. A novel phase portrait for neuronal excitability. *PLoS One*, 7(8):e41806, 2012.

[78] G. Drion, L. Massotte, R. Sepulchre, and V. Seutin. How modeling can reconcile apparently discrepant experimental results: the case of pacemaking in dopaminergic neurons. *PLoS Comput Biol*, 7(5):e1002050, 2011.

[79] G. Drion, T. O'Leary, J. Dethier, A. Franci, and R. Sepulchre. Neuronal behaviors: a control perspective. In *Proc 54th IEEE Conference on Decision and Control*, Osaka, Japan, 2015.

[80] P. F. Durieux, B. Bearzatto, S. Guiducci, T. Buch, A. Waisman, M. Zoli, S. N. Schiffmann, and A. de Kerchove d'Exaerde. D2R striatopallidal neurons inhibit both locomotor and drug reward processes. *Nat Neurosci*, 12(4):393–5, 2009.

[81] A. El Manira and P. Wallén. Mechanisms of modulation of a neural network. *News Physiol Sci*, 15(4):186–91, 2000.

[82] A. K. Engel and P. Fries. Beta-band oscillations–signalling the status quo? *Curr Opin Neurobiol*, 20(2):156–65, 2010.

[83] B. G. Ermentrout. Neural networks as spatio-temporal pattern-forming systems. *Rep Prog Phys*, 61(4):353, 1998.

[84] J. M. Fellous and C. Linster. Computational models of neuromodulation. *Neural Comput*, 10(4):771–805, 1998.

[85] R. J. Field and R. M. Noyes. Oscillations in chemical systems. IV. Limit cycle behavior in a model of a real chemical reaction. *J Chem Phys*, 60(5):1877–84, 1974.

[86] R. Fitzhugh. Impulses and physiological states in theoretical models of nerve membrane. *Biophys J*, 1(6):445–66, 1961.

[87] A. Franci, G. Drion, and R. Sepulchre. An organizing center in a planar model of neuronal excitability. *SIAM J Appl Dyn Syst*, 11(4):1698–722, 2012.

[88] A. Franci, G. Drion, and R. Sepulchre. Modeling the modulation of neuronal bursting: a singularity theory approach. *SIAM J Appl Dyn Syst*, 13(2):798–829, 2014.

[89] A. Franci, G. Drion, V. Seutin, and R. Sepulchre. A balance equation determines a switch in neuronal excitability. *PLoS Comput Biol*, 9(5):e1003040, 2013.

[90] A. Franci and R. Sepulchre. Realization of nonlinear behaviors from organizing centers. In *Decision and Control (CDC), 2014 IEEE 53rd Annual Conference on*, pages 56–61, 2014.

[91] K. Fujita, Y. Kashimori, and T. Kambara. Spatiotemporal burst coding for extracting features of spatiotemporally varying stimuli. *Biol Cybern*, 97(4):293–305, 2007.

[92] L. Garcia, G. D'Alessandro, B. Bioulac, and C. Hammond. High-frequency stimulation in Parkinson's disease: more or less? *Trends Neurosci*, 28(4):209–16, 2005.

[93] W. Gerstner and W. Kistler. *Spiking Neuron Models: Single Neurons, Populations, Plasticity*. Cambridge University Press, 2002.

[94] P. A. Getting. Emerging principles governing the operation of neural networks. *Annu Rev Neurosci*, 12:185–204, 1989.

[95] A. Gillies and D. Willshaw. Membrane channel interactions underlying rat subthalamic projection neuron rhythmic and bursting activity. *J Neurophysiol*, 95(4):2352–65, 2006.

[96] A. Gillies, D. Willshaw, and Z. Li. Subthalamic-pallidal interactions are critical in determining normal and abnormal functioning of the basal ganglia. *Proc Biol Sci*, 269(1491):545–51, 2002.

[97] J. A. Goldberg, U. Rokni, T. Boraud, E. Vaadia, and H. Bergman. Spike synchronization in the cortex/basal-ganglia networks of Parkinsonian primates reflects global dynamics of the local field potentials. *J Neurosci*, 24(25):6003–10, 2004.

[98] A. Goldbeter. A minimal cascade model for the mitotic oscillator involving cyclin and cdc2 kinase. *Proc Natl Acad Sci U S A*, 88(20):9107–11, 1991.

[99] M. S. Goldman, J. Golowasch, E. Marder, and L. F. Abbott. Global structure, robustness, and modulation of neuronal models. *J Neurosci*, 21(14):5229–38, 2001.

[100] D. Golomb and J. Rinzel. Dynamics of globally coupled inhibitory neurons with heterogeneity. *Phys Rev E Stat Phys Plasmas Fluids Relat Interdiscip Topics*, 48(6):4810–4, 1993.

[101] D. Golomb, X. J. Wang, and J. Rinzel. Synchronization properties of spindle oscillations in a thalamic reticular nucleus model. *J Neurophysiol*, 72(3):1109–26, 1994.

[102] D. Golomb, X. J. Wang, and J. Rinzel. Propagation of spindle waves in a thalamic slice model. *J Neurophysiol*, 75(2):750–69, 1996.

[103] J. Golowasch, L. F. Abbott, and E. Marder. Activity-dependent regulation of potassium currents in an identified neuron of the stomatogastric ganglion of the crab Cancer borealis. *J Neurosci*, 19(20):RC33+, 1999.

[104] J. Golowasch, M. Casey, L. F. Abbott, and E. Marder. Network stability from activity-dependent regulation of neuronal conductances. *Neural Comput*, 11(5):1079–96, 1999.

[105] B. C. Goodwin. Oscillatory behavior in enzymatic control processes. *Adv Enzyme Regul*, 3:425–38, 1965.

[106] C. M. Gray. Synchronous oscillations in neuronal systems: mechanisms and functions. *J Comput Neurosci*, 1(1-2):11–38, 1994.

[107] A. M. Graybiel. The basal ganglia: learning new tricks and loving it. *Curr Opin Neurobiol*, 15(6):638–44, 2005.

[108] J. S. Griffith. A field theory of neural nets: I. Derivation of field equations. *Bull Math Biophys*, 25:111–20, 1963.

[109] J. S. Griffith. A field theory of neural nets. II. Properties of the field equations. *Bull Math Biophys*, 27(2):187–95, 1965.

[110] J. S. Griffith. Mathematics of cellular control processes. I. Negative feedback to one gene. *J Theor Biol*, 20(2):202–8, 1968.

[111] J. S. Griffith. Mathematics of cellular control processes II. Positive feedback to one gene. *J Theor Biol*, 20(2):209–16, 1968.

[112] S. Grillner and P. Wallén. Central pattern generators for locomotion, with special reference to vertebrates. *Annu Rev Neurosci*, 8:233–61, 1985.

[113] P. J. Hahn and C. C. McIntyre. Modeling shifts in the rate and pattern of subthalamopallidal network activity during deep brain stimulation. *J Comput Neurosci*, 28(3):425–41, 2010.

[114] J. M. Halbertsma. The stride cycle of the cat: the modelling of locomotion by computerized analysis of automatic recordings. *Acta Physiol Scand Suppl*, 521:1–75, 1983.

[115] N. E. Hallworth, C. J. Wilson, and M. D. Bevan. Apamin-sensitive small conductance calcium-activated potassium channels, through their selective coupling to voltage-gated calcium channels, are critical determinants of the precision, pace, and pattern of action potential generation in rat subthalamic nucleus neurons in vitro. *J Neurosci*, 23(20):7525–42, 2003.

[116] C. Hammond, H. Bergman, and P. Brown. Pathological synchronization in Parkinson's disease: networks, models and treatments. *Trends Neurosci*, 30(7):357–64, 2007.

[117] R. M. Harris-Warrick. Neuromodulation and flexibility in central pattern generator networks. *Curr Opin Neurobiol*, 21(5):685–92, 2011.

[118] R. M. Harris-Warrick and E. Marder. Modulation of neural networks for behavior. *Annu Rev Neurosci*, 14:39–57, 1991.

[119] A. V. Hill. Excitation and accommodation in nerve. *Proc R Soc Lond B Biol Sci*, 119(814):305–55, 1936.

[120] A. L. Hodgkin and A. F. Huxley. A quantitative description of membrane current and its application to conduction and excitation in nerve. *J Physiol*, 117(4):500–44, 1952.

[121] J. J. Hopfield. Neural networks and physical systems with emergent collective computational abilities. *Proc Natl Acad Sci U S A*, 79(8):2554–8, 1982.

[122] J. J. Hopfield. Neurons with graded response have collective computational properties like those of two-state neurons. *Proc Natl Acad Sci U S A*, 81(10):3088–92, 1984.

[123] J. R. Huguenard and D. A. Prince. A novel T-type current underlies prolonged Ca(2+)-dependent burst firing in gabaergic neurons of rat thalamic reticular nucleus. *J Neurosci*, 12(10):3804–17, 1992.

[124] M. D. Humphries and K. N. Gurney. A pulsed neural network model of bursting in the basal ganglia. *Neural Netw*, 14(6-7):845–63, 2001.

[125] M. D. Humphries, N. Lepora, R. Wood, and K. Gurney. Capturing dopaminergic modulation and bimodal membrane behaviour of striatal medium spiny neurons in accurate, reduced models. *Front Comput Neurosci*, 3:26, 2009.

[126] M. D. Humphries, R. D. Stewart, and K. N. Gurney. A physiologically plausible model of action selection and oscillatory activity in the basal ganglia. *J Neurosci*, 26(50):12921–42, 2006.

[127] G. Indiveri, B. Linares-Barranco, T. J. Hamilton, A. van Schaik, R. Etienne-Cummings, T. Delbruck, S.-C. Liu, P. Dudek, P. Häfliger, S. Renaud, J. Schemmel, G. Cauwenberghs, J. Arthur, K. Hynna, F. Folowosele, S. Saighi, T. Serrano-Gotarredona, J. Wijekoon, Y. Wang, and K. Boahen. Neuromorphic silicon neuron circuits. *Front Neurosci*, 5:73, 2011.

[128] E. M. Izhikevich. Neural excitability, spiking and bursting. *Int J Bifurcat Chaos*, 10(6):1171–266, 2000.

[129] E. M. Izhikevich. *Dynamical Systems in Neuroscience: The Geometry of Excitability and Bursting (Computational Neuroscience)*. MIT Press, 1st edition, 2007.

[130] E. M. Izhikevich, N. S. Desai, E. C. Walcott, and F. C. Hoppensteadt. Bursts as a unit of neural information: selective communication via resonance. *Trends Neurosci*, 26(3):161–7, 2003.

[131] E. M. Izhikevich and G. M. Edelman. Large-scale model of mammalian thalamocortical systems. *Proc Natl Acad Sci U S A*, 105(9):3593–8, 2008.

[132] F. Jacob and J. Monod. Genetic regulatory mechanisms in the synthesis of proteins. *J Mol Biol*, 3:318–56, 1961.

[133] N. Jenkinson and P. Brown. New insights into the relationship between dopamine, beta oscillations and motor function. *Trends Neurosci*, 34(12):611–8, 2011.

[134] O. Jensen, M. A. Idiart, and J. E. Lisman. Physiologically realistic formation of autoassociative memory in networks with theta/gamma oscillations: role of fast NMDA channels. *Learn Mem*, 3(2-3):243–56, 1996.

[135] O. Jensen and A. Mazaheri. Shaping functional architecture by oscillatory alpha activity: gating by inhibition. *Front Hum Neurosci*, 4:186, 2010.

[136] X. Jin and R. M. Costa. Start/stop signals emerge in nigrostriatal circuits during sequence learning. *Nature*, 466(7305):457–62, 2010.

[137] S. R. Jones, C. E. Kerr, Q. Wan, D. L. Pritchett, M. Hämäläinen, and C. I. Moore. Cued spatial attention drives functionally relevant modulation of the mu rhythm in primary somatosensory cortex. *J Neurosci*, 30(41):13760–5, 2010.

[138] S. R. Jones, D. J. Pinto, T. J. Kaper, and N. Kopell. Alpha-frequency rhythms desynchronize over long cortical distances: a modeling study. *J Comput Neurosci*, 9(3):271–91, 2000.

[139] S. Kampakis. Investigating the computational power of spiking neurons with non-standard behaviors. *Neural Netw*, 43:41–54, 2013.

[140] J. Keener and J. Sneyd. *Mathematical Physiology*. Interdisciplinary applied mathematics. Springer, 1998.

[141] Z. M. Khaliq, N. W. Gouwens, and I. M. Raman. The contribution of resurgent sodium current to high-frequency firing in Purkinje neurons: an experimental and modeling study. *J Neurosci*, 23(12):4899–912, 2003.

[142] W. Klimesch, P. Sauseng, and S. Hanslmayr. EEG alpha oscillations: the inhibition-timing hypothesis. *Brain Res Rev*, 53(1):63–88, 2007.

[143] N. Kopell and G. Ermentrout. Mechanisms of phase-locking and frequency control in pairs of coupled neural oscillators. In B. Fielder, G. Iooss, and N. Kopell, editors, *Handbook of Dynamical Systems II: Towards Applications*, volume 2, chapter 1, pages 3–54. Elsevier B.V., Amsterdam, 2002.

[144] R. Krahe and F. Gabbiani. Burst firing in sensory systems. *Nat Rev Neurosci*, 5(1):13–23, 2004.

[145] M. L. Kringelbach, N. Jenkinson, S. L. F. Owen, and T. Z. Aziz. Translational principles of deep brain stimulation. *Nat Rev Neurosci*, 8(8):623–35, 2007.

[146] S. Kubota and J. E. Rubin. NMDA-induced burst firing in a model subthalamic nucleus neuron. *J Neurophysiol*, 106(2):527–537, 2011.

[147] A. A. Kühn, L. Doyle, A. Pogosyan, K. Yarrow, A. Kupsch, G.-H. Schneider, M. I. Hariz, T. Trottenberg, and P. Brown. Modulation of beta oscillations in the subthalamic area during motor imagery in Parkinson's disease. *Brain*, 129(Pt 3):695–706, 2006.

[148] A. A. Kühn, D. Williams, A. Kupsch, P. Limousin, M. Hariz, G.-H. Schneider, K. Yarrow, and P. Brown. Event-related beta desynchronization in human subthalamic nucleus correlates with motor performance. *Brain*, 127(Pt 4):735–46, 2004.

[149] A. Leblois, T. Boraud, W. Meissner, H. Bergman, and D. Hansel. Competition between feedback loops underlies normal and pathological dynamics in the basal ganglia. *J Neurosci*, 26(13):3567–83, 2006.

[150] D. K. Leventhal, G. J. Gage, R. Schmidt, J. R. Pettibone, A. C. Case, and J. D. Berke. Basal ganglia beta oscillations accompany cue utilization. *Neuron*, 73(3):523–36, 2012.

[151] R. Levy, P. Ashby, W. D. Hutchison, A. E. Lang, A. M. Lozano, and J. O. Dostrovsky. Dependence of subthalamic nucleus oscillations on movement and dopamine in Parkinson's disease. *Brain*, 125(Pt 6):1196–209, 2002.

[152] T. Lindeberg. Scale-space theory: A basic tool for analysing structures at different scales. *J Appl Stat*, pages 224–70, 1994.

[153] B. Lindner, A. Longtin, and A. R. Bulsara. Analytic expressions for rate and CV of a type I neuron driven by white gaussian noise. *Neural Comput*, 15(8):1761–88, 2003.

[154] J. E. Lisman. Bursts as a unit of neural information: making unreliable synapses reliable. *Trends Neurosci*, 20(1):38–43, 1997.

[155] Z. Liu, J. Golowasch, E. Marder, and L. F. Abbott. A model neuron with activity-dependent conductances regulated by multiple calcium sensors. *J Neurosci*, 18(7):2309–20, 1998.

[156] R. Llinás and M. Sugimori. Electrophysiological properties of in vitro Purkinje cell dendrites in mammalian cerebellar slices. *J Physiol*, 305:197–213, 1980.

[157] R. Llinás and M. Sugimori. Electrophysiological properties of in vitro Purkinje cell somata in mammalian cerebellar slices. *J Physiol*, 305:171–95, 1980.

[158] R. R. Llinás and M. Steriade. Bursting of thalamic neurons and states of vigilance. *J Neurophysiol*, 95(6):3297–308, 2006.

[159] Y. Loewenstein, S. Mahon, P. Chadderton, K. Kitamura, H. Sompolinsky, Y. Yarom, and M. Häusser. Bistability of cerebellar Purkinje cells modulated by sensory stimulation. *Nat Neurosci*, 8(2):202–11, 2005.

[160] W. Maass. Networks of spiking neurons: The third generation of neural network models. *Neural Netw*, 10(9):1659–71, 1997.

[161] W. Maass and H. Markram. On the computational power of circuits of spiking neurons. *J Comput Syst Sci*, 69(4):593–616, 2004.

[162] W. Maass, T. Natschläger, and H. Markram. Real-time computing without stable states: A new framework for neural computation based on perturbations. *Neural Comput*, 14(11):2531–60, 2002.

[163] S. G. Mallat. A theory for multiresolution signal decomposition: the wavelet representation. *IEEE Trans Pattern Anal Mach Intell*, 11:674–93, 1989.

[164] S. G. Mallat. *A Wavelet Tour of Signal Processing, Third Edition: The Sparse Way*. Academic Press, 2008.

[165] N. Mallet, A. Pogosyan, A. Sharott, J. Csicsvari, J. P. Bolam, P. Brown, and P. J. Magill. Disrupted dopamine transmission and the emergence of exaggerated beta oscillations in subthalamic nucleus and cerebral cortex. *J Neurosci*, 28(18):4795–806, 2008.

[166] E. Marder. Neuromodulation of neuronal circuits: back to the future. *Neuron*, 76(1):1–11, 2012.

[167] E. Marder, L. F. Abbott, G. G. Turrigiano, Z. Liu, and J. Golowasch. Memory from the dynamics of intrinsic membrane currents. *Proc Natl Acad Sci U S A*, 93(24):13481–6, 1996.

[168] E. Marder and D. Bucher. Central pattern generators and the control of rhythmic movements. *Curr Biol*, 11(23):R986–96, 2001.

[169] E. Marder and R. L. Calabrese. Principles of rhythmic motor pattern generation. *Physiol Rev*, 76(3):687–717, 1996.

[170] E. Marder and J.-M. Goaillard. Variability, compensation and homeostasis in neuron and network function. *Nat Rev Neurosci*, 7(7):563–74, 2006.

[171] E. Marder and V. Thirumalai. Cellular, synaptic and network effects of neuromodulation. *Neural Netw*, 15(4-6):479–93, 2002.

[172] K. E. Mathewson, A. Lleras, D. M. Beck, M. Fabiani, T. Ro, and G. Gratton. Pulsed out of awareness: EEG alpha oscillations represent a pulsed-inhibition of ongoing cortical processing. *Front Psychol*, 2:99, 2011.

[173] M. M. McCarthy, S. Ching, M. A. Whittington, and N. Kopell. Dynamical changes in neurological diseases and anesthesia. *Curr Opin Neurobiol*, 22(4):693–703, 2012.

[174] M. M. McCarthy, C. Moore-Kochlacs, X. Gu, E. S. Boyden, X. Han, and N. Kopell. Striatal origin of the pathologic beta oscillations in Parkinson's disease. *Proc Natl Acad Sci U S A*, 108(28):11620–5, 2011.

[175] D. A. McCormick. Cholinergic and noradrenergic modulation of thalamocortical processing. *Trends Neurosci*, 12(6):215–21, 1989.

[176] D. A. McCormick and T. Bal. Sleep and arousal: thalamocortical mechanisms. *Annu Rev Neurosci*, 20:185–215, 1997.

[177] D. A. McCormick and H. R. Feeser. Functional implications of burst firing and single spike activity in lateral geniculate relay neurons. *Neuroscience*, 39(1):103–13, 1990.

[178] D. A. McCormick and H. C. Pape. Properties of a hyperpolarization-activated cation current and its role in rhythmic oscillation in thalamic relay neurones. *J Physiol*, 431:291–318, 1990.

[179] C. Mead. *Analog VLSI and Neural Systems*. Addison-Wesley Longman Publishing Co., Inc., Boston, MA, USA, 1989.

[180] R. Milo, S. Shen-Orr, S. Itzkovitz, N. Kashtan, D. Chklovskii, and U. Alon. Network motifs: simple building blocks of complex networks. *Science*, 298(5594):824–7, 2002.

[181] J. W. Mink. The basal ganglia: focused selection and inhibition of competing motor programs. *Prog Neurobiol*, 50(4):381–425, 1996.

[182] J. Mo, C. E. Schroeder, and M. Ding. Attentional modulation of alpha oscillations in macaque inferotemporal cortex. *J Neurosci*, 31(3):878–82, 2011.

[183] C. Morris and H. Lecar. Voltage oscillations in the barnacle giant muscle fiber. *Biophys J*, 35(1):193–213, 1981.

[184] F. Nadim and D. Bucher. Neuromodulation of neurons and synapses. *Curr Opin Neurobiol*, 29C:48–56, 2014.

[185] F. Nadim, O. H. Olsen, E. De Schutter, and R. L. Calabrese. Modeling the leech heartbeat elemental oscillator. I. Interactions of intrinsic and synaptic currents. *J Comput Neurosci*, 2(3):215–35, 1995.

[186] J. Nagumo, S. Arimoto, and S. Yoshizawa. An active pulse transmission line simulating nerve axon. *Proc IEEE*, 50(10):2061–70, 1962.

[187] A. Nambu. Seven problems on the basal ganglia. *Curr Opin Neurobiol*, 18(6):595–604, 2008.

[188] A. Nambu and R. Llinas. Electrophysiology of globus pallidus neurons in vitro. *J Neurophysiol*, 72(3):1127–39, 1994.

[189] A. J. Nevado Holgado, N. Mallet, P. J. Magill, and R. Bogacz. Effective connectivity of the subthalamic nucleus-globus pallidus network during parkinsonian oscillations. *J Physiol*, 592(Pt 7):1429–55, 2014.

[190] A. J. Nevado Holgado, J. R. Terry, and R. Bogacz. Conditions for the generation of beta oscillations in the subthalamic nucleus-globus pallidus network. *J Neurosci*, 30(37):12340–52, 2010.

[191] Z. Ni, R. Bouali-Benazzouz, D. Gao, A. L. Benabid, and A. Benazzouz. Changes in the firing pattern of globus pallidus neurons after the degeneration of nigrostriatal pathway are mediated by the subthalamic nucleus in the rat. *Eur J Neurosci*, 12(12):4338–44, 2000.

[192] B. Novak and J. J. Tyson. Numerical analysis of a comprehensive model of M-phase control in Xenopus oocyte extracts and intact embryos. *J Cell Sci*, 106:1153–68, 1993.

[193] J. A. Obeso, C. Marin, C. Rodriguez-Oroz, J. Blesa, B. Benitez-Temiño, J. Mena-Segovia, M. Rodríguez, and C. W. Olanow. The basal ganglia in Parkinson's disease: current concepts and unexplained observations. *Ann Neurol*, 64 Suppl 2:S30–46, 2008.

[194] A. Olypher, G. Cymbalyuk, and R. L. Calabrese. Hybrid systems analysis of the control of burst duration by low-voltage-activated calcium current in leech heart interneurons. *J Neurophysiol*, 96(6):2857–67, 2006.

[195] A. Oppenheim, A. Willsky, and S. Nawab. *Signals and Systems*. Prentice-Hall signal processing series. Prentice Hall, 1997.

[196] T. Otsuka, T. Abe, T. Tsukagawa, and W.-J. Song. Conductance-based model of the voltage-dependent generation of a plateau potential in subthalamic neurons. *J Neurophysiol*, 92(1):255–64, 2004.

[197] T. Otsuka, F. Murakami, and W. J. Song. Excitatory postsynaptic potentials trigger a plateau potential in rat subthalamic neurons at hyperpolarized states. *J Neurophysiol*, 86(4):1816–25, 2001.

[198] D. Parker. Neuronal network analyses: premises, promises and uncertainties. *Philos Trans R Soc Lond B Biol Sci*, 365(1551):2315–28, 2010.

[199] A. Pavlides, S. J. Hogan, and R. Bogacz. Improved conditions for the generation of beta oscillations in the subthalamic nucleus–globus pallidus network. *Eur J Neurosci*, 36(2):2229–39, 2012.

[200] D. H. Perkel and B. Mulloney. Motor pattern production in reciprocally inhibitory neurons exhibiting postinhibitory rebound. *Science*, 185(4146):181–3, 1974.

[201] A. L. Person and I. M. Raman. Synchrony and neural coding in cerebellar circuits. *Front Neural Circuit*, 6:97, 2012.

[202] D. Plenz and S. T. Kitai. A basal ganglia pacemaker formed by the subthalamic nucleus and external globus pallidus. *Nature*, 400(6745):677–82, 1999.

[203] J. R. Pomerening, S. Y. Kim, and J. E. Ferrell, Jr. Systems-level dissection of the cell-cycle oscillator: bypassing positive feedback produces damped oscillations. *Cell*, 122(4):565–78, 2005.

[204] J. R. Pomerening, E. D. Sontag, and J. E. Ferrell, Jr. Building a cell cycle oscillator: hysteresis and bistability in the activation of Cdc2. *Nat Cell Biol*, 5(4):346–51, 2003.

[205] D. Prokhorov. Echo state networks: Appeal and challenges. In *Proc. of International Joint Conference on Neural Networks*, volume 3, pages 1463–6, Ford Res. & Adv. Eng., Dearborn, MI, USA, 2005.

[206] I. M. Raman and B. P. Bean. Resurgent sodium current and action potential formation in dissociated cerebellar Purkinje neurons. *J Neurosci*, 17(12):4517–26, 1997.

[207] I. M. Raman and B. P. Bean. Inactivation and recovery of sodium currents in cerebellar Purkinje neurons: evidence for two mechanisms. *Biophys J*, 80(2):729–37, 2001.

[208] E. J. Ramcharan, J. W. Gnadt, and S. M. Sherman. Burst and tonic firing in thalamic cells of unanesthetized, behaving monkeys. *Vis Neurosci*, 17(1):55–62, 2000.

[209] N. Rashevsky. Outline of a physico-mathematical theory of excitation and inhibition. *Protoplasma*, 20(1):42–56, 1933.

[210] P. Redgrave, N. Vautrelle, and J. N. J. Reynolds. Functional properties of the basal ganglia's re-entrant loop architecture: selection and reinforcement. *Neuroscience*, 198:138–51, 2011.

[211] J. Rinzel, D. Terman, X. Wang, and B. Ermentrout. Propagating activity patterns in large-scale inhibitory neuronal networks. *Science*, 279(5355):1351–5, 1998.

[212] J. E. Rubin, C. C. McIntyre, R. S. Turner, and T. Wichmann. Basal ganglia activity patterns in parkinsonism and computational modeling of their downstream effects. *Eur J Neurosci*, 36(2):2213–28, 2012.

[213] P. Sacré. *Systems analysis of oscillator models in the space of phase response curves*. PhD thesis, University of Liège, Belgium, 2013.

[214] R. A. Satterlie. Reciprocal inhibition and postinhibitory rebound produce reverberation in a locomotor pattern generator. *Science*, 229(4711):402–4, 1985.

[215] S. J. Schiff. Towards model-based control of Parkinson's disease. *Philos Trans A Math Phys Eng Sci*, 368(1918):2269–308, 2010.

[216] S. M. Sherman. Dual response modes in lateral geniculate neurons: mechanisms and functions. *Vis Neurosci*, 13(2):205–13, 1996.

[217] S. M. Sherman. Tonic and burst firing: dual modes of thalamocortical relay. *Trends Neurosci*, 24(2):122–6, 2001.

[218] S. M. Sherman and R. W. Guillery. Functional organization of thalamocortical relays. *J Neurophysiol*, 76(3):1367–95, 1996.

[219] S. M. Sherman and R. W. Guillery. On the actions that one nerve cell can have on another: distinguishing "drivers" from "modulators". *Proc Natl Acad Sci U S A*, 95(12):7121–6, 1998.

[220] S. M. Sherman and R. W. Guillery. *Exploring the Thalamus and Its Role in Cortical Function*. MIT Press, 2006.

[221] A. M. Sillito and H. E. Jones. Corticothalamic interactions in the transfer of visual information. *Philos Trans R Soc Lond B Biol Sci*, 357(1428):1739–52, 2002.

[222] E. Sitnikova. Thalamo-cortical mechanisms of sleep spindles and spike-wave discharges in rat model of absence epilepsy (a review). *Epilepsy Res*, 89(1):17–26, 2010.

[223] F. K. Skinner, N. Kopell, and E. Marder. Mechanisms for oscillation and frequency control in reciprocally inhibitory model neural networks. *J Comput Neurosci*, 1(1-2):69–87, 1994.

[224] F. K. Skinner, G. G. Turrigiano, and E. Marder. Frequency and burst duration in oscillating neurons and two-cell networks. *Biol Cybern*, 69(5-6):375–83, 1993.

[225] Y. Smith and R. Villalba. Striatal and extrastriatal dopamine in the basal ganglia: an overview of its anatomical organization in normal and parkinsonian brains. *Mov Disord*, 23 Suppl 3:S534–47, 2008.

[226] V. S. Sohal and J. R. Huguenard. Reciprocal inhibition controls the oscillatory state in thalamic networks. *Neurocomputing*, 44–46(0):653 – 9, 2002.

[227] W. J. Song, Y. Baba, T. Otsuka, and F. Murakami. Characterization of Ca^{2+} channels in rat subthalamic nucleus neurons. *J Neurophysiol*, 84(5):2630–7, 2000.

[228] M. Sorensen, S. DeWeerth, G. Cymbalyuk, and R. L. Calabrese. Using a hybrid neural system to reveal regulation of neuronal network activity by an intrinsic current. *J Neurosci*, 24(23):5427–38, 2004.

[229] O. Sporns. *Networks of the Brain*. MIT Press, 1st edition, 2011.

[230] O. Sporns and R. Kötter. Motifs in brain networks. *PLoS Biol*, 2(11):e369, 2004.

[231] M. Steriade. Corticothalamic resonance, states of vigilance and mentation. *Neuroscience*, 101(2):243–76, 2000.

[232] M. Steriade. Grouping of brain rhythms in corticothalamic systems. *Neuroscience*, 137(4):1087–106, 2006.

[233] M. Steriade, P. Gloor, R. R. Llinás, F. H. Lopes da Silva, and M. M. Mesulam. Basic mechanisms of cerebral rhythmic activities. *Electroen Clin Neuro*, 76(6):481–508, 1990.

[234] J. Stricker, S. Cookson, M. R. Bennett, W. H. Mather, L. S. Tsimring, and J. Hasty. A fast, robust and tunable synthetic gene oscillator. *Nature*, 456(7221):516–9, 2008.

[235] G. M. Süel, J. Garcia-Ojalvo, L. M. Liberman, and M. B. Elowitz. An excitable gene regulatory circuit induces transient cellular differentiation. *Nature*, 440(7083):545–50, 2006.

[236] D. J. Surmeier, J. Ding, M. Day, Z. Wang, and W. Shen. D1 and D2 dopamine-receptor modulation of striatal glutamatergic signaling in striatal medium spiny neurons. *Trends Neurosci*, 30(5):228–35, 2007.

[237] Y. Tachibana, H. Iwamuro, H. Kita, M. Takada, and A. Nambu. Subthalamo-pallidal interactions underlying parkinsonian neuronal oscillations in the primate basal ganglia. *Eur J Neurosci*, 34(9):1470–84, 2011.

[238] C.-H. Tai, Y.-C. Yang, M.-K. Pan, C.-S. Huang, and C.-C. Kuo. Modulation of subthalamic T-type Ca^{2+} channels remedies locomotor deficits in a rat model of Parkinson's disease. *J Clin Invest*, 121(8):3289–305, 2011.

[239] D. Terman, A. Bose, and N. Kopell. Functional reorganization in thalamocortical networks: transition between spindling and delta sleep rhythms. *Proc Natl Acad Sci U S A*, 93(26):15417–22, 1996.

[240] D. Terman, J. E. Rubin, A. C. Yew, and C. J. Wilson. Activity patterns in a model for the subthalamopallidal network of the basal ganglia. *J Neurosci*, 22(7):2963–76, 2002.

[241] G. Thut, C. Miniussi, and J. Gross. The functional importance of rhythmic activity in the brain. *Curr Biol*, 22(16):R658–63, 2012.

[242] P. H. Tiesinga, J. M. Fellous, J. V. José, and T. J. Sejnowski. Computational model of carbachol-induced delta, theta, and gamma oscillations in the hippocampus. *Hippocampus*, 11(3):251–74, 2001.

[243] I. Timofeev and M. Bazhenov. Mechanisms and biological role of thalamocortical oscillations. In F. Columbus, editor, *Trends in Chronobiology Research*, chapter 1, pages 1–47. Nova Science Publishers, Inc., 2005.

[244] G. Turrigiano, G. LeMasson, and E. Marder. Selective regulation of current densities underlies spontaneous changes in the activity of cultured neurons. *J Neurosci*, 15(5 Pt 1):3640–52, 1995.

[245] J. J. Tyson. Modeling the cell division cycle: cdc2 and cyclin interactions. *Proc Natl Acad Sci U S A*, 88(16):7328–32, 1991.

[246] J. J. Tyson, R. Albert, A. Goldbeter, P. Ruoff, and J. Sible. Biological switches and clocks. *J R Soc Interface*, 5 Suppl 1:S1–8, 2008.

[247] J. J. Tyson, K. C. Chen, and B. Novak. Sniffers, buzzers, toggles and blinkers: dynamics of regulatory and signaling pathways in the cell. *Curr Opin Cell Biol*, 15(2):221–31, 2003.

[248] J. J. Tyson and B. Novak. Temporal organization of the cell cycle. *Curr Biol*, 18(17):R759–68, 2008.

[249] J. J. Tyson and B. Novák. Functional motifs in biochemical reaction networks. *Annu Rev Phys Chem*, 61(1):219–40, 2010.

[250] P. J. Uhlhaas and W. Singer. Neural synchrony in brain disorders: relevance for cognitive dysfunctions and pathophysiology. *Neuron*, 52(1):155–68, 2006.

[251] D. Verstraeten, B. Schrauwen, M. D'Haene, and D. Stroobandt. An experimental unification of reservoir computing methods. *Neural Netw*, 20(3):391–403, 2007.

[252] M. W and B. C. M. *Pulsed Neural Networks*. MIT press, 2001.

[253] X.-J. Wang. Neurophysiological and computational principles of cortical rhythms in cognition. *Physiol Rev*, 90(3):1195–268, 2010.

[254] X. J. Wang, D. Golomb, and J. Rinzel. Emergent spindle oscillations and intermittent burst firing in a thalamic model: specific neuronal mechanisms. *Proc Natl Acad Sci U S A*, 92(12):5577–81, 1995.

[255] X.-J. Wang and J. Rinzel. Alternating and synchronous rhythms in reciprocally inhibitory model neurons. *Neural Comput*, 4(1):84–97, 1992.

[256] X. J. Wang and J. Rinzel. Spindle rhythmicity in the reticularis thalami nucleus: synchronization among mutually inhibitory neurons. *Neuroscience*, 53(4):899–904, 1993.

[257] M. Weinberger and J. O. Dostrovsky. A basis for the pathological oscillations in basal ganglia: the crucial role of dopamine. *Neuroreport*, 22(4):151–6, 2011.

[258] M. Weinberger, W. D. Hutchison, and J. O. Dostrovsky. Pathological subthalamic nucleus oscillations in PD: can they be the cause of bradykinesia and akinesia? *Exp Neurol*, 219(1):58–61, 2009.

[259] T. Wichmann and J. Dostrovsky. Pathological basal ganglia activity in movement disorders. *Neuroscience*, 198:232–44, 2011.

[260] S. R. Williams, S. R. Christensen, G. J. Stuart, and M. Häusser. Membrane potential bistability is controlled by the hyperpolarization-activated current IH in rat cerebellar Purkinje neurons in vitro. *J Physiol*, 539(2):469–83, 2002.

[261] C. J. Wilson and M. D. Bevan. Intrinsic dynamics and synaptic inputs control the activity patterns of subthalamic nucleus neurons in health and in Parkinson's disease. *Neuroscience*, 198:54–68, 2011.

[262] H. R. Wilson. *Spikes, Decisions, and Actions: The Dynamical Foundations of Neurosciences*. Oxford University Press, Incorporated, 1999.

[263] H. R. Wilson and J. D. Cowan. Excitatory and inhibitory interactions in localized populations of model neurons. *Biophys J*, 12(1):1–24, 1972.

[264] H. R. Wilson and J. D. Cowan. A mathematical theory of the functional dynamics of cortical and thalamic nervous tissue. *Kybernetik*, 13(2):55–80, 1973.

[265] T. Womelsdorf, T. A. Valiante, N. T. Sahin, K. J. Miller, and P. Tiesinga. Dynamic circuit motifs underlying rhythmic gain control, gating and integration. *Nat Neurosci*, 17(8):1031–9, 2014.

[266] M. S. Worden, J. J. Foxe, N. Wang, and G. V. Simpson. Anticipatory biasing of visuospatial attention indexed by retinotopically specific alpha-band electroencephalography increases over occipital cortex. *J Neurosci*, 20(6):RC63, 2000.

[267] Z. Xiang, A. D. Thompson, J. T. Brogan, M. L. Schulte, B. J. Melancon, D. Mi, L. M. Lewis, B. Zou, L. Yang, R. Morrison, T. Santomango, F. Byers, K. Brewer, J. S. Aldrich, H. Yu, E. S. Dawson, M. Li, O. McManus, C. K. Jones, J. S. Daniels, C. R. Hopkins, X. S. Xie, P. J. Conn, C. D. Weaver, and C. W. Lindsley. The discovery and characterization of ML218: A novel, centrally active T-type calcium channel inhibitor with robust effects in STN neurons and in a rodent model of Parkinson's disease. *ACS Chem Neurosci*, 2(12):730–42, 2011.

[268] M. M. Yartsev, R. Givon-Mayo, M. Maller, and O. Donchin. Pausing Purkinje cells in the cerebellum of the awake cat. *Front Syst Neurosci*, 3:2, 2009.